technische universität
dortmund

Ultraviolet photoelectron spectroscopy and scanning tunnelling microscopy of silver and copper clusters on HOPG, noble metals and rare gas layers

Dissertation

Zur Erlangung des Doktorgrades der Naturwissenschaften der Fakultät Physik der Technischen Universität Dortmund

Vorgelegt von
Natalie Janina Miroslawski

Oktober 2013

Gutachter:

Erstgutachter: apl. Prof. Dr. Heinz Hövel

Zweitgutachter: Prof. Dr. Markus Betz

TABLE OF CONTENTS

1 Introduction

Ever since humans had an interest in understanding how the phenomena they could observe in nature work. Therefore they started to observe and investigate the nature around them and with this the science field of physics was born. In the beginning physics (from Greek φύσις which means "nature") was a part of the natural philosophy which has its origins in Greece and became a separate science in the early modern Europe.

Two fields of modern physics today are solid state physics and particle physics. The first field investigates the interaction of solid matter. The second field investigates the interaction of single particles and the composition of these particles, which are the basic module of solid matter. In both fields different physical concepts are used and they can be treated separately. A link between these two independent fields is the physics of clusters. A cluster is a small particle consisting of only a few atoms ($3 - 10^5$) which changes its physical properties from particle like to bulk like depending on its size.

The investigation of clusters began in the 1950s although the special size dependent properties of clusters were already used by the ancient Egyptians 3500 years ago [1]. They colored glass by adding metal compounds. In melted glass the metal atoms are released and assemble to clusters of different size. The longer the glass is held at high temperatures the bigger the clusters become. Depending on the cluster size the electronic and optical properties of the clusters change resulting in a change of the color of the glass (for silver clusters from red for small clusters to green for big clusters) [2]. The same principle was used for the coloring of church windows.

Today the field of application for clusters is much bigger. For example, they are used in cosmetics for sun protecting cremes and deodorants. In the latter case mostly silver nanoparticles are used to prevent the development of bacteria due to their antimicrobial activity [3]. In addition magnetic clusters can be used in medicine for drug delivery, as magnetic resonance imaging contrast agents and for cancer therapy [4]. In the latter case magnetic nanoparticles are transported to the cancer cells where they are heated up due to an external magnetic field which results in a suppression of the cancer cells.

A big area of application exists for clusters deposited on surfaces, e.g. for catalysis [5]. For example small gold clusters (with ≤ 20 atoms per cluster) are deposited on magnesia and then catalyse the reaction of CO to CO_2 while bulk gold shows no catalytic reaction. Other applications for deposited clusters are, e.g. data storage and the building of nanoelectronics [4].

Although clusters are widely used today, their properties are not yet fully understood and need further investigation. Therefore the investigation of the geometrical and electronical properties of clusters deposited on surfaces is the subject of this thesis.

An overview about the general properties of clusters and the used substrates is depicted in **chapter 2&3**. Then the experimental setup is described (**chapter 4**), consisting of the cluster source facility and a surface science facility. This is followed by the methods used for sample preparation and cluster deposition (**chapter 5**). Within this thesis the clusters were investigated with scanning tunnelling microscopy (STM) and ultraviolet photoelectron spectroscopy (UPS). These two measuring techniques used are described in **chapter 6**. In the course of this thesis results of UPS measurements of deposited clusters are compared with results of UPS measurements of free beam clusters. The data for free beam clusters were made available by *Bernd von Issendorff* from the Albert-Ludwig-Universität in Freiburg and extracted from other sources in the literature. For a better comprehension a short overview about the measuring procedure of free beam clusters as used by the group of *Bernd von Issendorff* is given in **chapter 7**. The results for deposited copper and silver clusters on various substrates and the comparison of the UPS results with results of free beam spectra are presented in **chapter 8**. Besides UPS measurements STM measurements are presented which are compared with computer simulations from *Michael Moseler* and *Tommi Järvi* from the Fraunhofer Institute for Mechanics of Materials IWM in Freiburg. **Chapter 9** gives a summary of the results achieved during this work and an outlook on future experiments.

2 Cluster

According to the *Concise Oxford Dictionary* a cluster is explained as "a group of similar things". In accordance with this the word *cluster* is common in many fields. For example, in astrophysics the term is used for an accumulation of stars or for an agglomeration of computers in the IT-sector.
In cluster physics the term *cluster* describes a conglomeration of N atoms or molecules with $N=3 - 10^5$ and a height of a few to a several hundred nano meters. Depending on their composition clusters may exhibit different binding types, like van der Waals attraction (He or Ar clusters), covalent chemical bonds (Si clusters) or metallic bonds (Na and Cu clusters) [6]. Additionally, they show different geometries and electronic structures. Clusters show properties intermediate between those of single atoms, with discrete energy states and bulk matter, characterized by continua or bands of states [7]. They represent a link between the fields of molecular and solid state physics. Methods and concepts of both fields have to be understood to describe the physical properties of clusters. In cluster physics the observed phenomena are discussed as a function of the cluster size. For example, the binding character of the atoms in silver clusters changes from a covalent bonding for small clusters [6] to a metallic bonding for large clusters or micro crystallites due to the fact that clusters have quantized or bulk-like properties depending on the cluster size.

Clusters can be subdivided in four groups depending of the number of atoms per cluster [2]:

- Microclusters (2<N<13 atoms): all atoms can be found at the surface of the cluster. Here a cluster can be treated like a molecule at low temperatures.
- Small clusters (13≤N≤100 atoms): multiple isomers exist. As a result there are different energy levels and the methods of molecular physics begin to break down. First bulk-like properties begin to occur.
- Large clusters (100<N≤1000 atoms): the transition to a bulk begins.
- Micro crystallites (N>1000 atoms): most of the bulk properties are reached.

The ratio between atoms on the surface of a cluster to atoms in the volume is very high [6, 2]. This is shown mathematically in [2]:
Reckoning a spherical cluster with a volume $V_{sphere}= 4/3\pi R^3$ and a surface $A_{sphere}= 4\pi R^2$ (R= radius of the cluster) it becomes clear the smaller a cluster is the more atoms are at the surface:

$$K \propto \frac{A_{sphere}}{V_{sphere}} = \frac{3}{R} \propto \frac{1}{R}, \tag{1.1}$$

with K as the ratio between the atoms on the surface of a cluster to the atoms in the volume. For a cluster with N atoms with a radius r for one atom the cluster radius R is $R \propto \sqrt[3]{N}r$. So the ratio K becomes $K \propto N^{-\frac{1}{3}}$.

The main focus of this work is the investigation of the properties of metal clusters, especially silver and copper clusters, particularly with regard to their electronic and geometric properties. The clusters have been deposited onto different surfaces which change the general properties of the clusters compared with free beam clusters [8].

Certain cluster sizes show an enhanced stability due to electronic or geometric shell closings. This is described in detail in the two following chapters.

2.1. Electronic magic clusters

A model to describe the binding of small metal clusters is the spherical jellium model [9, 10, 11, 12]. It assumes a uniform background of positive charge, which replaces the positive ions, where electrons can move and are exposed to an external potential [6]. Simple forms of such a potential are an infinite harmonic potential or a spherical box potential with infinitely high walls. A more realistic potential is the Wood-Saxon potential, a finite deep box potential with rounded walls. The solution of the single electron Schrödinger equation for the three potentials is shown in figure 1.

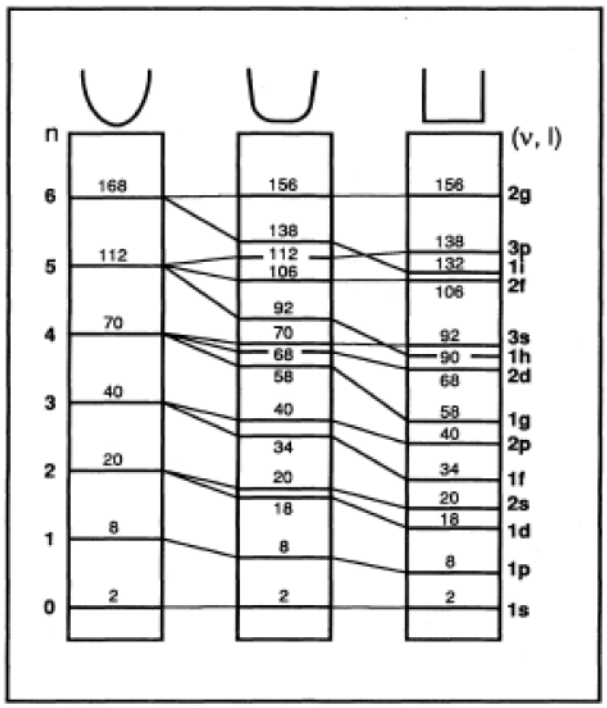

Figure 1: Energy-level occupations for different spherical symmetric potentials (harmonic, Wood-Saxon and box potential). In cluster physics the quantum numbers follow the nuclear convention, so each shell is characterized by a radial quantum number *n* and an angular quantum number *l*. Levels with the same angular momentum are connected. The numbers on the levels indicate the accumulated electron count. [13]

Clusters with closed electronic shells are the most stable ones. This is the case when the electronic levels are filled completely and a large gap exists between the highest

occupied level and the lowest unoccupied level in the cluster. The clusters are then called electronically magic clusters. So the magic numbers of the Wood-Saxon potential are: 2, 8, 18, 20, 34,…. etc. In 1982 KAPPES [14] and in 1984/85 KNIGHT et al [15][16] observed electronically magic clusters in mass spectra of sodium and potassium clusters for the first time. The spectra showed relatively high peaks for clusters with 8, 20, 40 and 58 atoms (figure **2**), indicating enhanced stability for this cluster sizes. This implies that the effective potential of a cluster is somewhere between a box and a Wood-Saxon potential [17].

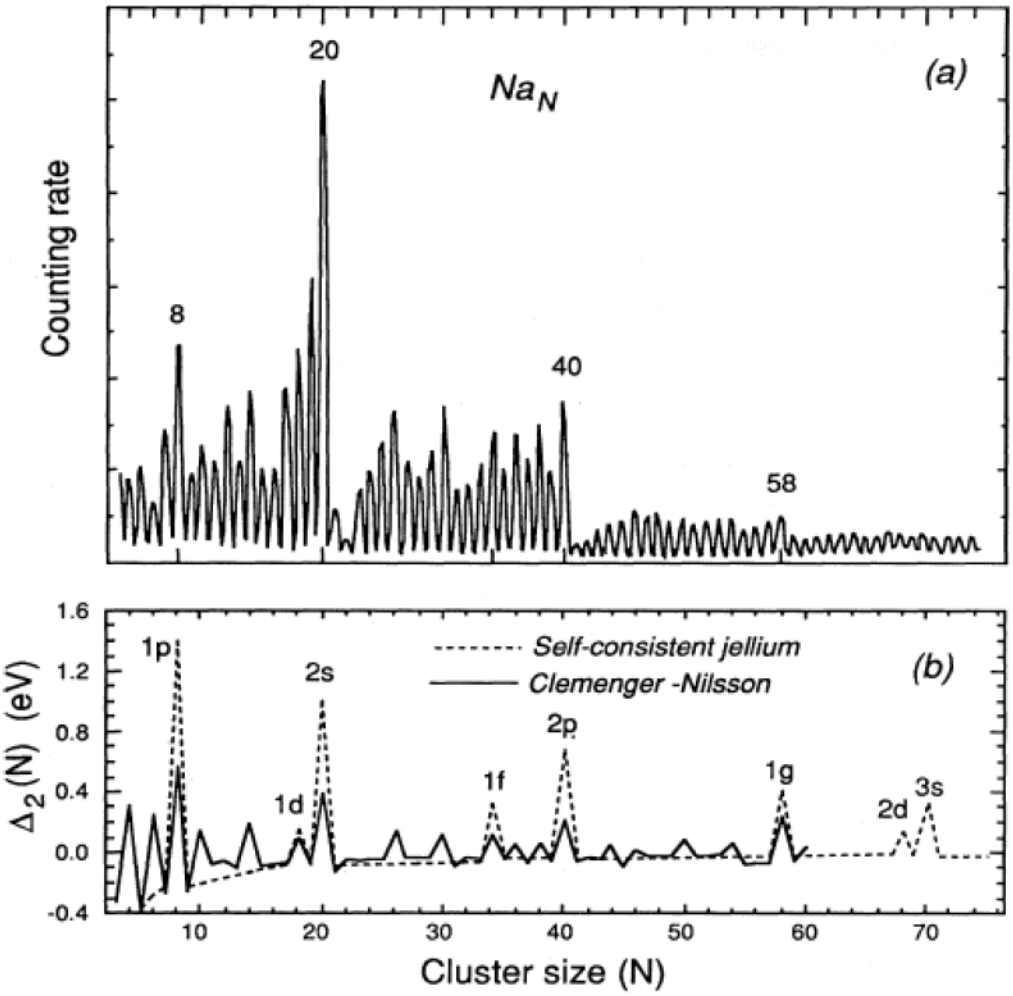

Figure 2: Spectrum of sodium clusters. (a) experimental [15]; (b) dashed line, using Woods-Saxon potential [15]; solid line, using Clemenger-Nilsson model [18, 19].[13]

In this sense a cluster is treated like one atom to describe its electronic properties. The atoms of the cluster are treated like the atom core and the valence electrons of all atoms are put together to form orbitals as in an atom, i.e. a cluster can be treated mathematically like an atom. Thus, in spherical clusters electrons occupy orbitals, as in an atom. With growing cluster size the orbitals get filled with electrons and when an electronic shell is full, enhanced stability occurs. This magic cluster sizes are equivalent to the rare gas atoms in the periodic system. Clusters with newly opened shells are less

stable because the electrons in these shells are less tightly bound. Thereby the mass spectra show an abrupt decrease in intensity after an electronically magic cluster size.

In the spherical jellium model the clusters are supposed to be spheres. But this approximation is only reasonable for electronically closed shells. Open-shell clusters are unstable towards distortion due to the asymmetric distribution of the electrons in the cluster. This effect is called the Jahn-Teller effect [20]. In 1985 CLEMENGER [21] adapted the deformed nuclear shell model of NILSSON [22] to alkali clusters and found that nearly all of the fine structure in the spectrum appears within this model (figure **2**). This model is called the Clemenger-Nilsson model. The assumption is that clusters with not totally filled shells can reduce their total energy by a deformation of the cluster shape and by the lifting of the degeneracy of the electronic shells.

The Clemenger-Nilsson model [21] defines a distortion parameter δ which is defined by [17]

$$\delta = \frac{R_z - R_x}{R_z + R_x}, \tag{1.2}$$

where R_z is the cluster radius along the rotational symmetry axis and R_x is the radius perpendicular to it. Additionally, the model assumes that the single particle potential is effectively the one of a three-dimensional harmonic oscillator. The resulting single-electron levels are shown in figure **3**.

For $\delta = 0$ the clusters are spherical and show the same electronically magic numbers, indicating closed shells, as in the experiment. For $\delta \neq 0$ the clusters deform to minimize their energy. A prolate deformation occurs typically when the uppermost shell is less than half filled and an oblate deformation occurs for an almost filled shell. The electrons in the distorted clusters are localised in subshells which have a lower energy than the electrons in the spherical clusters. Additionally, the spherical distortions cause subshell closings which can also be seen in the spectra [13] (figure **2**).

In this thesis silver and copper clusters are investigated. The theories described in this chapter for sodium and potassium clusters can be adopted to silver and copper clusters because they also have a s^1-electron [23]. Therefore the same electronic magic numbers can be found for these two metals. The clusters in this thesis are positively charged for the purpose of mass selection (chapter 4.1.3 and 5.2). So the magic numbers are as follows: Ag_3^+, Ag_9^+, Ag_{20}^+… Due to the positive charge, the electronic shells are closed for one cluster size higher.

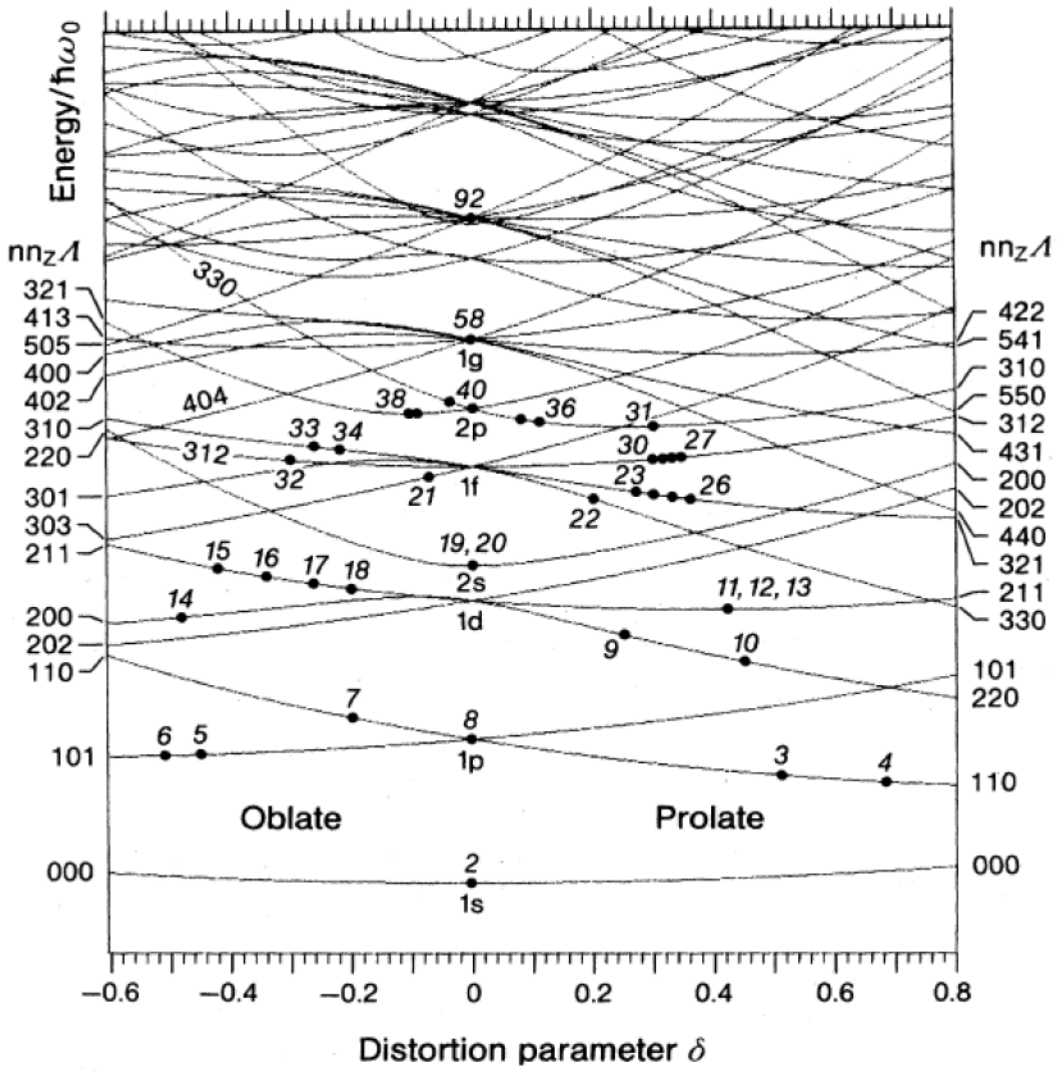

Figure 3: Nilsson diagram of cluster energy levels as a function of the distortion parameter δ. The points in the figure indicate the position of the highest occupied level for each cluster, at the value of δ corresponding to the assigned ground state. [21]

2.2. Geometric magic clusters

A second possibility to enhance the stability of clusters is the arrangement of the atoms to closed shells. This was observed for the first time 1981 by ECHT [24] for free xenon clusters (figure **4**) and later by MARTIN [25] (experimentally) and STAMPFLI [26] (theoretically) for metal clusters. The clusters form so called closed-shell MACKAY icosahedra [27] (figure **5**).

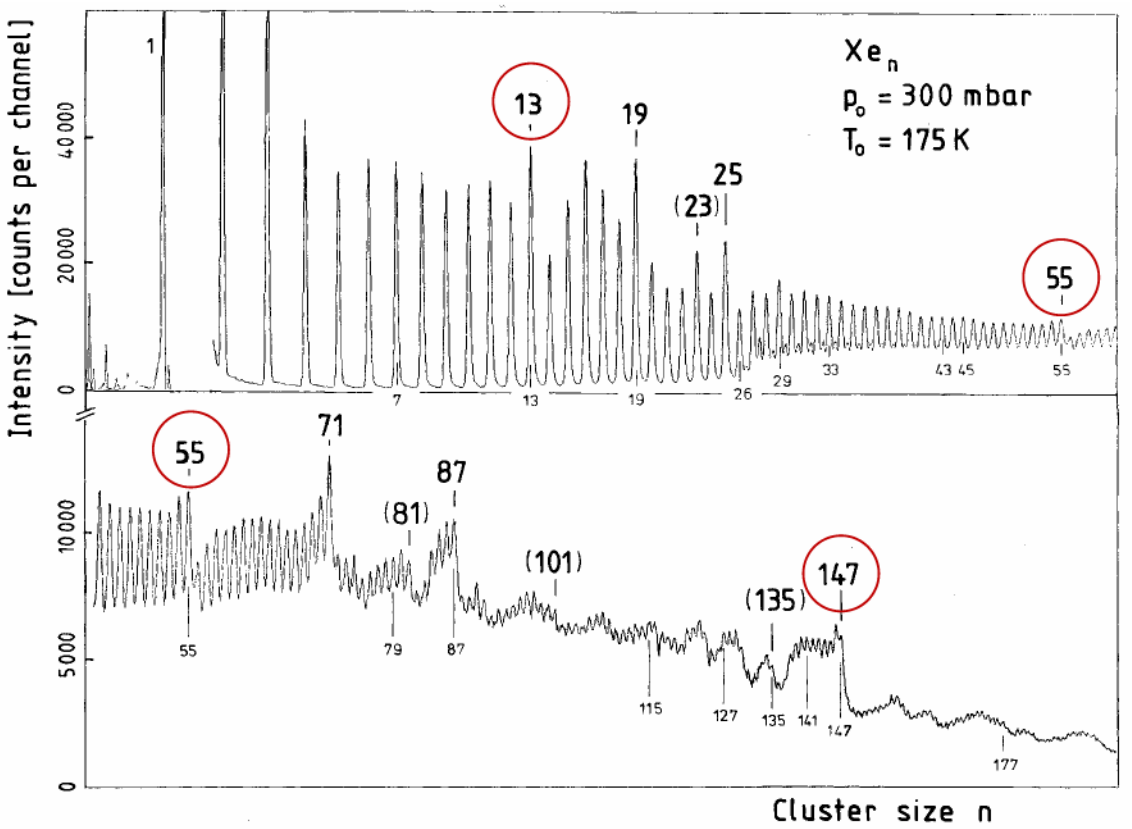

Figure 4: Mass spectrum of xenon clusters. The observed geometric magic numbers are marked (13, 55, 147). The other numbers exhibit additional caps on closed shell clusters (19 & 25 for the first closed shell cluster and 71 & 87 for the second). The numbers in brackets show a smaller effect. [24]

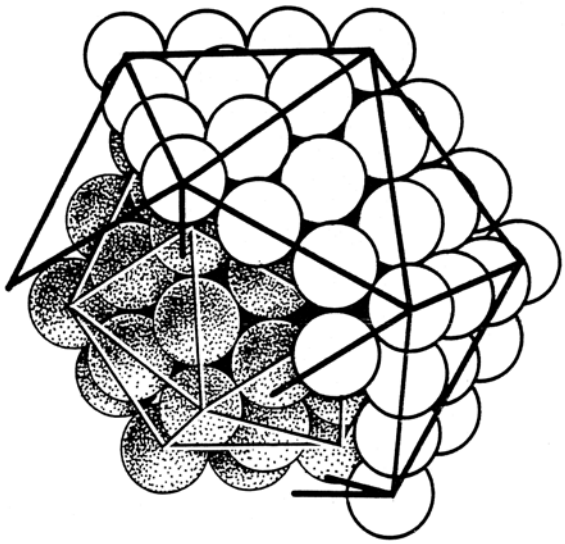

Figure 5: A closed-shell 55 atom icosahedron and a portion of the next shell. [28]

In the mass spectrum these geometric magic numbers show peaks with higher intensity indicating increased stability. Here, Xe_{13}, Xe_{55} and Xe_{147} show geometrically closed shells and form MACKAY icosahedrons. The first icosahedron, with 13 atoms, is build from a shell of 12 atoms with a five-fold symmetry around one atom in the center. The other geometric magic clusters are formed by the attachment of new closed shells

(figure **5**), e.g., the second geometric magic cluster (55 atoms) is formed by attaching 42 atoms to the first icosahedron, forming an icosahedral lattice when the shell is completed [29]. The number of atoms to form an icosahedron with k shells is given by:

$$N = 1 + \sum_{i=1}^{k} \left(10i^2 + 2\right). \tag{2.1}$$

The enhanced stability of clusters with the shape of an icosahedron comes from the high number of next neighbor bonds due to the five-fold symmetry and the resulting high binding energy [26]. This also explains the rapid decrease in intensity after the magic numbers. During cluster formation, clusters with slightly more atoms than the geometric magic numbers, can easily evaporate atoms to regain the magic cluster size, whereas a high energy barrier prevents the evaporation of atoms for magic cluster sizes [24].

A comparison of simulated and measured electron density of states shows that for cold metal clusters the electronic structure is highly degenerated for geometric magic clusters [30]. Furthermore sizes slightly below the closed shell ones maintain the MACKAY icosahedron geometry. But, in the intermediate size range, clusters close to electronic magic clusters and electronic magic clusters themselves still favour a more spherical shape due to the closed electron shells.

Increased cluster stability due to the closing of atomic shells occurs especially for large clusters (for Na cluster, N>1500) [25, 26, 28]. For small clusters the atoms are highly mobile and thus have no difficulties to arrange themselves into a sphere-like confirmation due to electronic shell closings. For small metal clusters (sodium clusters with less than 20 atoms) it was shown that electronic effects dominate the shell structure [31]. Clusters with more than 1500 atoms are rigid, thereby new attached atoms stay where they condense and further growth takes place by the accumulation of shells of atoms [25, 28]. The exact cluster size for the transition from electronically dominated cluster stability to geometrically dominated cluster stability depends partially on the melting point of the cluster material [26]. Clusters with more than 10^4 atoms prefer the fcc structure. For bigger icosahedra the nonconstant distance between the atoms leads to an increasing potential energy and thus a decreasing binding energy. Hence the fcc structure becomes energetically favorable [2].

3 Substrates

This chapter briefly discusses the properties of the substrate materials used for cluster deposition. The substrates used were highly oriented pyrolytic graphite (HOPG), Ag(111), Cu(111) and Au(111). Additionally, 60 monolayers of xenon were adsorbed on the substrate materials to decouple the clusters from the substrate.

3.1. HOPG

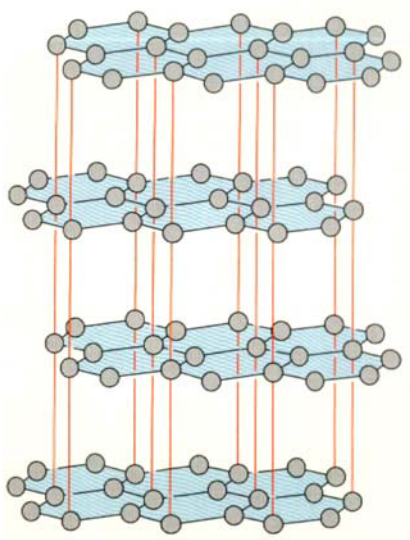

Figure 6: Alignment of atoms in HOPG. [33]

Graphite is a soft, black solid with a metallic shine. It is formed of layers with a honeycomb arrangement of carbon atoms which are strongly covalent bonded to each other. The distance between nearest neighbors is 0.142 nm, whereas the in-plane lattice constant is 0.246 nm [32]. In one layer each carbon atom develops three σ-bonds, with three other carbon atoms using a sp^2-hybridisation [33]. Each carbon atom contributes with three valence electrons to the σ-bonds. The remaining valence electron contributes to a p-orbital perpendicular to the layers. The p-orbital of one carbon atom overlaps with the p-orbitals of the other carbon atoms forming a delocalized π-orbital which ranges over the whole layer. All π-orbitals together form an energy band which is half filled. Consequently, the conductivity parallel to a layer is high, but perpendicular to the layers low [33].
The interaction between the layers is weaker, so they can easily be shifted against each other or separated. The layers are held together by van der Waals forces and are spaced apart about 0.335 nm. Neighboring layers are shifted relative to each other and form an ABAB… stacking sequence and a lattice constant of 0.670 nm perpendicular to the layers [32].

Highly oriented pyrolytic graphite (HOPG) is a form of hexagonal graphite (figure **6**). HOPG has a large grain size (about 3-10 µm) and a good c-axis orientation. The misorientation angle of the HOPG samples used in this thesis was 0.4°±0.1°.

3.2. Fcc metals

The metals used as substrate materials in this thesis are copper (electron configuration: Ar $3d^{10}$ $4s^1$), silver (Kr $4d^{10}$ $5s^1$) and gold (Xe $4f^{14}$ $5d^{10}$ $6s^1$). They have a face centered cubic (fcc) crystal structure. All metal samples used had a special orientation. If the metal crystal is cut along a plane given by the Miller indices (111), the resulting surface has the orientation (111) (figure **7**).

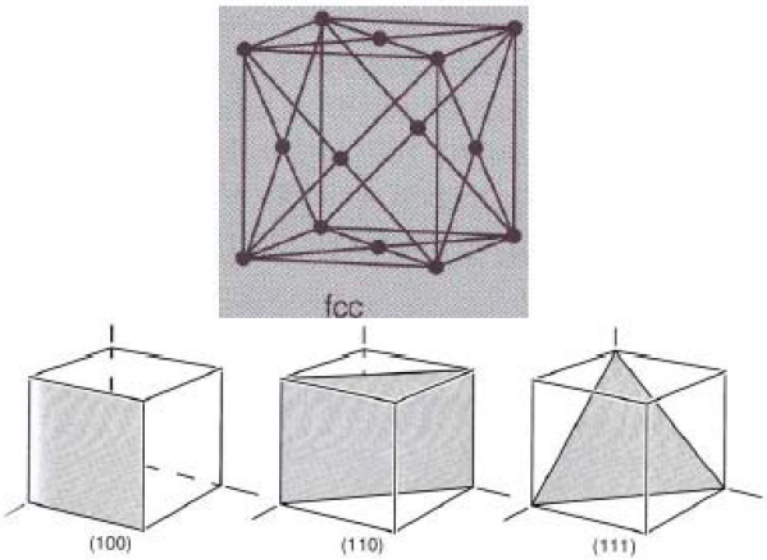

Figure 7: Above: fcc-structure; below: planes given by the Miller indices. [34]

The Au(111) surface shows an extraordinary composition of the surface atoms. Gold shows significant deviations from an ideal fcc lattice structure on the surface due to missing bonding partners at the top layer. Au(111) forms a reconstruction at the surface with a $(23 \pm 1) \times \sqrt{3}$ unit cell [35]. Gold is the only fcc metal that exhibits a reconstruction of the closed packed (111) surface [35, 36]. At the surface regions with a fcc structure alternate with regions with a hcp structure (hcp= hexagonal closed packed), due to the fcc bulk structure of gold the regions with fcc stacking are wider than the domains with a hcp structure. The regions with hcp and fcc stacking are connected by partial Shockley dislocations. These dislocations add one atom per reconstructed unit cell, resulting in a contraction of the surface layer along the $(1\bar{1}1)$ direction [35, 36]. In figure **8** a STM image of the reconstructed Au(111) surface is shown.

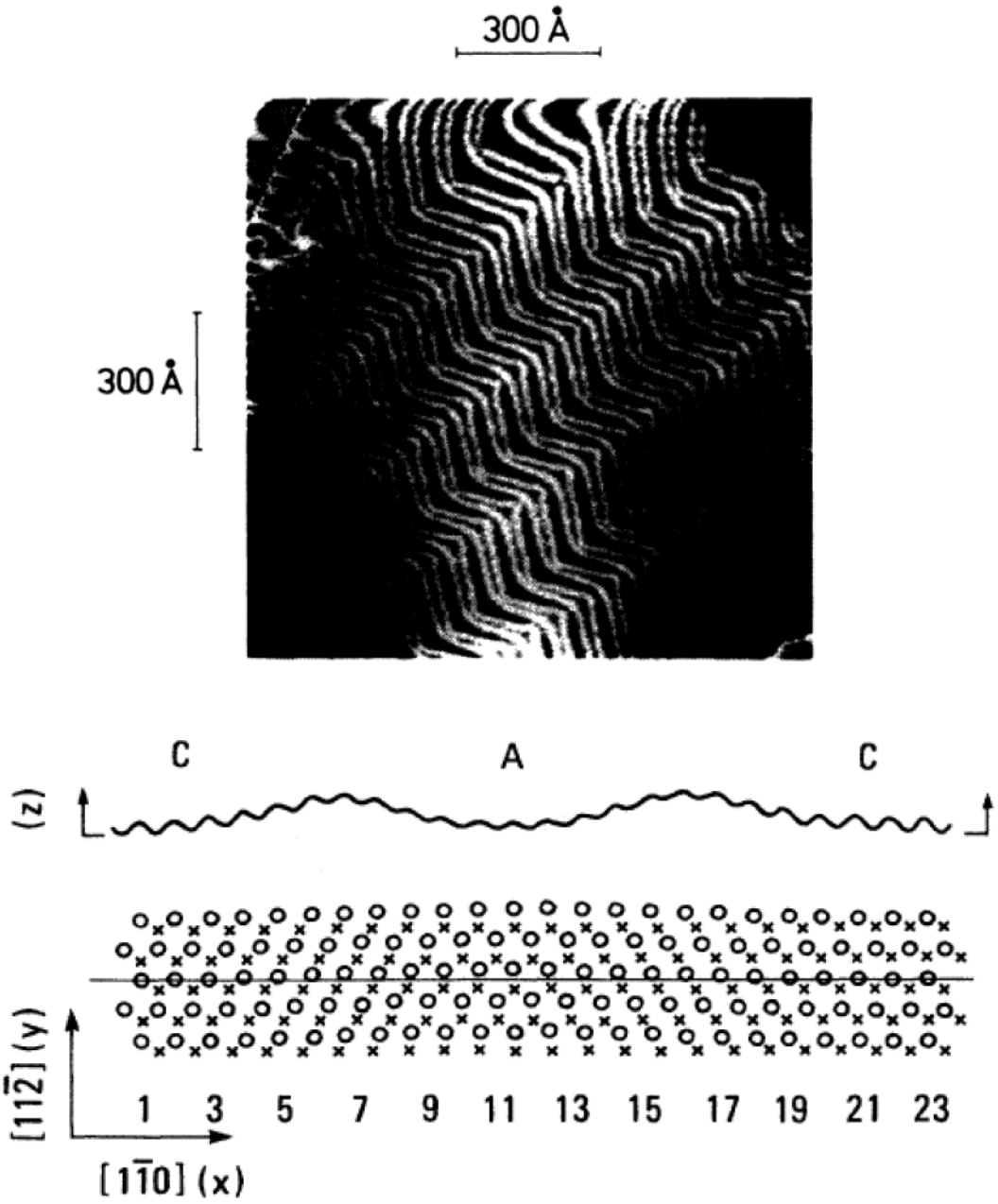

Figure 8: Above: STM image of a Au(111) surface from ref. [36]. The reconstruction is clearly visible; below: Model of the reconstruction of the Au(111) surface. The crosses denote the positions of atoms in the second layer, whereas open circles denote the positions of atoms in the reconstructed top layer. C and A mark the regions of ABC (fcc) and ABA (hcp) stacking. The lattice defect at the boundary between these two regions corresponds to a bulk Shockley partial dislocation. The displacement of the atoms from the straight line which has been drawn in the $(1\bar{1}0)$ direction is clear. [35]

(111) noble metals have an interesting property in common. They develop Shockley surface states [37] which can be observed with ultraviolet photoelectron spectroscopy (chapter 6.2). These surface states are prototype quasi-two-dimensional electron states that appear in a projected energy gap of the bulk bands, due to the termination of the infinite crystal by the surface [37, 38]. They can only be found in the first few layers (figure 9).

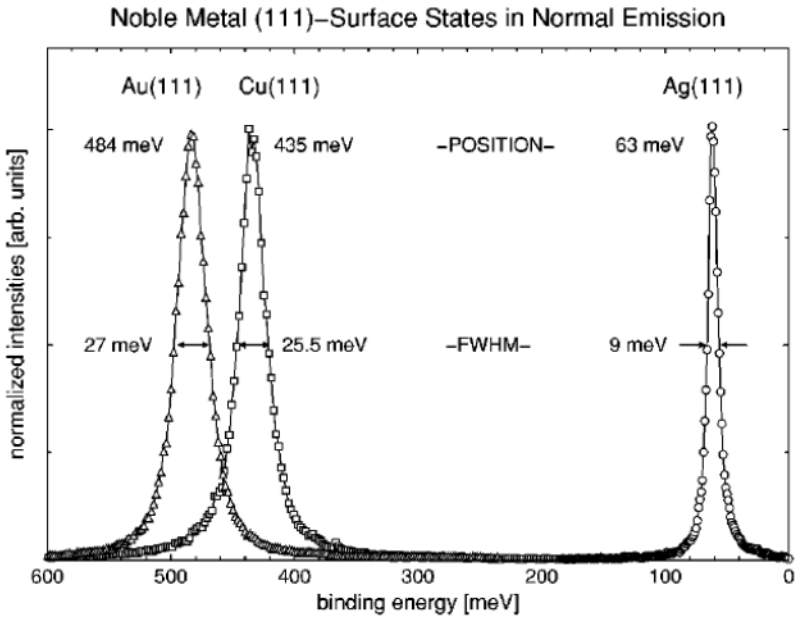

Figure 9: Surface states at normal emission and T= 30 K for Au(111), Cu(111) and Ag(111) on a common energy scale, measured with He I radiation (hv= 21.23 eV). [38]

In a one-dimensional model the metal surface can be described as a semi-infinite periodic chain of identical atoms with the spacing a and a screening by the conducting electrons [39]. The termination of the chain represents the surface, where the potential tries to attain the vacuum level in the form of a step function, see figure **10**. The resulting potential in the one-dimensional nearly-free electron model is

$$V(z) = -V_0 + 2V_g \cos gz\,, \tag{3.1}$$

where $g = 2\pi/a$ is the shortest reciprocal lattice vector of the chain, V_0 the vacuum energy and V_g defines the amplitude. The solution of the one dimensional Schrödinger equation for the surface state is shown in figure **10**. The electron density shows an exponential decay into the vacuum and the bulk and a maximum at the surface.

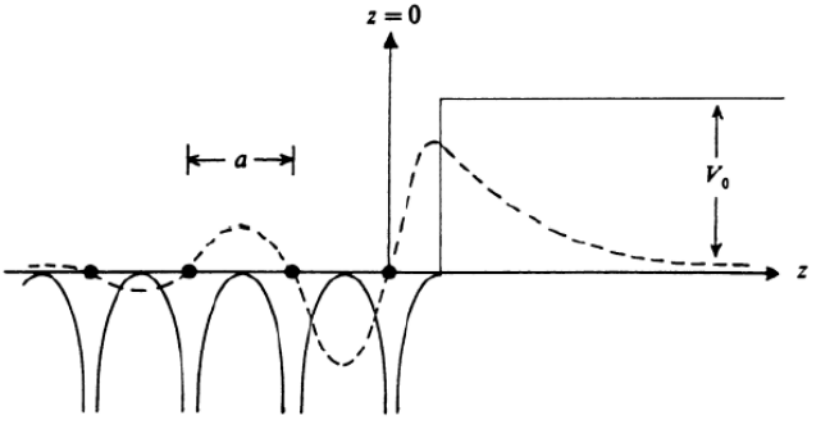

Figure 10: One-dimensional semi-infinite lattice model potential (solid curve) and an associated surface state (dashed curve). [39]

The Schrödinger equation has to be calculated separately for $z>0$ and $z<0$. As a result, one obtains that the energy of the surface state falls in an energy gap of the width of $2V_g$ and that it has to decay in the direction of the bulk, because these electronic states are forbidden in the crystal. For a more detailed description of the surface state see ref. [37, 39].

This consideration can be transferred to a three-dimensional theory [39].

3.3. Xenon

Xenon is a colourless, inert gas. Rare gases are characterized by a closed shell electronic structure and a weak interaction with substrates and among themselves due to van der Waals interaction.

Xenon is used here as a buffer layer for cluster deposition and to shield the clusters from the influence of the substrate. If metal clusters are deposited directly on a metal surface, they deform due to the strong interaction between the cluster and the substrate [40]. In order to avoid this 60 monolayers (ML) of xenon are adsorbed on the surface (see chapter 5.1), thus, quasi-free clusters are created.

With photoemission of adsorbed xenon (PAX) [41] it is possible to investigate some properties of surfaces, e.g, the work function of the substrate. The binding energy of the Xe $5p_{1/2}$ peak shifts with the work function of the underlying substrate. The dependence of the binding energy E^F_B of the Xe $5p_{1/2}$ peak on the work function Φ_C is depicted in figure **11**.

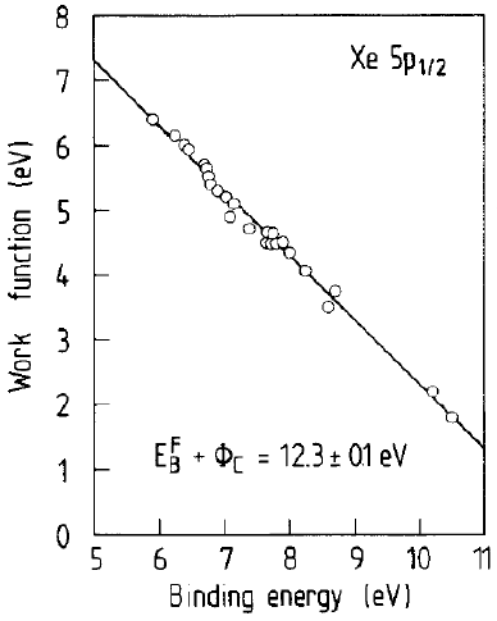

Figure 11: Dependence of the binding energy E^F_B of the xenon $5p_{1/2}$ peak on the work function, Φ_C, of clean low-index planes of transition metals, noble metals, semiconductors and oxides. [41]

The equation in figure **11** describes this dependence and was found via numerous experiments [41]. Considering two different uniform surfaces *i* and *j* one obtains from this equation:

$$\Delta E_B^F(i,j) = -\Delta\Phi_C(i,j), \tag{3.2}$$

with $\Delta E_B^F(i,j)$ as the difference in the binding energy of the two surfaces and $\Delta\Phi_C(i,j)$ as the difference in the surface work functions. Thus, the shift of the Xe $5p_{1/2}$ peak observed for uniform surfaces seems to be completely associated with the difference in the work function of the substrates [41].

In addition the position of the Xe $5p_{1/2}$ peak shifts to higher electron binding energies with the amount of xenon adsorbed on a surface [42, 43]. The reason for this shift is the work function decrease of the substrate due to the adsorption of xenon [43], i.e., using the example of the first two monolayers, the first monolayer changes the work function of the surface and therefore the position of the $5p_{1/2}$ peak of the second xenon monolayer shifts. A surface covered with one momolayer of xenon is equivalent to a new sample with a work function $\Phi_1 = \Phi_0 + \Delta\Phi_1(Xe)$. Hence the electron binding energy of one xenon atom in the second layer is shifted by $\Delta E_B = \Phi_1 - \Phi_0 = \Delta\Phi_1(Xe)$ [43].

4 Experimental Setup

For cluster production different methods can be used [7], e.g., gas aggregation, super sonic expansion or laser vaporization. The method used for this thesis will be described in the following chapter, along with the process of mass selection of simply charged clusters. Additionally, the surface science facility of the "Lehrstuhl für experimentelle Physik E1a" of the "Technische Universität Dortmund" used for the experiments will be presented.

4.1. Cluster Source Facility

The cluster deposition machine (figure 12) at TU Dortmund is composed of three parts:

- **Cluster source:** Here the clusters are generated by gas aggregation. A solid target is evaporated into an aggregation chamber filled with a cold inert gas [7]. After reaching supersaturation and after many collisions with the gas the atoms nucleate and form clusters of different size. The same principle is responsible for the formation of fog in nature. The cluster source used here is a magnetron-sputter-gas-aggregation source [44].
- **Cryo chamber:** In this chamber the cluster beam is focussed and the rare gas necessary for cluster production is pumped.
- **Mass selector:** In this chamber the clusters are mass selected before deposition. The mass selector used here is a time-of-flight mass selector [45].

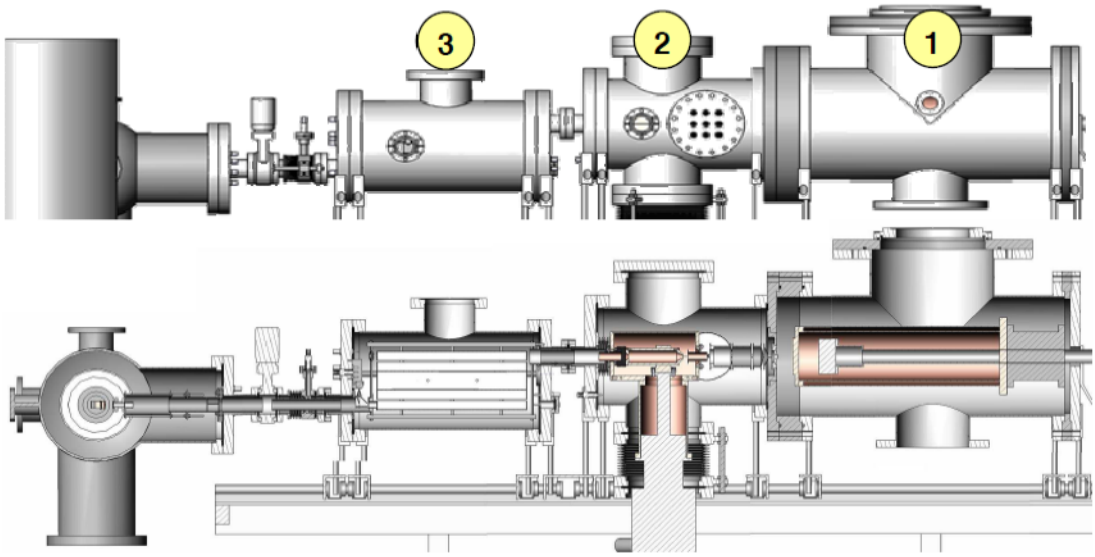

Figure 12: Top: the cluster source facility with the magnetron-sputter-gas-aggregation source (1), the cryo chamber (2) and the time-of-flight mass selector (3); below: a cross section of the cluster source facility. [47]

The individual components of the cluster source facility will be described in the following sections. For a more detailed description see [46].

4.1.1. Magnetron-Sputter-Gas-Aggregation Source

The clusters used here are produced by bombarding a target with argon ions. Argon gas is let into the target chamber and ionized. Then the argon ions are accelerated on the target due to a magnetron-cathode behind the target (figure **13**). Because of the high kinetic energy of the ions metal atoms and electrons can be knocked out of the target. The electrons are forced in cycloid tracks due to a magnetic field applied vertically to the target. These electrons keep the ionization of the argon atoms running. An electric field is applied perpendicular to the magnetic field so the electrons move on closed circular type tracks perpendicularly to the cycloid tracks. The circular sputtered region of the used silver and copper targets are presented in figure **14**.

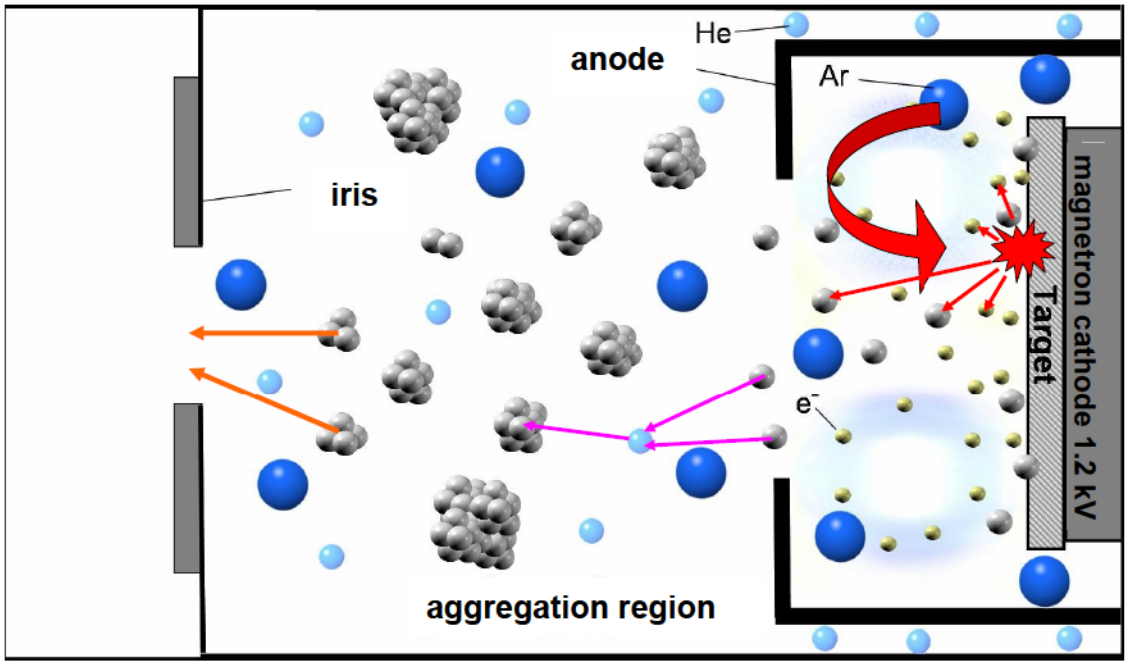

Figure 13: Schematic illustration of the sputter and aggregation process in the cluster source. Red arrows: argon ions are accelerated on the target and knock out atoms and electrons. Pink arrows: the atoms coalesce to clusters due to collisions with argon and helium atoms. Orange arrows: Due to the negative charge of the iris the clusters leave the aggregation region.

The resulting metal atoms and molecules drift through the aggregation chamber where they collide with helium and argon atoms. Due to these collisions they lose a part of their kinetic energy, cool down and coalesce to clusters.

In general the kinetic energy of the metal atoms (Me) has to be smaller then the binding energy of a dimer [2] so a stable metal dimer (Me_2) can be build:

$$Me + Me + Ar \rightarrow Me_2 + Ar$$

These dimers build condensation nuclei to grow bigger clusters. For a cluster source using argon ions the former condensation process changes slightly because argon dimers are very stable:

$$Ar_2^+Me_N + Me + Ar \rightarrow Ar_2^+Me_{N+1} + Ar$$

After the agglomeration of several metal atoms (5-10) the positive charge goes to the metal cluster and the now neutral argon atoms desorbs from the cluster [2].

Figure 14: Copper and silver targets used for cluster production. The circular sputtered region can clearly be seen on both targets. The silver target is an American silver eagle.

The pressure in the aggregation chamber is very small (10^{-7} mbar without gas, 10^{-2} mbar during operation) and the target is cooled down to -170 °C to abet the building of pure metal clusters. Due to the low pressure a collision with foreign atoms can be prevented.

The clusters move through a negatively charged iris and ring to a negatively charged skimmer at the end of the aggregation source to enter the next chamber. The skimmer cuts the diffuse boundary area of the cluster beam and focuses it. Most components of the cluster machine are negatively charged to guide the positively charged clusters through the machine. At the skimmer one usually applies a voltage of 0 V to -10 V to guide the clusters through the opening.

4.1.2. Cryo chamber

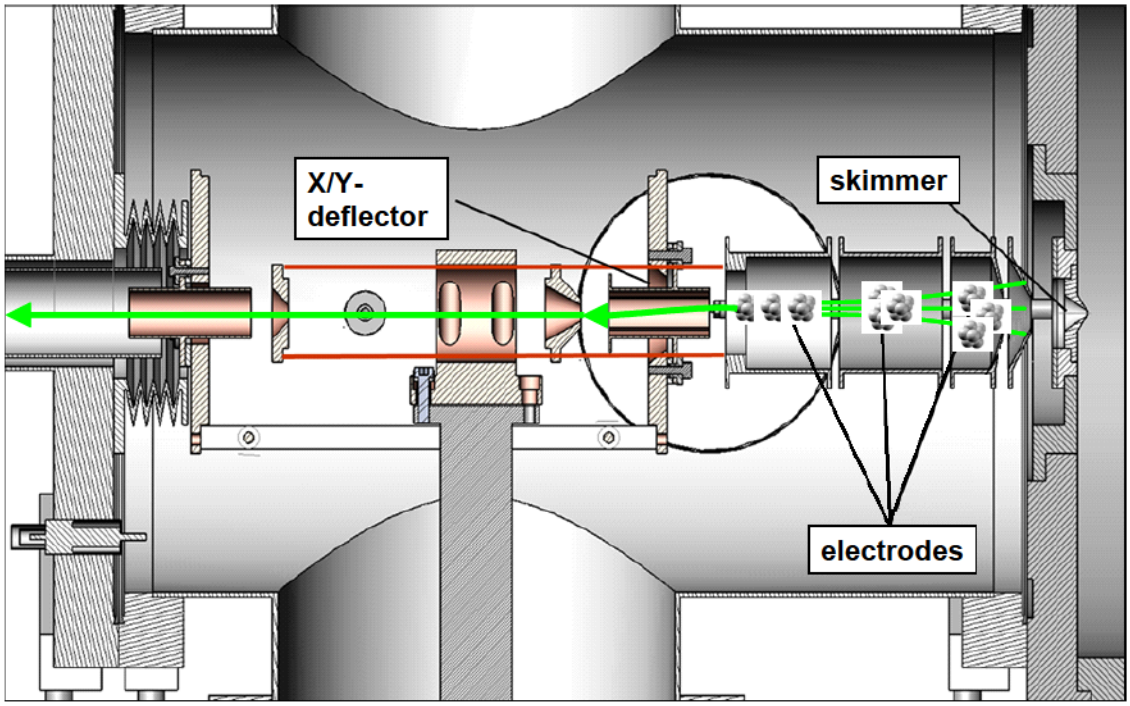

Figure 15: Schematic illustration of the clusters going through the cryo chamber. The green arrows picture the way of the cluster beam. The skimmer cuts off the diffuse boundary area of the cluster beam. Afterwards, the cluster beam reaches the ion optics. These three electrodes focus the incoming beam and the X-/Y-deflector plates change the vertical or horizontal direction. Therefore, the cluster beam can be led through the chamber. The rare gas atoms from the cluster source coming through the skimmer are pumped with a turbo molecular pump and a cryo pump.

After passing the skimmer, a cone-shaped lens which cuts the diffuse boundary area of the cluster beam, the cluster beam enters the cryo chamber. Three electrodes forming an ion lens are stationed behind the skimmer (figure **15**). At each electrode one can apply a different voltage (up to -1 kV) to focus the cluster beam. Afterwards, the cluster beam passes a X-/Y-deflector which is also under high voltage. With this deflector the cluster beam can be moved horizontally or perpendicularly. The goal is to perfectly guide the cluster beam to another lens called focus, marking the entrance in the time-of-flight mass selector (see next chapter).

In addition the cryo chamber has the function to guarantee optimal vacuum conditions. Through the skimmer helium and argon from the cluster aggregation flow into the chamber and would also drift in the mass selector. This would lead to a contamination of the deposited clusters. To avoid this, turbo molecular pumps [48] are attached to the chamber which can keep the pressure low enough (10^{-8} mbar-10^{-6} mbar). Additionally, a cryo pump [48] is installed which supports the pumping down of argon. This pump works as follows: aeriform helium is pressed under a pressure of 15 bar through a pipe in a chamber at the cold head of the pump. There the helium experiences a change in pressure and cools down. The cold head can now reach a temperature of approx. 10 K and freeze the argon out. Unfortunately, the temperature is still too high to freeze out helium, so this gas can only be evacuated by the turbo pumps.

4.1.3. Mass selector

In the mass selector the cluster beam is split up into parallel cluster beams containing only one mass. The positively charged clusters are accelerated in an electric field where they have a different acceleration depending on their mass. So it is possible to deposit only one cluster mass on the sample.

A schematic drawing of the mass selector and the process of the mass selection is given in figure **16**.

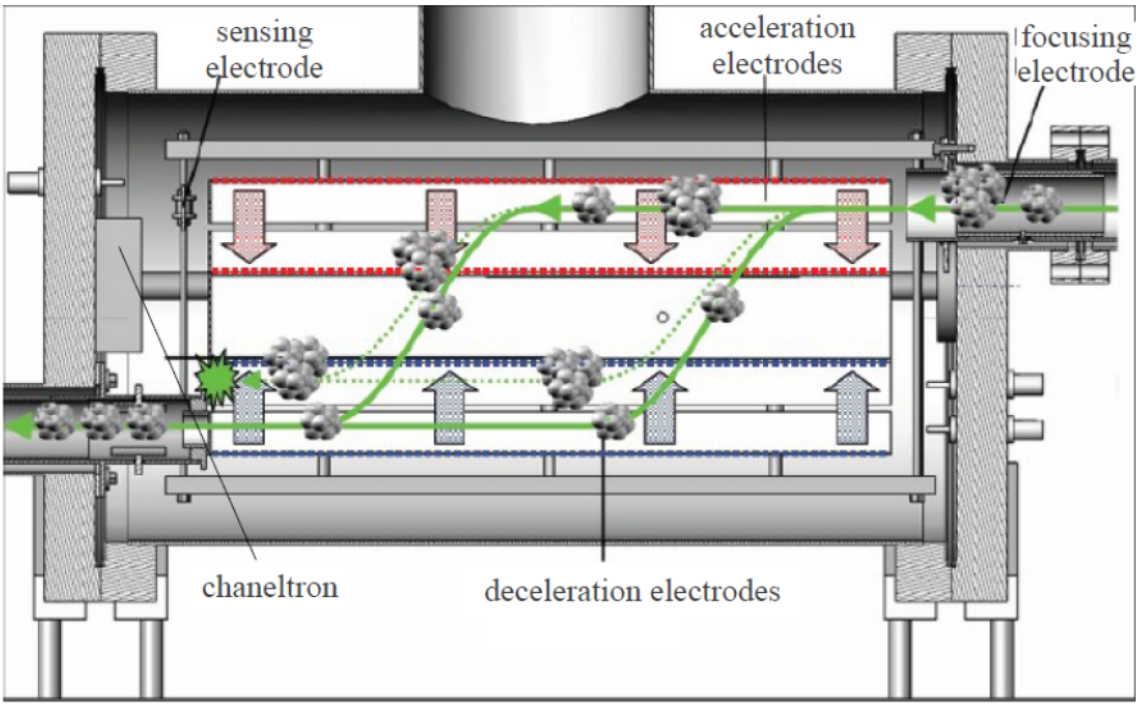

Figure 16: Schematic of the time-of-flight mass selector. The incoming cluster beam is displaced vertically by an acceleration pulse and splits up due to different cluster masses. After a short drifting time a deceleration pulse stops the vertical movement and only the chosen cluster mass can leave through the exit slit.

The mass selector works with the time-of-flight method [45]. The cluster beam enters the mass selector after passing a focussing electrode. The clusters are deflected downwards by a short high voltage pulse. The length of the pulse is chosen so that no clusters can leave the region between the two acceleration plates during the pulse. Because of their different masses but equal charge the cluster beam splits in several cluster beams containing one mass a time. With a force F affecting a particle with a charge q and a mass m in a homogeneous electric field E between two plates with a distance d the acceleration a for one particle is:

$$F = m \cdot a = q \cdot E \rightarrow a = \frac{U}{d} \cdot \frac{q}{m}, \tag{4.1}$$

with U as the applied voltage between the acceleration plates. As a consequence, the clusters are deflected the more the smaller they are.

After a short acceleration time the electric pulse is shut down and the clusters move downwards with a constant speed. Then a second pulse is applied between the two deceleration plates which stops the movement downwards so the clusters move horizontally. Only the cluster mass which can go through the exit slit can be deposited. The other cluster masses hit the wall of the mass selector and remain in the chamber. The time the positive charged clusters need to travel from the acceleration region to the deceleration region depends on their mass, i.e. the timing of the two pulses is crucial for the transmitted cluster mass. When the acceleration pulse is over the acceleration region is again filled with clusters of the incoming cluster beam and the mass selection starts anew after a certain waiting time. Figure **17** shows a schema of the timing for the acceleration and deceleration pulses.

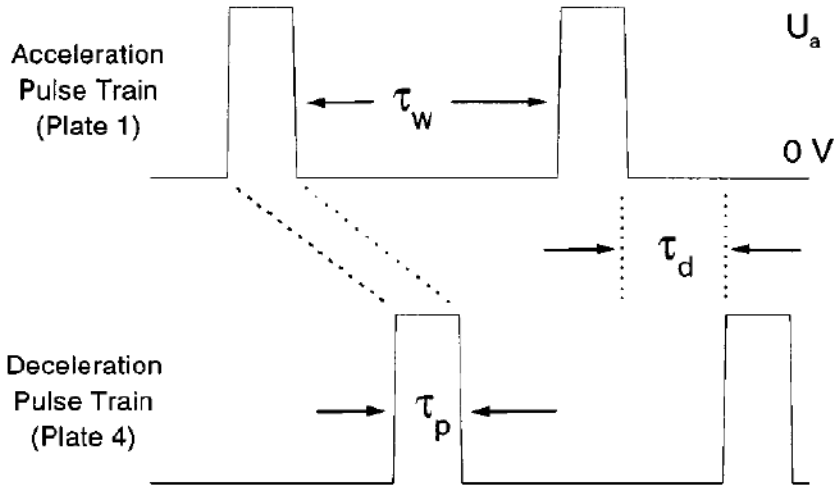

Figure 17: Schematic of the timing of the high voltage pulses. τ_p: pulse length, τ_d: drift time between acceleration and deceleration pulse, τ_w: time between consecutive acceleration pulses. U_a is the voltage applied to the acceleration and deceleration plates, respectively. [45]

The mass resolution R of this mass selector is at the moment $R = 50 - 70$, i.e. clusters with up to 50-70 atoms (depending on the calibration) can be resolved separately. For detailed information about the mass resolution see ref. [45, 46, 47].

4.2. Surface science facility

In the low temperature-ultra high vacuum (LT-UHV) surface science facility (Omicron Nanotechnology) samples for cluster deposition can be prepared and analysed before and after deposition. The surface science facility [49] consists of a preparation chamber with an ultraviolet photoelectron spectroscopy (UPS) analysis system and an analysis chamber containing the LT scanning tunnelling microscope (STM) [50]. The two chambers are separated from each other by a valve. This valve is only opened when samples are transported from one chamber into the other by an x-y-z-sample manipulator. The sample manipulator has three sample holders. With the so called heatable (HB) -sample holder samples can be heated up to 800 K and in the LT-sample

holder they can be cooled down to T≈ 10 K with the help of a liquid helium (LHe) flow cryostat [51]. In the third sample holder STM tips can be prepared in situ [52].

Samples can be transferred into the preparation chamber with the help of a load-lock and a magnetic transfer rod, which can be pumped separately, and prepared in situ in the preparation chamber via cycles of heating and sputtering. Therefore, a sputter gun operated with argon [53] is attached to the preparation chamber. Additionally, they can be exposed to xenon to grow rare gas layers.

The LT-STM is surrounded by two cryostats and can be cooled down to 77 K with the help of liquid nitrogen or down to 5 K with liquid helium. The STM is free of vibrations due to the use of spring suspension with eddy current damping.

The pressure in both chambers is $< 10^{-10}$mbar which is kept up by a system of turbo pumps, titan sublimation pumps and ion getter pumps [48]. The low pressure is important to prevent a contamination of the sample.

A schematic of the surface science facility is shown in figure **18**.

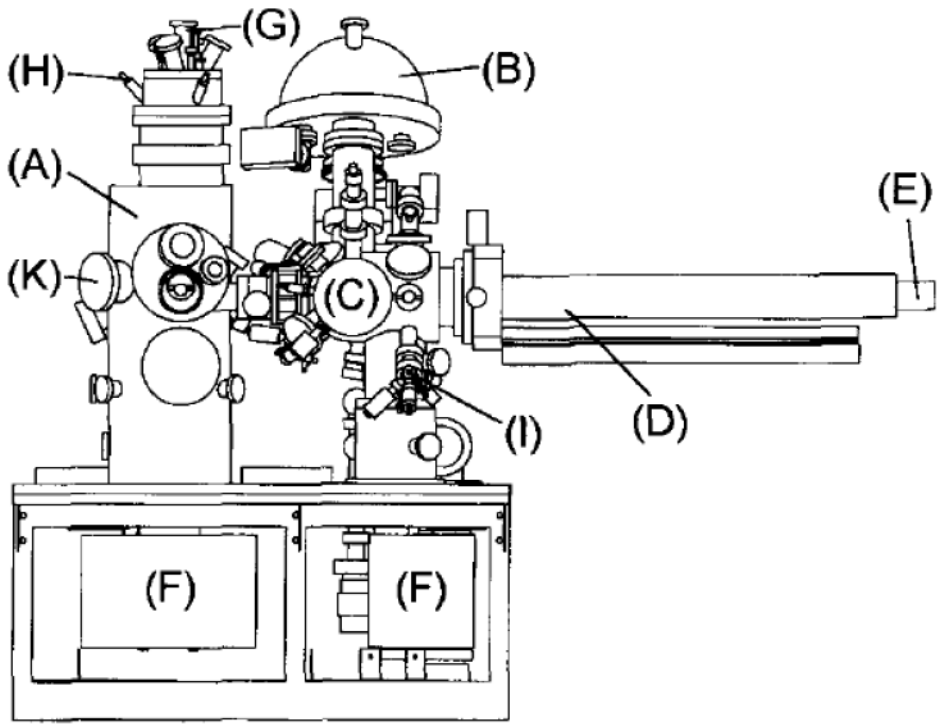

Figure 18: Side view of the surface science facility. (A) LT-STM; (B) energy analyser; (C) connection to the cluster source facility; (D) x-y-z-sample manipulator; (E) custom-build LHe flow cryostat with full 360° of rotation; (F) ion getter and titan sublimation pumps; (G) LHe bath cryostat; (H) liquid nitrogen (LN_2) dewar; (I) metal evaporation source; (K) storage carousel. [49]

5 Sample preparation

Before cluster deposition the samples have to be prepared. This chapter describes the preparation procedures of the used substrates (HOPG and fcc metals) and the adsorption of the xenon layer. In addition, the process of cluster deposition will be explained.

5.1. Substrates

5.1.1. HOPG

HOPG is chemical inert, therefore, the first preparation step can be done outside the UHV preparation chamber. As described in chapter 3.1, carbon atoms in HOPG are strongly bound in one layer but the layers are only weakly bound to each other. To obtain a clean and smooth surface it is sufficient to remove the first few layers by adhesive tape. Afterwards the HOPG sample is mounted onto a sample plate (figure **19**) and transferred into the preparation chamber.

Due to the exposure to air the sample is covered with a thin water layer. This water layer is removed by heating the HOPG sample for one hour at 600°C. After the sample cooled down it is clean and can be used as a substrate for cluster deposition.

Additionally, 60 ML of xenon can be adsorbed on HOPG. Therefore, the sample has to be cooled down to 30 K and xenon is let into the preparation chamber at a pressure of $7.5 \cdot 10^{-7}$ mbar for 19 minutes. It was shown experimentally in previous works that at this pressure and after the given amount of time 60 ML of xenon grow on the HOPG sample [42].

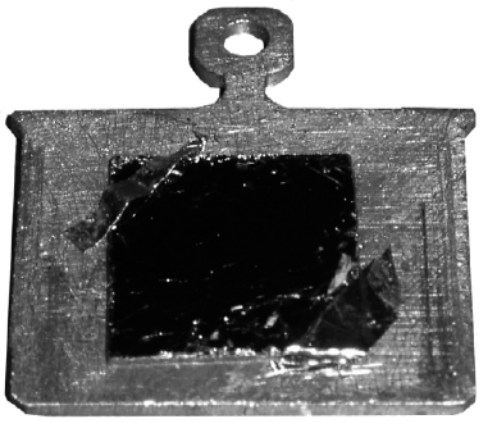

Figure 19: Photograph of a HOPG sample mounted on a sample plate with two tantalum stripes.

5.1.2. Metals

The metals have to be prepared in a different way than the HOPG sample. After attaching the metal sample to a sample holder and transferring it into the preparation chamber it has to undergo several preparation steps.

The first step is to heat the sample up to several hundred degrees for one hour. Thereby the water layer is removed from the sample and impurity atoms located in the bulk can diffuse to the surface. In a second step the sample is sputtered [53] for one hour with 1 keV argon ions at room temperature. This removes the top monolayers from the sample and removes adsorbates from the surface. After this procedure the surface is full of defects. These defects can be healed out by an additional annealing step. It is important that the second annealing step takes place at a lower temperature than the first one to avoid a new diffusion of impurity atoms to the surface. The three preparation steps for the different metal samples are shown in table **1**.

The result of the preparation can be checked for the (111) single crystals with the help of ultraviolet photoelectron spectroscopy (UPS). The Shockley surface state is only visible when the surface is free of adsorbates and other impurities. Thus, when the surface state is clearly visible in the spectra the sample preparation was successful otherwise the preparation has to be repeated.

substrate	1st annealing step	Sputtering with 1 keV Ar ions	2nd annealing step
Ag(111) single crystal	1 h at 550°C	1 h at RT	1 h at 430°C
Cu(111) single crystal	1 h at 500°C	1 h at RT	1 h at 400°C
Au(111) single crystal	1 h at 600°C	1 h at RT	1 h at 475°C
Au(111)/mica	1 h at 500°C	1 h at RT	1 h at 300°C

Table 1: Preparation steps for the used metal substrates.

Au(111)/mica is a substrate used for STM measurements. Mica includes a group of sheet silicate minerals with a close to perfect basal cleavage. This nearly perfect cleavage comes from the hexagonal sheet-like arrangement of its atoms. This extremely flat surface leads to the growth of (111) oriented gold terraces, if gold is evaporated on mica at T= 500°C [54].

The adsorption of 60 ML of xenon on the single crystals works like already described for HOPG. The sample is exposed to xenon at a pressure of $7.5 \cdot 10^{-7}$ mbar for 19 minutes at 30 K respectively 45 K, to avoid desorption of the xenon layers the sample is cooled down afterwards. The higher adsorption temperature of 45 K was used in later experiments to form a smoother xenon surface.

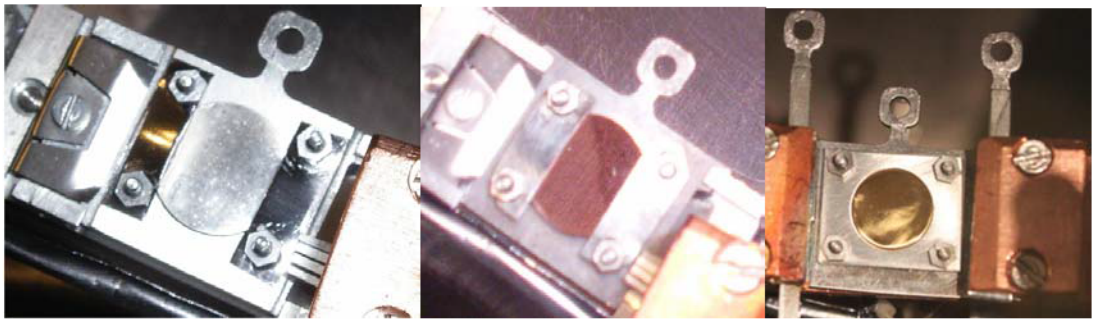

Figure 20: Metal samples used. Left: Ag(111); Middle: Cu(111); Right: Au(111).

5.2. Cluster deposition

After the substrates are prepared clusters can be deposited on the samples. Thereto the desired cluster size has to be adjusted. This is possible with two Labview programs [55] where the mass of a cluster can be selected. With the help of these programs a mass spectrum can be taken. This is necessary because of the mass resolution of the mass selector. Cluster sizes up to 50 atoms can be resolved separately but for bigger clusters the masses have to be evaluated. Therefore, the peak position of the small cluster sizes has to be defined, from this the masses of the bigger clusters can be deduced. For this procedure *David Engemann* wrote a program in his diploma thesis which automatically finds the peak maxima in a mass spectrum and calculates the masses for the desired cluster sizes [56]. In figure **21** a mass spectrum and the corresponding best-fit line of the cluster sizes is depicted.

The cluster current of the desired cluster mass is measured with the help of a Faraday cup [46] positioned in the preparation chamber. For a successful deposition the cluster current must be at least 1 pA. To avoid cluster fragmentation during deposition the clusters are slowed down before reaching the sample i.e. their kinetic energy is reduced. This is called soft landing [57, 58]. For this purpose a countervoltage is applied to the sample which is defined as follows. The cluster current is measured for different voltages applied to the sample (figure **22**). From a certain voltage forward the current begins to decrease i.e. not all cluster have enough energy to reach the sample. For soft landing the countervoltage applied to the sample is the voltage where 80% of the clusters reach the sample.

The average energy of the clusters is the energy where only half of the clusters reach the sample. The kinetic energy of the clusters deposited when 80% of the clusters reach the sample can be calculated as follows:

$$E_{kin}(cluster)=E_{kin}(50\%\ reach\ the\ sample)-E_{kin}(80\%\ reach\ the\ sample)$$

The cluster coverage is given by the cluster current and the deposition time (coverage[pAmin]=current[pA]*time[min]). It is important to choose a coverage where the clusters do not coalesce but stay well separated from each other. On the other hand the coverage must be high enough to guarantee good measurement conditions i.e. there must be enough clusters on the sample for a sufficient signal. The coverage for each experiment and for the different cluster sizes can be found in the appendix.

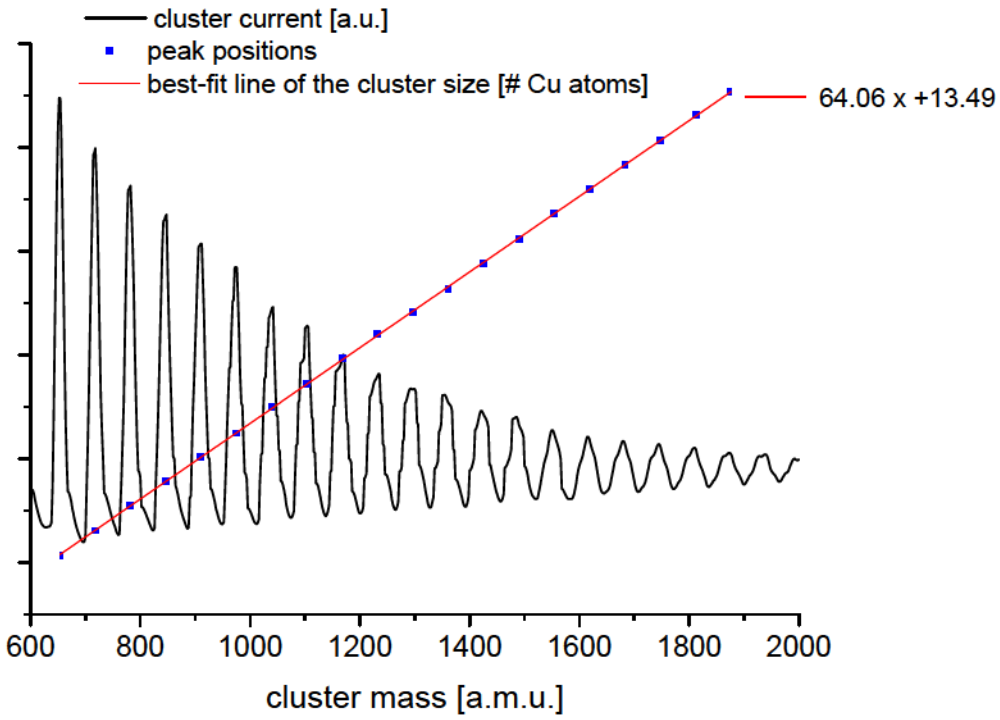

Figure 21: The black curve represents a mass spectrum of copper clusters taken with the equipment described above. The red line represents the best-fit line for bigger cluster sizes and the resulting formula as calculated with the program of *David Engemann*. [56]

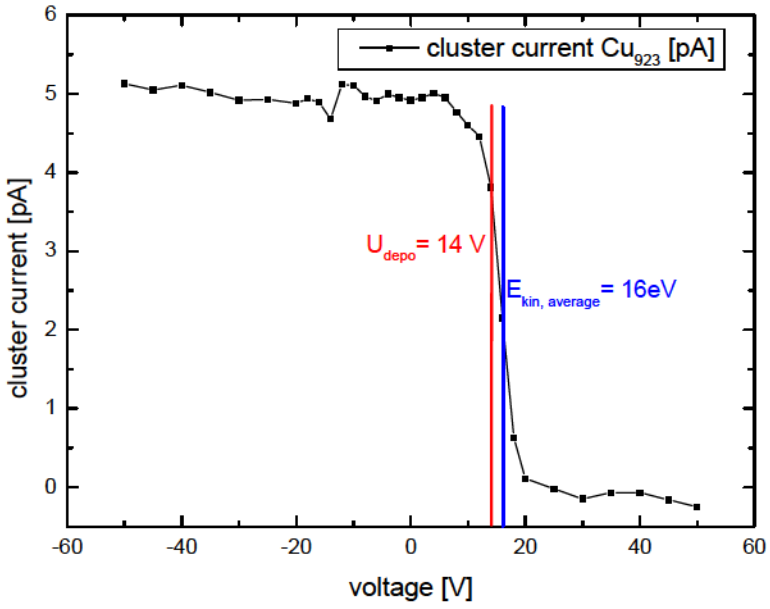

Figure 22: Cluster current versus sample voltage using the example of Cu_{923} clusters. The red line marks the counter voltage of the sample the clusters were deposited on and the blue line marks the average energy of the clusters (only half the clusters have enough energy to reach the sample at this counter voltage).

The deposition spot has a diameter of 1 mm due to a new movable focus lens attached to the ion optics of the cluster source facility [59] build by *Niklas Grönhagen*. For UPS measurements the deposition spot contains approx. 9500 cluster/μm^2 and for STM measurements approx. 1900 cluster/μm^2.

For a more detailed description of the procedure of cluster deposition see ref. [47, 59].

6 Measuring techniques

The deposited, mass selected clusters were investigated with scanning tunnelling microscopy and ultraviolet photoelectron spectroscopy. The working principle and the measurement procedure of these two techniques are described in this chapter. Additionally, the working principle and implementation of a heatable LiF window for an argon gas discharge lamp are presented.

6.1. Scanning tunnelling microscopy

Scanning tunnelling microscopy (STM) is a measuring technique to take topographic pictures of conductors and semi-conductors with atomic resolution. Thereto, a sharp metal tip is scanned in a certain distance over the surface of a sample and the current between tip and sample is measured as a function of the position [60]. The STM was developed by BINNING and ROHRER in 1982 [61, 62].

The distance between tip and surface represents a potential barrier (figure **23**), due to the quantum mechanical tunnelling effect [63] electrons can pass through this barrier with a certain probability. This tunnelling current I is given by the height of the potential barrier and by the distance d between the tip and the sample. Tunnelling through a one dimensional barrier is, e.g., described in [64]. For small voltages applied between tip and sample the tunnelling current simplifies further to:

$$I \propto e^{-2qd} \text{ with } q = \sqrt{2m_e/\hbar^2 \, \Phi}\,, \tag{6.1}$$

with m_e as the free-electron mass, Φ as the effective height of the potential barrier and the Planck constant $\hbar$. From this it follows that the tunnelling current is higher the smaller the distance between tip and sample is.

The topographic images taken with the STM do not picture atoms directly, but the local density of states (LDOS) of the surface near the Fermi energy [65]. Thus, the LDOS of the surface and the tip have an influence on the topographic image and it represents a contour map of constant surface LDOS. Depending on the polarity of the applied voltage it is possible to image the occupied states of the sample (negative voltage applied to the sample) or the unoccupied states (positive voltage applied to the sample).

The STM tip used here is made of a tungsten tip which is etched electrochemically in KOH or NaOH ensuing a cycle of in-situ sputtering, heating and self-sputtering. The goal is to create a clean tip with ideally one atom on top. The tip is approached to the sample to less than 1 nm distance and then scanned over the sample, thereby the tip is moved by piezo elements [66]. Piezo elements are ceramics which change their dimensions due to an applied voltage. The STM used during this thesis has a piezo element in the shape of a tube. Applying a voltage to one side of the tube leads to a

change of the dimensions of this side so the tube bends to one direction. Thus, the tip can be moved in x- and y- direction over the sample. If a voltage is applied to the whole tube the tip moves in z-direction.

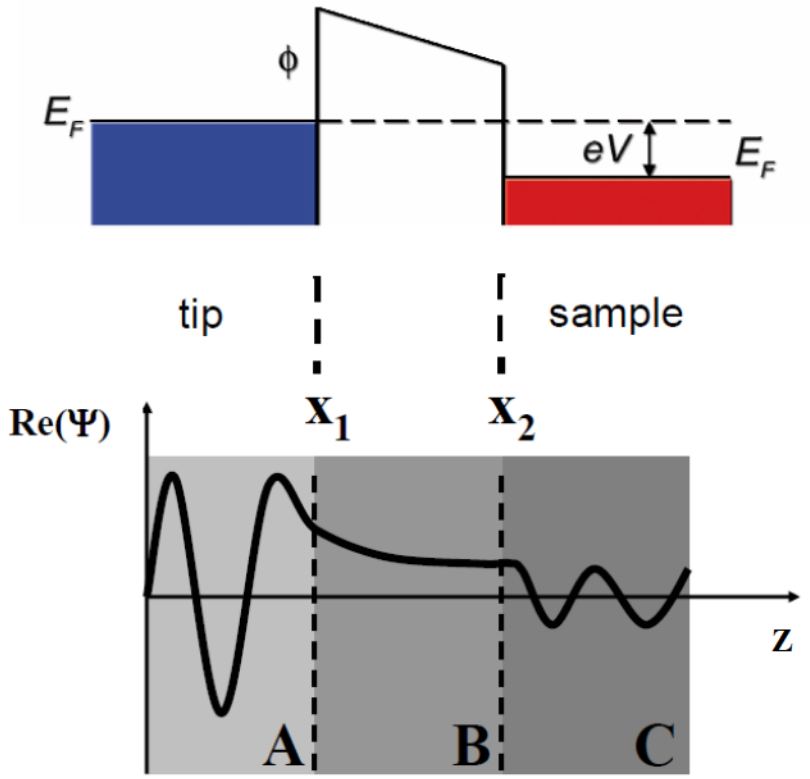

Figure 23: Top: model of a one dimensional potential barrier between tip and sample, which have an equal work function Φ. Bottom: a wave (A) penetrates a potential barrier, decays exponentially (B) and leaves the barrier with a smaller amplitude than before (C). [47]

A STM can be operated in two different modes (figure **24**):

- Constant height mode: In this mode the distance between tip and sample is kept constant. Scanning over the sample changes the tunnelling current due to the roughness of the surface and the resulting change in distance between tip and surface.
- Constant current mode: In this mode the tunnelling current is kept constant. The topographic image emerges from the changing z- position of the tip which is regulated with the help of an electronic circuit.

The method of choice to measure clusters on surfaces is the constant current mode. This mode is slower than the constant height mode but more secure because collisions with objects on the surface (e.g., clusters) can be avoided.

The disadvantage of scanning tunnelling microscopy of clusters is that the height of pictured objects can be defined precisely, but not their width. This behaviour is shown in figure **25**. A real STM tip is an inhomogeneous 3D body. When the tip approaches an object a tunnelling current flows from the side of the tip. The result is that the tip "sees" the approaching object and no collision occurs between the tip and the object (constant

current mode). But, additionally, the object is imaged wider than it actually is. Thus, the STM image is a convolution of the shape of the tip and the imaged object.

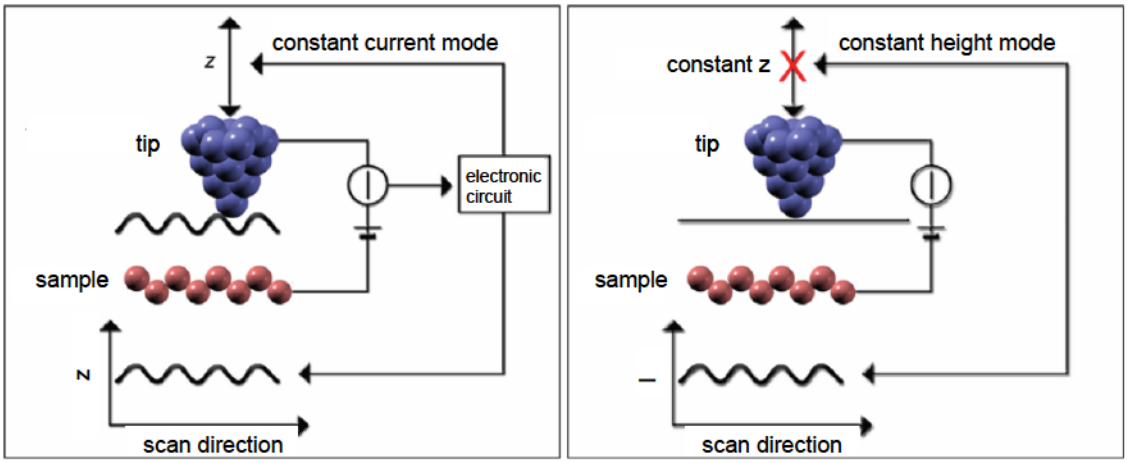

Figure 24: Schematic of the two operation modes. Left: constant current mode, right: constant height mode. In this thesis only the constant current mode was used.

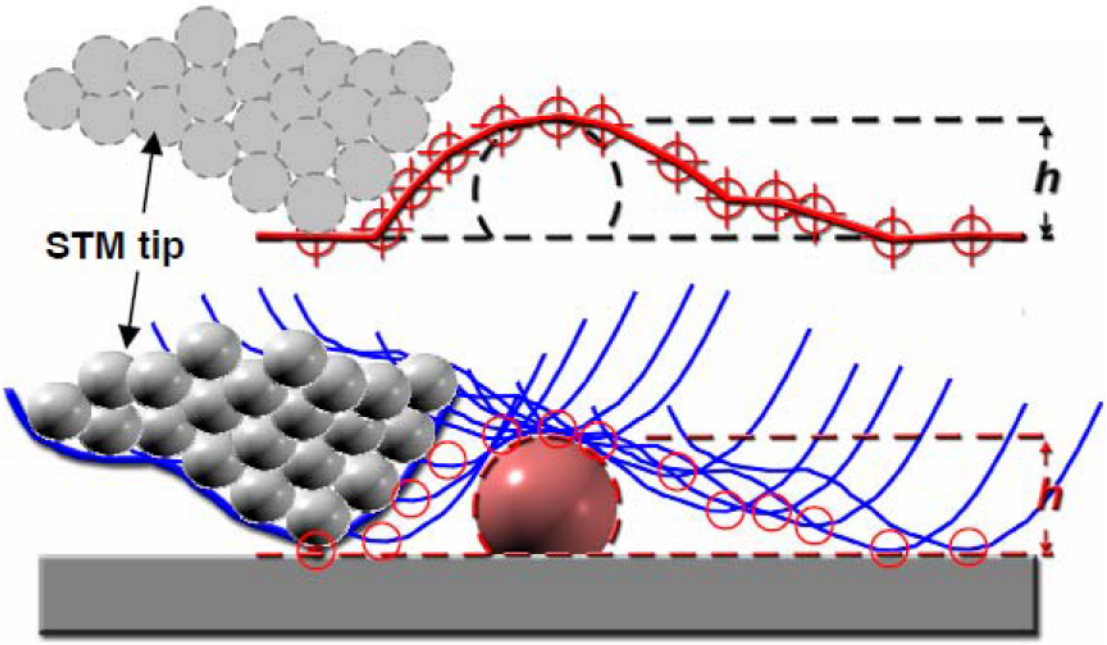

Figure 25: Top: line profile of a surface scanned by a STM tip and broadening effect due to the convolution of tip shape and object on the surface. Bottom: Trajectory and shape of the same STM tip. [47]

As mentioned above, the contrast in a STM image is linked to the LDOS of the sample. Therefore, "bright colors" in a STM image do not always mean a "high" object. In [67] it was shown that adsorbates with a low electronegativity (e.g., carbon) are pictured as bumps in a STM image whereas adsorbates with a high electronegativity (e.g., oxygen) show depressions. Thus, the interpretation of STM images is not always easy.

For more detailed information about scanning tunnelling microscopy see, e.g., ref [66, 68].

For a STM measurement different cluster sizes are deposited on up to nine deposition spots on the same sample (figure **26**) to ensure the same experimental conditions. This makes it easier to compare the obtained results. The size of a deposition spot is approx. 1 mm in diameter. The cluster spots are then measured in turn with the STM at 77 K or 5 K, respectively.

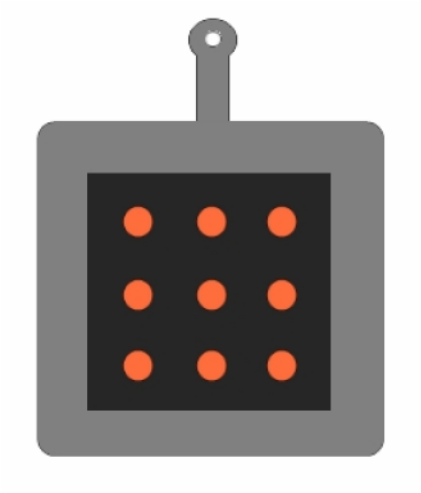

Figure 26: Schematic of a sample with nine deposition spots (red). Each spot can contain another cluster size and different coverages.

6.2. Ultraviolet photoelectron spectroscopy

Ultraviolet photoelectron spectroscopy (UPS) enables the measurement of occupied electronic states in a sample. It is based on the phenomenon of photoemission which was detected for the first time by HERTZ [69] in 1887. In 1905 EINSTEIN [70] was able to explain the photoelectric effect by invoking the quantum nature of light. For this achievement he obtained the Nobel price in 1921.

The principle of an UPS experiment is sketched in figure **27**. A sample is irradiated by a light source (here a gas discharge lamp) and the photons transfer their energy to the electrons in the sample. The impinging photon is absorbed by an electron which, thus, is excited, then the electron is transported to the surface and can afterwards escape through this surface. This is called the three-step-model [71, 72]. The detected electrons exhibit spectra which represent the electronic bands the electrons come from. Knowing the kinetic energy of the emitted electrons E_{kin}, the energy of the light $\hbar\omega$ and the work function Φ the binding energy of the electrons E_B can be determined with the EINSTEIN equation:

$$E_{kin} = \hbar\omega - \Phi - E_B . \tag{6.2}$$

The photoelectron spectrum is proportional to the joint density of states (JDOS), taking into account the initial and final electron state [71, 73]. With increasing photon energy the structure of the final states disappears, thus, the measured signal shows the occupied

electronic states of the sample. In figure **27** a schematic shows the relation between the energy levels in a solid and the electron energy distribution obtained with UPS.

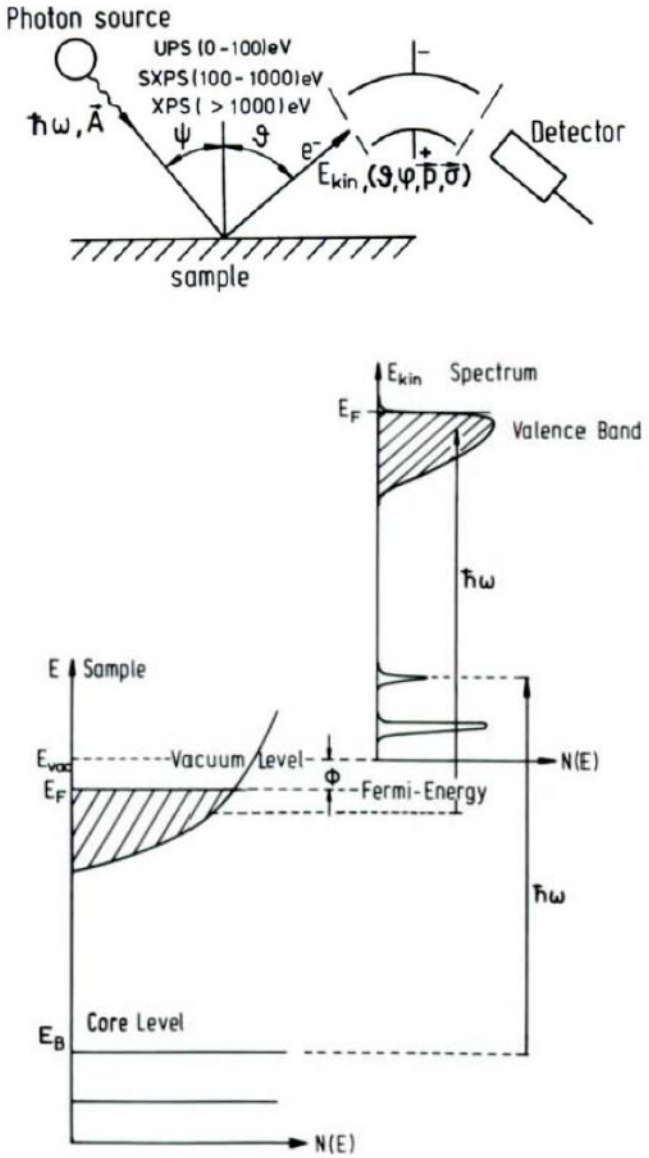

Figure 27: Top: Schematic of an UPS experiment. Bottom: Relation between the energy levels in a solid (metal) and the electron energy distribution produced by photons of the energy $\hbar\omega$. [71]

The photon energy used for UPS lies in the ultraviolet regime (11.62 eV and 21.22 eV here) and it is therefore very surface sensitive. With the help of the photon energy it is possible to adjust the sensibility of the photo emission for particular electronic states [74]. In general, one can say the lower the photon energy, the better electronic states near the Fermi edge can be measured. The detection depth for UPS measurements is in the region of ≈ 1 nm [73, 74]. Thus, it is very important to work with atomically clean surfaces and under UHV conditions.

For the interpretation of UPS measurements on clusters it is important to know how the intensity of the UPS signal depends on the cluster size. This dependence is explained in detail in [75] and will be discussed only shortly in the following.

Within the three-step model the excited electron is transported through the sample until it reaches the surface. The probability of the escape of an electron is dependent on its initial depth z (considering a cluster z is the cluster height h; and at the surface of the sample it is $z= 0$) and is limited by the inelastic mean free path (IMFP) λ. The number of emitted electrons per time n for a cluster is:

$$n = n_0 \cdot \int_0^h A(z) e^{-z/\lambda} dz \,, \tag{6.3}$$

where n_0 is the number of excited photoelectrons per time and sample volume (n_0 is assumed to be constant since the overall photon penetration depths is much bigger than the electron IMFP) and $A(z)$ is the cluster area.

For simplicity a cylindrical cluster is assumed which has the same height and diameter ($d= h$). This results in a cluster volume of $V = \pi/4\, h^3$. From this follows for the number of emitted electrons:

$$n(V) = n_0 \cdot V^{2/3} \cdot \left(\frac{\pi}{4}\right)^{1/3} \cdot \lambda \cdot \left[1 - \exp\left(-\frac{1}{\lambda}\left(\frac{V}{(\pi/4)}\right)^{1/3}\right)\right]. \tag{6.4}$$

In addition to the number of emitted electrons the overall intensity of an UPS spectrum I is dependent on the cluster density ρ_C in the measuring spot:

$$I \propto \rho_C \cdot n(V). \tag{6.5}$$

Equation (6.4) has two limits: for small clusters the intensity of the UPS signal is directly proportional to the average cluster volume V because the IMFP is bigger than the cluster heights. For large clusters the signal is proportional to $V^{2/3}$ because the emission of the projected cluster surface dominates [75]. In figure **28** the change of the photoelectron intensity depending on the cluster volume is presented. The electron escape depth was determined with the following formula from ref. [76] for copper and silver clusters measured with ArI radiation:

$$\lambda = \frac{A}{E_{kin}^2} + B\sqrt{E_{kin}} \quad \text{with } A= 143\ nm{\cdot}eV^2 \text{ and } B= 0.054\ nm{\cdot}eV^{1/2}\,. \tag{6.6}$$

The reference energy for E_{kin} is the Fermi level of the sample (here $E_{kin}= 7\ eV$).

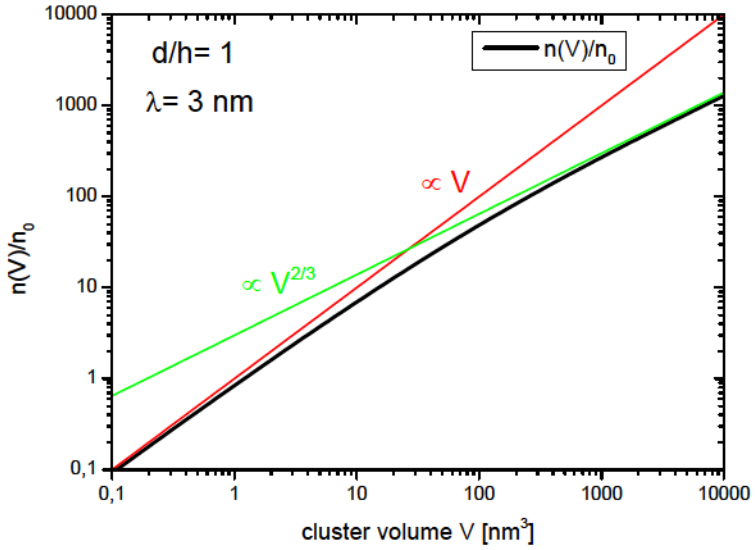

Figure 28: Calculated photoelectron intensity versus cluster volume for a cylindrical cluster with *d/h=1*. The electron escape depth was calculated with the help of equation (6.6) for copper clusters measured with ArI light (11.62 eV).

An effect which has to be taken into account while interpreting UPS spectra of clusters is the so-called dynamic-final-state-effect [73, 77]. A schematic of this effect is presented in figure **29**. For free clusters the final state effect is characterized by the excited electron and the corresponding hole in the cluster. This positive charge state remains constant over a time scale sufficient to let the electron leave the cluster. The results are well defined, sharp spectral electron lines. For deposited metal clusters the size dependent energetic shift is changed due to the interaction with the surface. Directly after the electron escapes the cluster the electron hole interaction is just like for free clusters. But after a certain time τ the photohole can be screened or neutralized, and the resulting change of the interaction affects the kinetic energy of the electron. This leads to a broadening of the spectral lines.

The UPS facility consists of a gas discharge lamp and a spherical electron analyzer [71]. The electrons emitted by excitation with the gas discharge lamp exit the sample under normal emission[1]. The extracted electrons are then focused by an electrostatic lens and enter the analyzer trough an entrance slit. After passing the spherical electron analyzer the electrons reach five independently working channeltrons [78] through an exit slit.

The measurement spot of the electron analyzer has a diameter of 1.2 mm. The size of the spot was measured by mounting a thin tantalum wire on an HOPG sample and measuring the metal signal with UPS (figure **30**) [56]. The size of the deposition spot is approx. 1 mm in diameter (chapter 5.2). Thus, it is possible to measure the whole deposition spot with one UPS measurement. But this also means that the measured spectra are averaged spectra of the whole irradiated area. With UPS it is not possible to measure individual cluster spectra, but only average spectra of all clusters deposited in one deposition spot.

[1] However, the angle of the sample can be changed with the help of the sample manipulator so that angle resolved measurements are possible.

Another method using the photoelectric effect is XPS (X-ray photoelectron spectroscopy) using X-ray radiation (> 1000 eV) [71]. This method is less sensitive with respect to electronic states near the surface, but can detect electronic states deeper in the bulk. The method of inverse photoelectron spectroscopy [71, 79] uses electrons with an energy E which impinges the sample and, by being decelerated, emit bremsstrahlung which is then detected. With this method it is possible to measure the density of unoccupied states in the sample.

For more detailed information about ultraviolet photoelectron spectroscopy see, e.g., ref [71, 72].

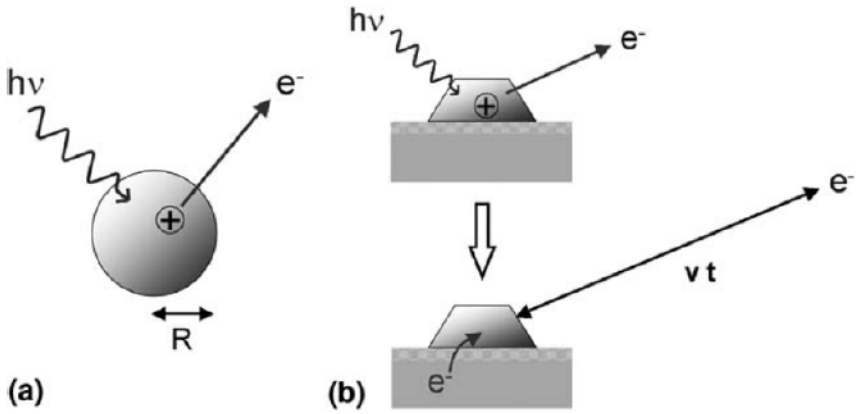

Figure 29: Schematic of the photoemission process from a metal cluster. (a) For a free cluster the photohole persists within the relevant electron-hole interaction time and the kinetic energy of the photoelectron is lowered. (b) Immediately after the photoexcitation in a supported cluster the electron-hole interaction is like in (a), but after a certain time *t* the photohole may be screened or neutralized and the corresponding change of the interaction affects the kinetic energy of the electron. The smaller the distance *vt* at the time *t*, the larger the influence on the kinetic energy. [73]

For UPS measurements four deposition spots are deposited on one sample. In a first step a cluster spot with a very high coverage is deposited. The position of this deposition spot is detected with the help of UPS (figure **31**) and from the position of this spot the positions of the other spots can be calculated before deposition. From these "empty" spots (the positions of the later deposition spots) UPS spectra are taken as reference to extract the cluster signal from the background after deposition. Afterwards the other three cluster spots are deposited and measured via UPS.

In addition to the actual measurements of the deposition spots measurements of an area without clusters are made. These substrate spectra are taken before and after cluster deposition and after the whole measurement. A comparison of the spectra of the same empty spot taken at different times gives information about the contamination of the sample during the measurement.

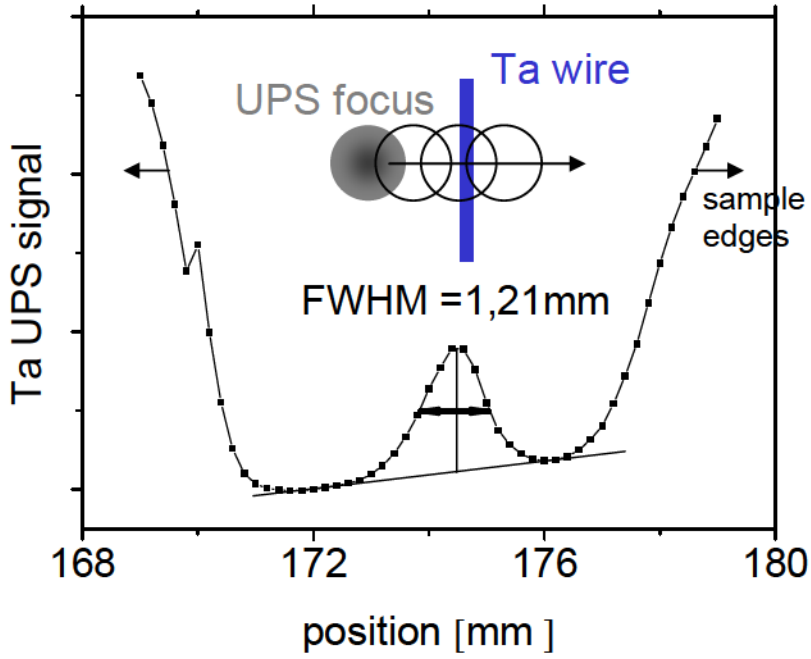

Figure 30: Size of the UPS spot measured with the help of a tantalum wire with a diameter of 0.2 mm. The x-axis describes the position of the sample manipulator. The manipulator was moved in a way so that the measurement spot crosses the tantalum wire and the tantalum UPS signal was measured. From the full width at half maximum (FWHM) the size of the UPS spot can be depicted.

After all deposition spots are measured the rare gas layer is desorbed from the surface by heating up the sample. When the rare gas layer completely vanished the position of the Fermi edge of the sample holder is measured. The position of the Fermi energy is later used as reference energy and set to zero.

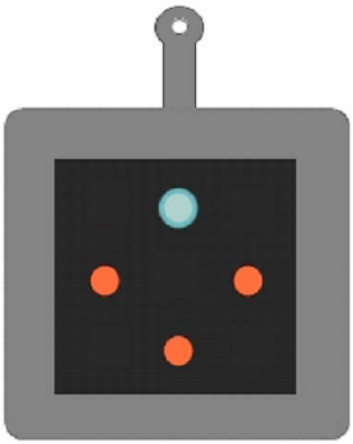

Figure 31: Schematic of a sample with four deposition spots for UPS measurements (red). Each spot contains another cluster size with a different coverage. The blue dot marks the UPS measurement spot. It covers the whole deposition spot.

6.3. Argon discharge lamp

In the course of my diploma thesis [80] a construction for a heatable LiF window for the existing gas discharge lamp was developed which was launched during this dissertation. For construction details see [80].

Before the change to argon the gas discharge lamp was operated with helium. A schematic of the gas discharge lamp and the additional construction for the LiF window is depicted in figure 32. During the operation with helium the gas was able to float into the preparation chamber which causes a contamination of the sample due to residual gas in the helium. Another disadvantage of the helium gas discharge lamp was the low sensibility for the electronic states near the Fermi edge as described above. Therefore, the operating gas of the gas discharge lamp was changed to argon.

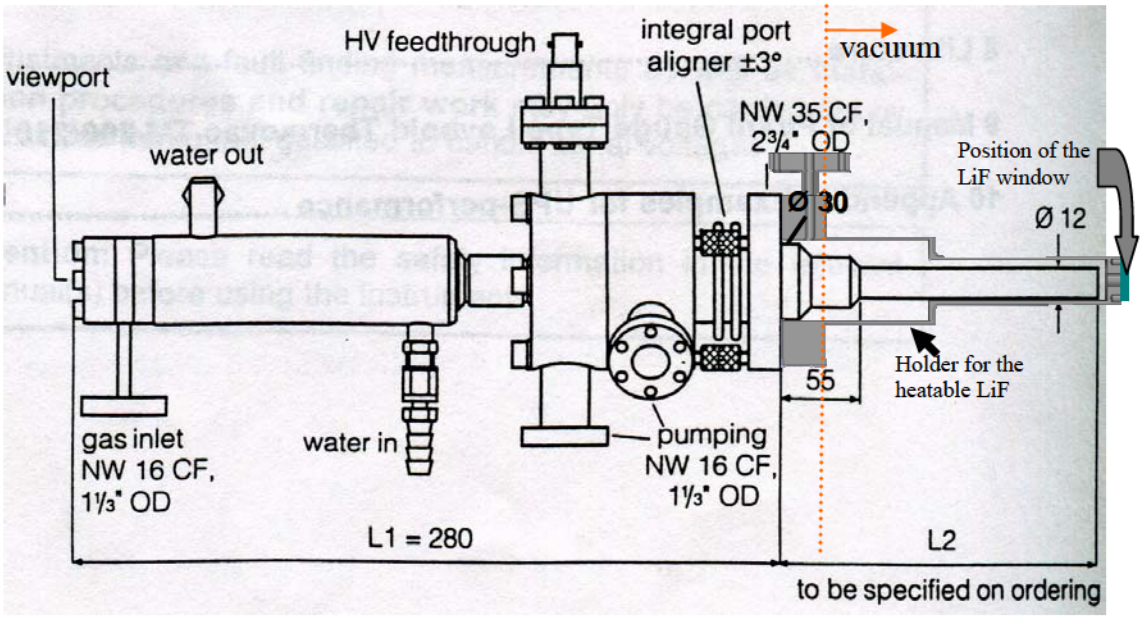

Figure 32: Schematic of the gas discharge lamp [81] and the construction for the heatable LiF window [80].

The spectrum of an argon gas discharge lamp is shown in figure 33. The argon spectrum consists of several spectral lines from which the first (ArI= 11.62 eV) and the second (ArII= 11.83 eV) lie close to each other. Measuring with an argon gas discharge lamp in the energy region of the ArI line, thus, leads to a doubling of the spectral features, i.e. all peaks in an UPS spectrum are imaged twice. This phenomenon can be eliminated by positioning a LiF window in front of the gas discharge lamp and heating it to a certain temperature. The transmission cutoff of the LiF window travels with increasing temperature to smaller energies. For a certain temperature all peaks except the ArI line are cut off resulting in a monochromatic light source. This is described in more detail in [82, 83].

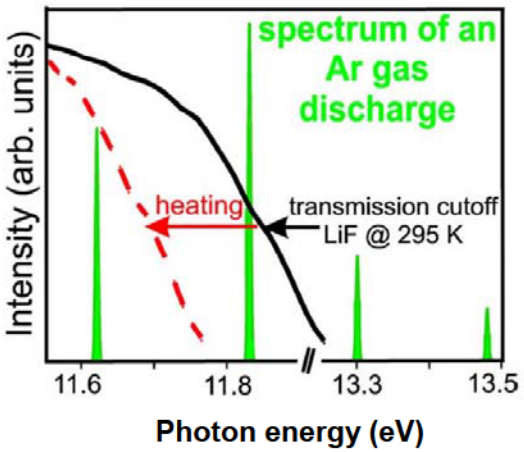

Figure 33: VUV spectrum of an Ar gas discharge. The black (dashed red) line represents the transmission cutoff of LiF. [82]

In figure **34** the surface state of an Ag(111) surface is illustrated for different window temperatures. The left peak comes from the ArI line and the right peak from the ArII line. With increasing window temperature the right peak disappears. At a window temperature of 345 K the peak resulting from the ArII line is so small that it disappears in the background signal and the peak resulting from the ArI line remains. However, the intensity of the first peak also decreases a bit whereby a further increasing of the window temperature would be counterproductive.

The holder for the LiF window was constructed in such a way that the gas of the discharge lamp cannot enter the preparation chamber and, therefore, no contamination of the sample occurs even at very low sample temperatures. The pressure in the chamber before the installation of the LiF window was 10^{-8} mbar during UPS measurements due to the gas from the discharge lamp. Now the pressure during an UPS measurement is in the region of 10^{-11} mbar.

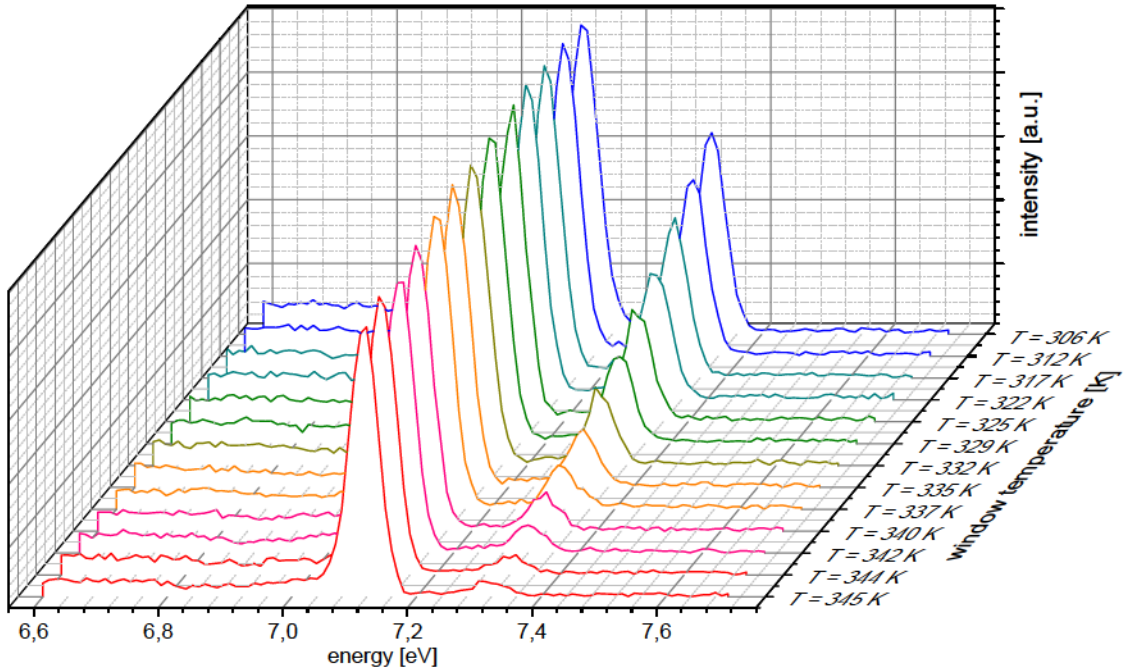

Figure 34: Temperature dependent transmission of the LiF window measured at the Ag(111) surface state. With increasing window temperature the surface state caused by the ArII line disappears until at 345 K the peak perishes in the underground signal.

7 Free beam clusters

In the course of this thesis the results obtained with UPS for deposited clusters are compared with results of UPS measurements of free beam clusters. The data for free beam clusters presented in this thesis come from two sources: Most of the data were measured at the Albert-Ludwig-Universität in Freiburg and were taken by the group of *Bernd von Issendorff* (measured with 6.43 eV). Additional data were extracted from two papers of CHESHNOVSKY et al. [84, 85] (measured with 7.9 eV). Therefore, a short introduction to the measurement procedure of free beam clusters will be given in this chapter as used by the group of *Bernd von Issendorff*. For a more detailed description of this topic see ref. [8, 17].

7.1. Experimental setup

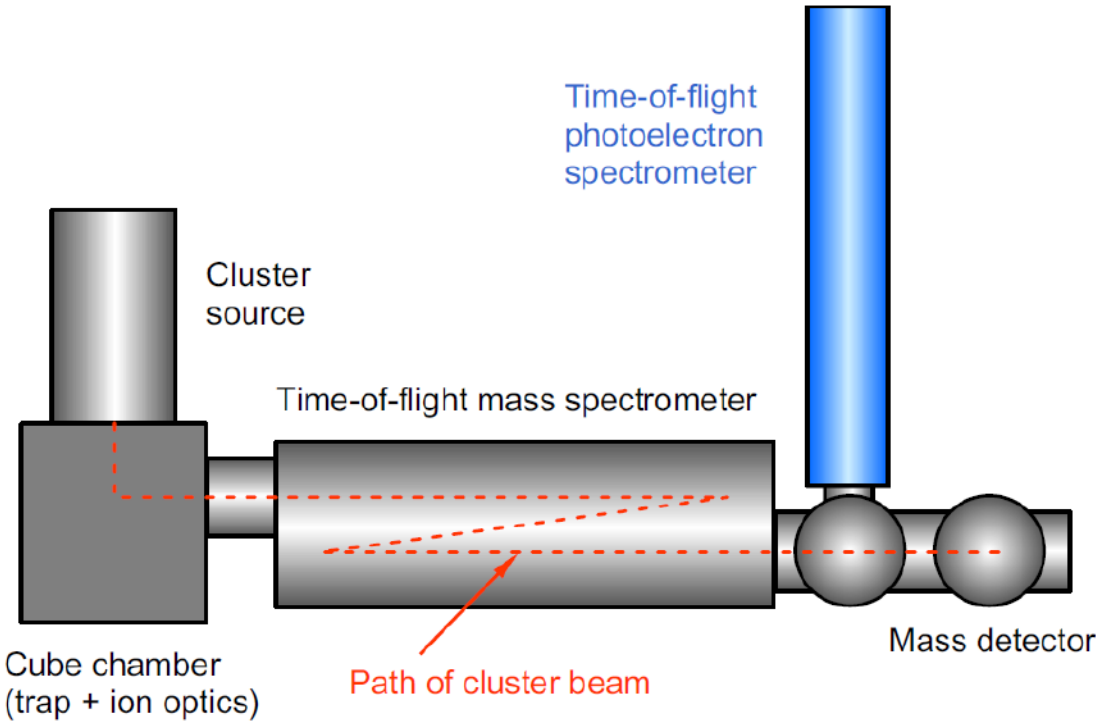

Figure 35: Scheme of the experimental setup as used for the production and measurement of mass selected free beam clusters. [8]

The clusters are produced in the cluster source (used here: magnetron sputter source or thermal evaporation source [2]) and, in the case of the thermal evaporation source, charged by an additional discharge ring mounted at the end of the aggregation tube of the cluster source. Then they reach a tandem-reflectron time-of-flight mass spectrometer [8] after passing a cube chamber. In the cube chamber the clusters can be cooled down

and stored. The stored clusters can then be released into the time-of-flight mass selector. The storing of the clusters increases the cluster beam intensity because more clusters enter the mass selector, but this leads to a pulsed cluster current. The mass selected clusters are then decelerated and irradiated by an ultraviolet laser pulse in the interaction region of a magnetic bottle type time-of flight photoelectron spectrometer [8, 86]. There the kinetic energy of the electrons is measured and converted into electron binding energy. With the help of an applied magnetic field nearly all electrons emitted from the clusters can be detected independent of the direction the electrons are emitted. The electron spectra are accumulated for a few thousand laser shots to reduce the statistical error. Figure **35** shows a schematic of the experimental setup.

Free beam binding energy spectra of copper clusters taken by the group of *Bernd von Issendorff* are presented in figure **36**. In contrast to UPS spectra of deposited clusters the reference energy (*E=0* in the graphs) here is the vacuum energy E_{vac} of the system. The position of the vacuum energy is determined by calibrating the spectrometer with the known photoelectron spectrum of Pt^- [87]. Mathematically the binding energy in the spectra is determined by subtracting the photon energy from the electron kinetic energy spectrum. For deposited clusters the reference energy is the Fermi energy E_F of the apparatus ($E_F = 0$). Based on the Fermi energy as highest occupied level the energy scale for deposited clusters is negative for energy levels deeper in the cluster. The reason for this is that also unoccupied levels can be investigated which are depicted with a positive energy scale. Therefore the occupied levels measured with UPS are depicted with a negative sign and the energy scale is referred to as "energy". For free beam spectra the energy scale is positive and is from now on referred to as "binding energy".

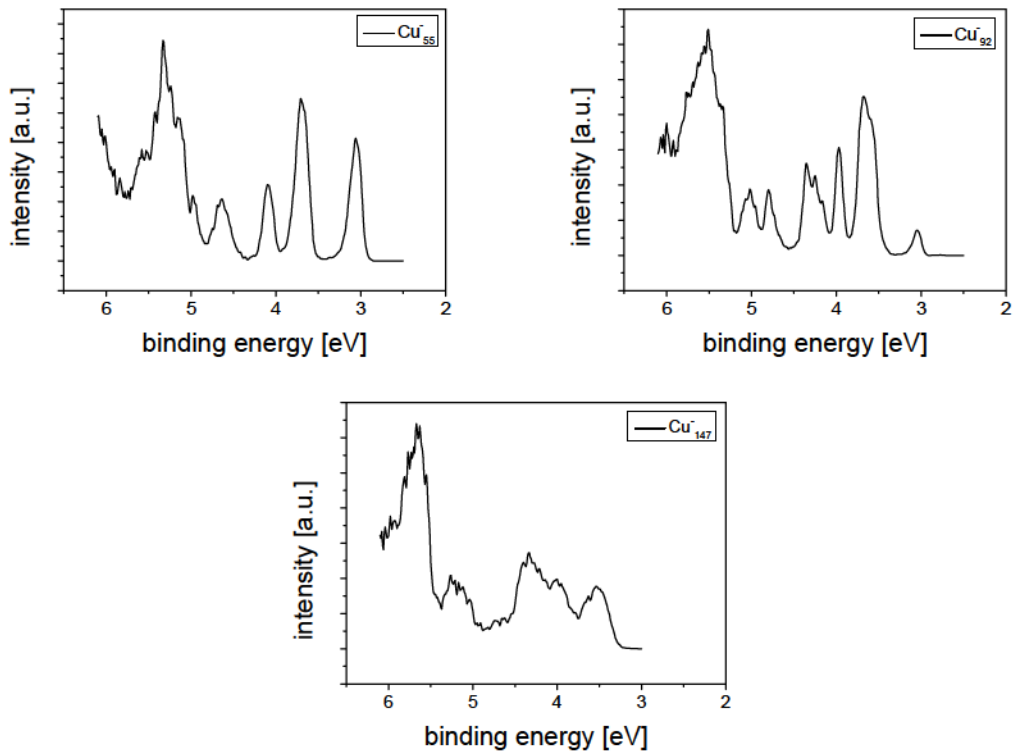

Figure 36: Free beam spectra of mass selected, negatively charged copper clusters with 55, 92 and 147 atoms. [8]

7.2. Comparison of free beam spectra with spectra of deposited clusters

As mentioned above, the free beam clusters measured by the group in Freiburg and CHESHNOVSKY et al. are negatively charged. Our deposited clusters on the other hand are neutral due to charge transfer with the substrate. For a comparison of the UPS spectra of the negatively charged free beam clusters with the neutral deposited clusters the shift in the spectra due to the charge of the clusters has to be taken into account.

The ionization energy needed to extract an electron from a big cluster is given by

$$E_i = \Phi + (Z + \alpha)\frac{e^2}{4\pi\varepsilon(R+\delta)}, \tag{7.1}$$

with Φ for the work function of the material, Z is the cluster charge, α a material dependent constant value, ε the dielectricity constant for the surroundings of the cluster, R the radius of the cluster and δ the spill-out of the electrons [88]. The spill-out of the electrons δ describes the distance (1 Å in this case) the LDOS of the electrons exceeds the cluster radius R given by the atoms. For smaller clusters (N= *20-200*) the situation is not so simple, because the ionization energy changes strongly with the cluster size due to the closing of electronic shells at electronic magic clusters sizes [8]. But, this behaviour does not change the results of the following discussion.

The effective shift between neutral (Z=*0*) and negatively charged clusters (Z= *-1*) is given by

$$\Delta E_i = \frac{e^2}{4\pi\varepsilon(R+\delta)}. \tag{7.2}$$

In the previous section it was mentioned that free beam clusters have a different reference energy than deposited clusters. For deposited clusters the reference energy is the Fermi energy E_F of the substrate and for free beam clusters it is the vacuum energy E_{vac} of the system. For a comparison of the UPS spectra it is hence necessary to change the reference energy of the free beam spectra from the vacuum energy to the Fermi energy.

For cluster anions in a free beam the onset of their spectra can be arranged at the electron affinity underneath the vacuum energy. The electron affinity is the binding energy needed to extract an electron from a negatively charged atom, molecule or cluster. Its binding energy marks the beginning of the free beam spectrum. With the Fermi energy of the substrate as reference energy, the onset of the cluster spectra for free beam clusters can be arranged at $\Phi_{substrate}$-$E_{binding\ energy}$. To compare the neutral deposited clusters with the charged free beam clusters an additional shift is needed which comes from the charge of the free beam clusters and shifts the spectrum to smaller energies (ΔE_i). The resulting shift to compare the UPS spectra of charged free beam clusters with the UPS spectra of neutral clusters deposited on rare gas layers looks as follows (figure **37**):

$$E_{energy}=\Phi_{substrate}-E_{binding\ energy}-\Delta E_i. \quad (7.3)$$

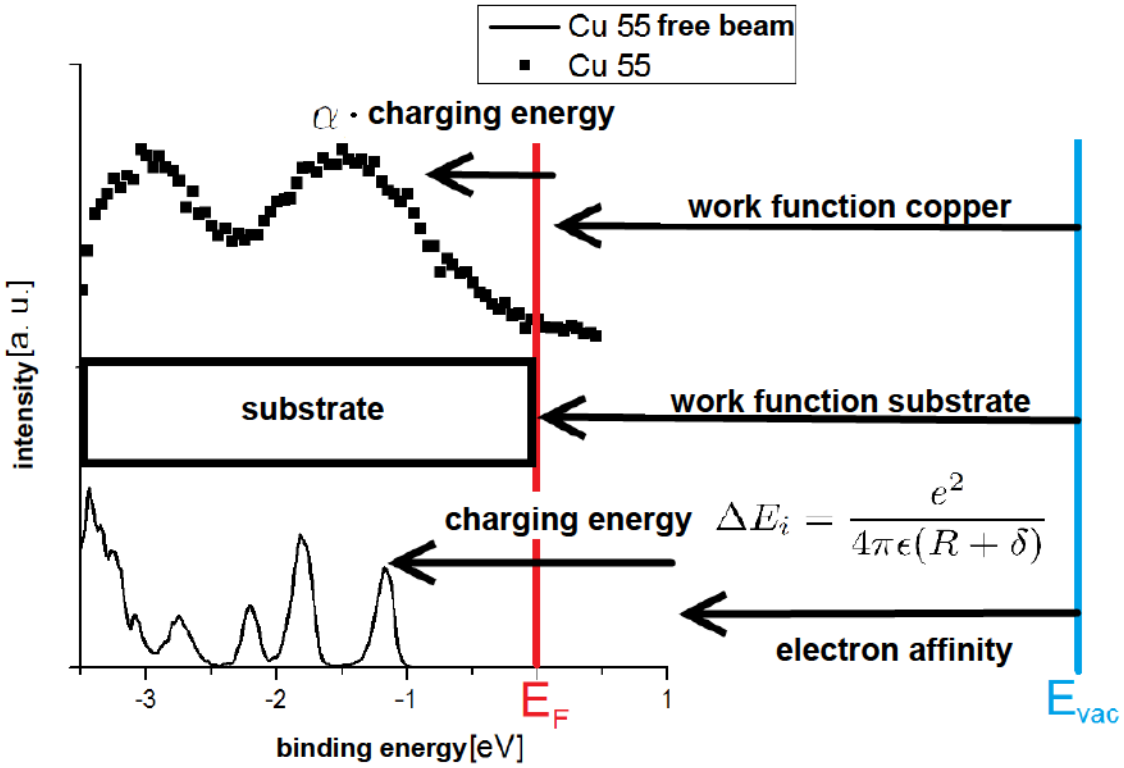

Figure 37: Schematic of the shift of deposited clusters and free beam clusters using the example of Cu_{55} clusters. The Fermi edge of the substrate lies under the vacuum energy by the value of its work function. The deposited Cu_{55} clusters are isolated from the substrate due to the rare gas layer. Therefore, the spectrum of the deposited clusters lies by the value of the charging energy times α plus the work function of copper under the vacuum energy. The free beam clusters are also isolated because they were measured in vacuum and are negatively charged. Therefore, the spectrum has to be shifted by the amount of the electron affinity and the charging energy to lower energies to compare free beam cluster spectra with those of deposited clusters. [89]

In this thesis clusters deposited on rare gas layers with a thickness of 60 ML are investigated. These clusters experience nearly no interaction with the substrate due to the isolating rare gas layer and are called "free clusters on a substrate" [90]. Their highest occupied electronic states do not align to the Fermi energy. Instead they can be compared to free beam clusters, as discussed above. In ref. [90] it is shown that for big gold clusters (N> 1000) deposited on 60 ML xenon on a Pb(111) substrate the onset of the cluster spectrum lies about the amount of the difference of the work function between cluster and substrate (ΔΦ) and α times the charging energy ($E_C = \alpha \frac{e^2}{4\pi\varepsilon(R+\delta)}$) below the Fermi energy (figure **38**). The contribution from the charging energy comes from the final state of the photoemission process (see chapter 6.2).

If the work function of the cluster material is equal or close to that of the substrate material (e.g., for polycrystalline copper on HOPG or Cu(111)), mainly the charging

energy remains as shift from the Fermi energy for larger clusters (see top curve in figure 37). However, changes due to variations in α and the dielectricity constant ε of the surroundings have to be considered.

But, it has to be mentioned that also clusters deposited on conducting surfaces (e.g. HOPG) show a shift of the onset of the cluster spectrum. The reason for this is that the clusters show a gap between the highest occupied orbital and the lowest unoccupied orbital (this is not visible with UPS) which is located around the Fermi edge for conducting surfaces. This is indicated, e.g., by STS experiments [47, 59, 80]. This gap becomes smaller for bigger clusters and closes if the bulk limit is reached.

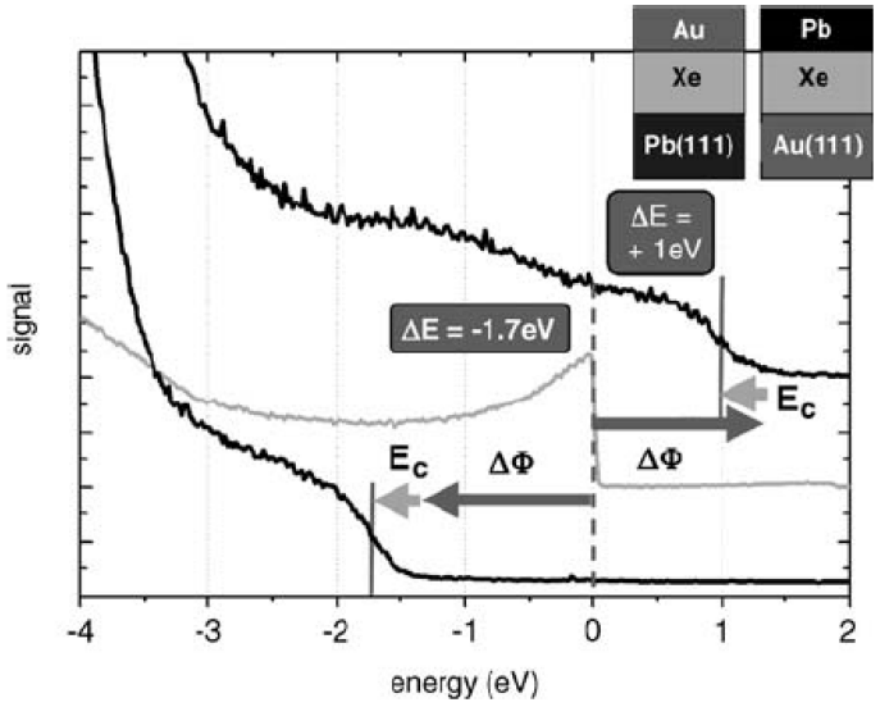

Figure 38: Shift of the Fermi edge due to the work function difference $\Delta\Phi$ (dark grey arrows) between Au and Pb. The difference between the shifts for Au/Xe/Pb and Pb/Xe/Au could be explained by the cluster charging energy ($E_C = \alpha \Delta E_i$; light grey arrows). [90]

8 Experimental results

This chapter presents the experimental results received during this work. It begins with measurements of clusters deposited on pure substrates. Clusters deposited directly on HOPG, Ag(111) and Au(111) are measured with UPS and STM with regard to the cluster surface interaction and the right amount of deposited clusters. Afterwards clusters on rare gas layers are probed with UPS. Here the clusters show a very weak interaction with the surface and can be treated as "quasi-free". The obtained UPS spectra of this "free clusters on a substrate" are then compared with free beam cluster spectra.

The programs used for the analysis of the measured data are *EIS Sphera* of the Omicron company and *Origin 8.5* for UPS measurements. For measurements with the STM the programs *WSxM* [91] from the Nanotech company, *Scala SPM SO 2.2* from the Omicron company and a program developed by *Niklas Grönhagen* during his diploma thesis called *clusterizer* [92] were used.

8.1. Clusters on pure substrates

Clusters deposited on substrates interact with the surface. This interaction can cause a change in the properties of the cluster depending on, e.g., its electronic and/or geometric structure [40, 93]. This has to be taken into account when working with deposited clusters. However, not all surfaces have the same effect on a cluster, e.g. a metal surface causes a metal cluster (as used in this thesis) to deform strongly [40], whereas HOPG causes nearly no deformation [94]. This arises from the different properties of the substrate materials. As already mentioned HOPG is an inert material (chapter 3.1) and, therefore, the clusters are only weakly bound to the substrate, thus, the electronic and geometric properties of the cluster are preserved which makes it a good substrate for the investigation of deposited clusters.

8.1.1. UPS on silver and copper clusters deposited on HOPG

The measurements presented in this chapter were made with the helium gas discharge lamp before the change of the operating gas to argon and the application of the heatable LiF window. The results for silver clusters on HOPG were obtained in collaboration with *Niklas Grönhagen* and were also a part of his dissertation [59].

HOPG is well qualified as a substrate for UPS measurements of deposited clusters due to its weak cluster-surface interaction and UPS spectrum. This chapter investigates the d-band region of deposited clusters. Figure **39** shows two UPS spectra of a silver bulk

and HOPG. The region of interest of the metal is the region 4 eV below the Fermi edge; this is the region in the HOPG spectrum with nearly no structure. This is also the energy region where the d-band signal of metal clusters can be found [84, 95, 96].

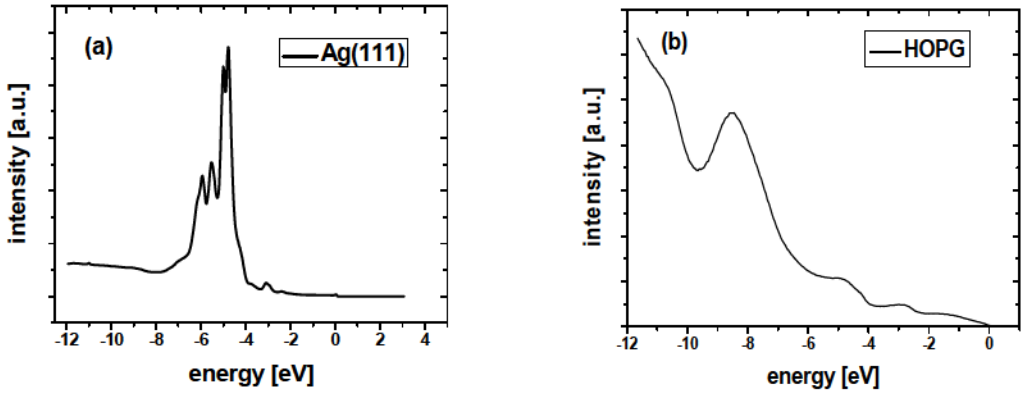

Figure 39: UPS spectra of (a) Ag(111) and (b) HOPG surfaces taken with the helium gas discharge lamp.

8.1.1.1. Silver clusters deposited on HOPG

In two independent experiments silver clusters in the size range of Ag_{55}-Ag_{923} were deposited at 70 K (Ag_{55}-Ag_{147}) and 125 K (Ag_{147}-Ag_{923}) directly on an HOPG substrate and investigated at a substrate temperature of 125 K with the helium gas discharge lamp. The UPS spectra as measured are presented in figure **40**.

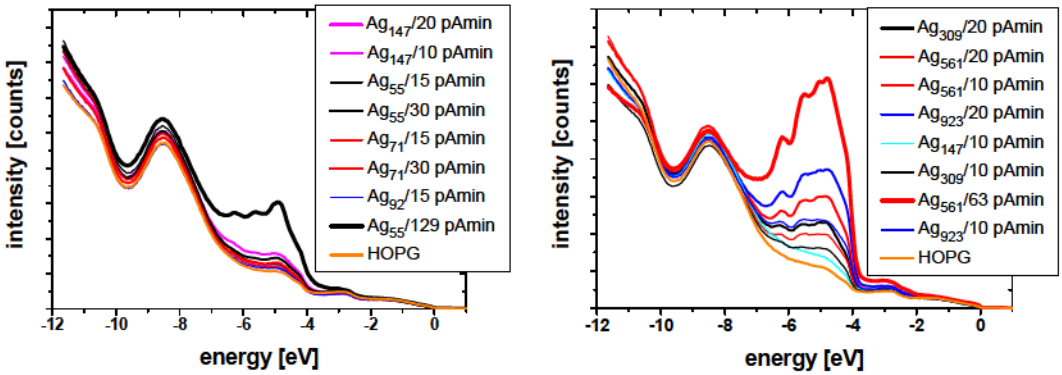

Figure 40: UPS spectra of HOPG (orange line) and clusters deposited directly on HOPG in the size range Ag_{55}-Ag_{923} with different coverages. The coverage is given in terms of the ion dose (current*time) for the 1mm cluster spot as measured with the Faraday cup. The spectra are referenced to the Fermi edge (E_F=0 eV).

Afterwards the HOPG signal is subtracted from measured cluster spectra. For this procedure *David Engemann* wrote the program *varalpha* during his diploma thesis [56]. The cluster d-band begins 4 eV below the Fermi edge and ends approx. 7 eV or 8 eV below the Fermi edge. The rest of the spectrum comes from the HOPG substrate. But with cluster deposition the UPS signal in the region from -8 eV changes so it is difficult

to subtract the underlying HOPG signal straight forward because this causes a distortion of the spectra in the region below -8 eV. To minimize this distortion the spectra are subtracted in a way where the region below -8 eV resembles silver bulk spectra. For a more detailed description of this program see ref. [56, 59]. UPS spectra of the clusters after a subtraction of the underlying HOPG signal are presented in figure **41**.

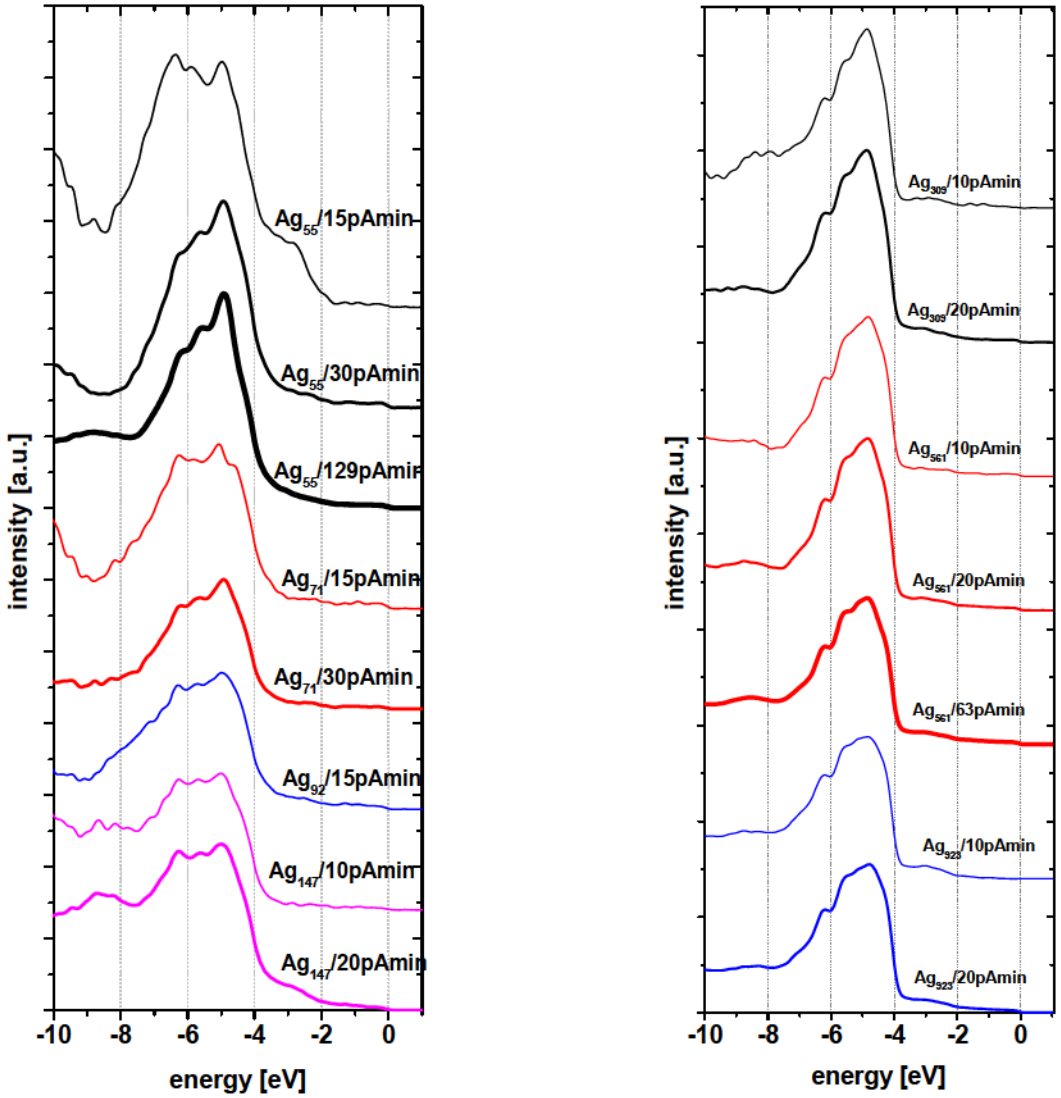

Figure 41: UPS spectra of Ag_{55}-Ag_{923} clusters after the subtraction of the HOPG substrate signal by using the program *varalpha*. For a better comparability the spectra are normalized by dividing the spectra by the cluster size times the coverage (i.e. the amount of silver) and shifted relatively to each other. (Ag_{147} deposited with 10 pAmin has an intensity too low for a proper investigation). These spectra were smoothed with the FFT smoothing method of origin using k=3 [56].

The d-band signal of the deposited silver clusters is clearly visible. Comparing these spectra with UPS spectra of polycrystalline silver and bulk Ag(111) (figure **42**), some similarities can be noticed. The spectra of small clusters deposited with a low coverage (≤ 20 pAmin) resemble the UPS spectrum of polycrystalline silver. UPS spectra of small clusters deposited with a high coverage or spectra of big clusters (independent of the coverage) look like the spectrum of Ag(111).

The similarity of the small-cluster spectra to the polycrystalline silver spectrum is a hint that the clusters did not coalesce at the given coverage and sample temperature (T= 125 K). The clusters lie random on the HOPG substrate with no predominant direction. When the clusters coalesce they build islands with an Ag(111) orientation due to the orientation of the facets of the cluster surfaces.

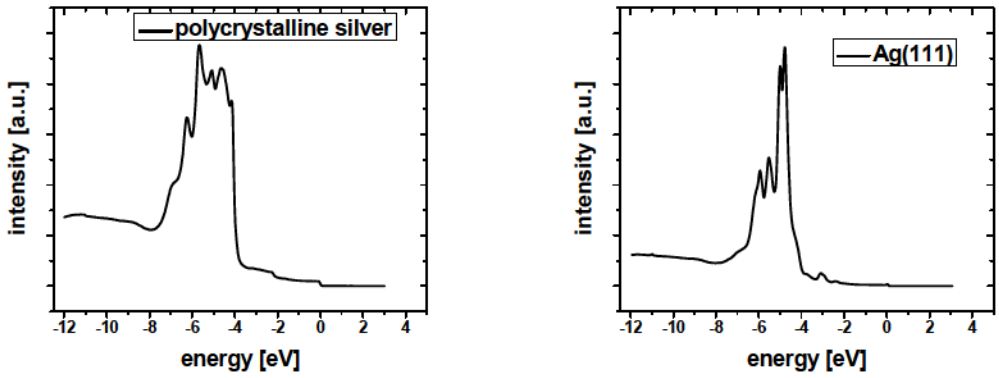

Figure 42: UPS spectra of polycrystalline silver and Ag(111) taken with the helium gas discharge lamp.

In contradiction to the small clusters, the similarity of the cluster spectra for big clusters to the Ag(111) spectrum is not a hint that the clusters coalesced. Given that the smaller clusters, which are more mobile at the substrate, did not coalesce at the same coverage and sample temperature, it is improbable that the bigger clusters did. For bigger clusters the facets on the cluster surface with an Ag(111) direction are bigger. If the clusters show a dominant orientation with Ag(111) facets parallel to the surface the resulting cluster spectrum resembles an Ag(111) spectrum.

The sample with the cluster sizes Ag_{147}-Ag_{923} was annealed stepwise up to room temperature (RT) for one hour and afterwards cooled down to T= 125 K and measured again. UPS spectra before and after annealing are presented in figure **43**. Not all spectra are shown in this graph because they all show the same effect. As mentioned above, the spectra before annealing look similar to the spectrum of Ag(111) independent of cluster size and coverage. After annealing the spectra resemble polycrystalline silver except for Ag_{561}/63 pAmin. In this case the Ag(111) like structure has become even more prominent. Before annealing the cluster lie on the surface with aligned facets (figure **44**). During the annealing process they receive more energy due to the increased temperature, thus, they can move over the surface and move to step edges and/or surface defects where they accumulate with a random orientation. This results in UPS spectra which look like polycrystalline silver. The Ag_{561} clusters with the highest coverage coalesced after annealing due to the high coverage. The annealing procedure leads to an Ag(111) film and to a more prominent Ag(111) like UPS spectrum. A schematic of this effect can be found in figure **44**.

Concluding, one can say that the cluster coverage useful for UPS measurements depends on the cluster size and sample temperature. The coverage must be high enough for a good UPS signal, but low enough to avoid coalescence. For the observed cluster sizes in this chapter (Ag_{55}-Ag_{923}) and the given sample temperature (T= 125 K) a

coverage ≤ 20 pAmin seems ideal. But, note that for lower temperatures clusters are less mobile and, therefore, a higher coverage could be possible without coalescence. Additionally, the substrate plays an important role. On substrates with a higher sticking coefficient (e.g. C_{60} covered surfaces or metals [80]) the clusters are bound more tightly to the surface and, as a consequence, need more energy to move over the surface.

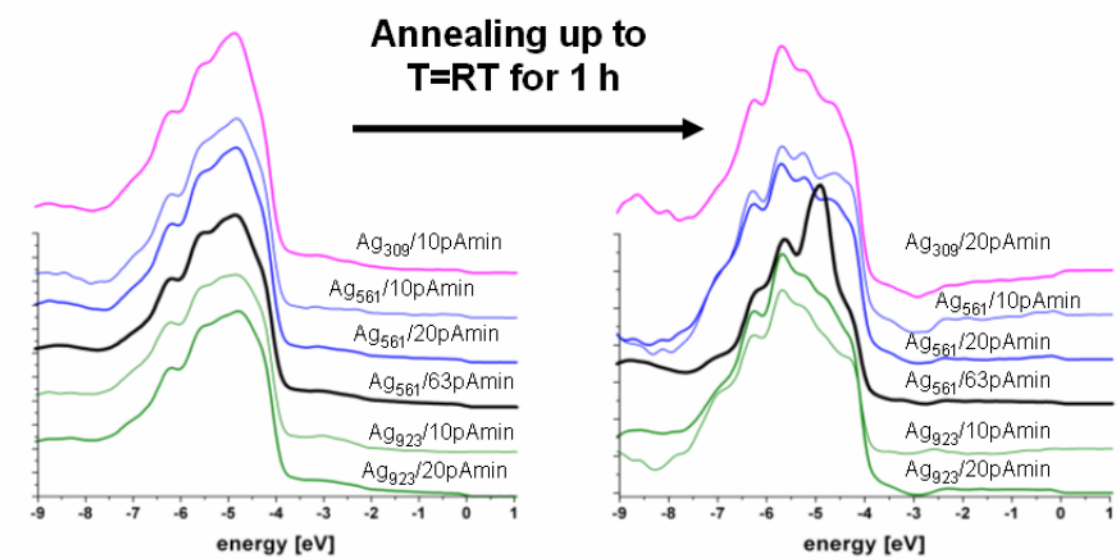

Figure 43: UPS spectra of Ag_{309}-Ag_{923} clusters with different coverages before and after annealing to RT. All spectra presented were measured at T= 125 K. Before annealing all spectra resemble Ag(111), after annealing they look more like the spectrum of polycrystalline silver, except for Ag_{561}/63 pAmin. Here the Ag(111) like spectrum becomes even more prominent. These spectra were smoothed with the SG smoothing method of Origin using n=5 [109].

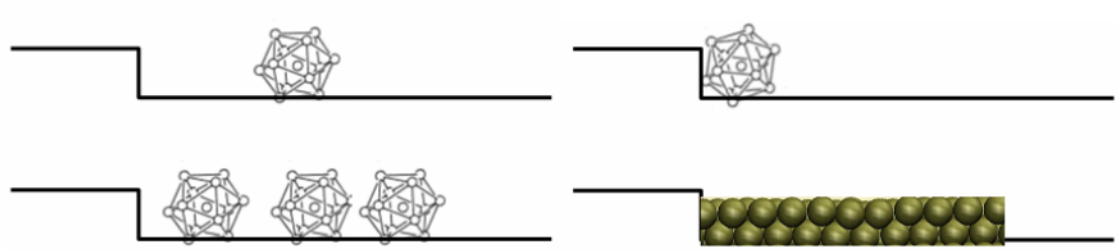

Figure 44: Left image (before annealing): *above* for low coverage, *below* for high coverage. The clusters are oriented with the hexagonally closed packed facets parallel to the flat HOPG surface; right image (after annealing): *above* clusters are attached, e.g., to step edges and lie randomly oriented on the surface, *below* for a high coverage (111) oriented islands are formed.

8.1.1.2. Copper clusters deposited on HOPG

Copper clusters in the size range of Cu_{34}-Cu_{92} were deposited with different coverages on HOPG at T= 125 K and measured with the helium gas discharge lamp (HeI= 21.2 eV) at the same temperature. The UPS spectra as measured are presented in figure **45**. It is eye-catching that the intensity of the cluster d-band signal is substantially lower than for the measurements of silver clusters on HOPG in the previous chapter although similar coverages and cluster sizes were used. The clusters were deposited in

the following order: Cu_{58}/70 pAmin → Cu_{92}/20 pAmin → Cu_{55}/30 pAmin → Cu_{55}/15 pAmin → Cu_{58}/30 pAmin → Cu_{58}/15 pAmin → Cu_{34}/40 pAmin → Cu_{71}/15 pAmin → Cu_{71}/30 pAmin. The cluster current was measured directly before and after this sequence. Unfortunately, the cluster current broke down to only 60% of the initial value during deposition and it is not possible to say at which point exactly the current broke down. Therefore, in the following discussion the coverage calculated with the cluster current at the start of the deposition will be used. But this can be one reason for the low intensity of the cluster signal in the UPS spectra.

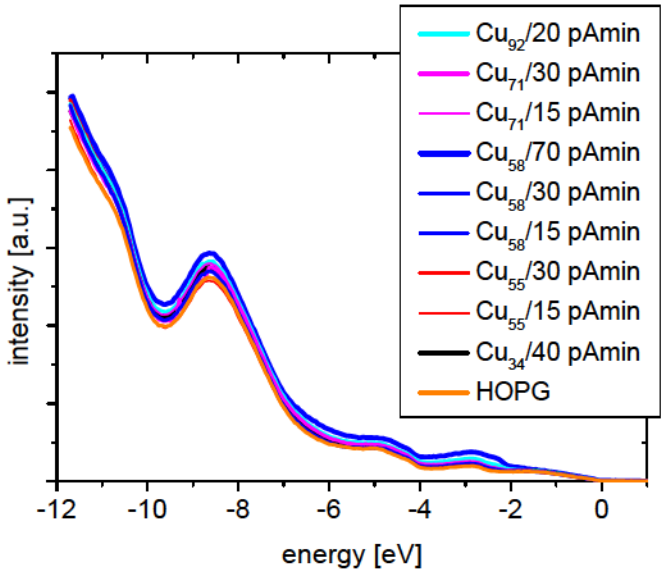

Figure 45: UPS spectra of HOPG (orange line) and clusters deposited directly on HOPG in the size range Cu_{34}-Cu_{92} at T= 125 K with different coverages. The spectra are referenced to the Fermi edge (E_F=0 eV).

The HOPG underlying signal was subtracted from the cluster spectra with the help of the program *varalpha*. The resulting cluster spectra are shown in figure **46** along with UPS spectra of polycrystalline copper and Cu(111) [97]. The d-band signal of the clusters is visible. In contrast to the spectra of polycrystalline silver and Ag(111), the copper bulk spectra look very similar. This makes it difficult to distinguish if the cluster spectra resemble more polycrystalline copper or Cu(111). The highest peak in the spectrum of polycrystalline copper is at nearly the same position as for Cu(111). Therefore, the shoulder at lower energies in the spectrum of polycrystalline copper (green circle, see figure **46**) is used for identification, because here the shoulder has more intensity than in the case of Cu(111) with regard to the main peak between -2 eV and -3 eV. Indeed for Cu_{92}/20 pAmin, Cu_{58}/30 pAmin plus 15 pAmin and Cu_{55}/15 pAmin such a shoulder could be identified. This would be a hint that the clusters did not coalesce and lie randomly oriented on the surface. But, in the case of Cu_{92}/20 pAmin the overall spectrum looks also very similar to the spectrum of Cu(111) due to the high intensity of the first peak in the cluster d-band, therefore in this case it is not really possible to make a clear statement. For Cu_{58}/70 pAmin the highest peak in the Cu(111) spectrum (orange circle, see figure **46**) can be found in the cluster spectrum, which could be a hint that the clusters already coalesced.

Due to the resemblance of the spectra of Cu(111) and polycrystalline copper and the poor statistics of the cluster spectra a clear classification of the spectra is very difficult and the above-mentioned assumptions must be treated carefully.

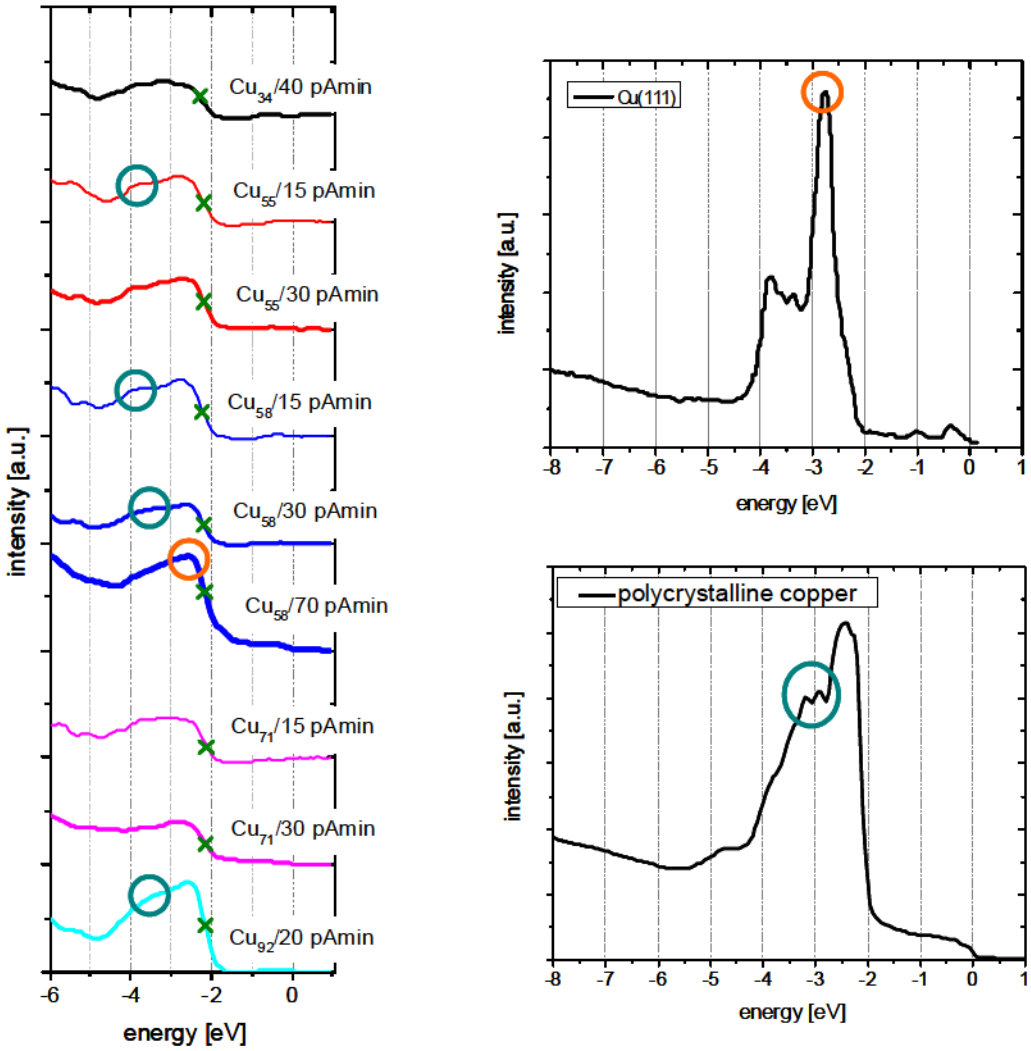

Figure 46: Left: UPS spectra of Cu_{34}-Cu_{92} clusters after the subtraction of the HOPG substrate signal with *varalpha*. For a better comparability the spectra are normalized with the amount of copper (see figure 41) and shifted relatively to each other. Right: UPS spectrum of Cu(111) (from ref. [97]) and of polycrystalline copper taken with the helium gas discharge lamp. The green and orange circle marks the position of the dominant peak of the Cu(111) spectrum and of the shoulder in the polycrystalline copper spectrum. This peak can be found in the cluster spectra of Cu_{92}, Cu_{58} and Cu_{55} on the left side. These spectra were smoothed with the FFT smoothing method of origin using k=5 [56]. The green crosses mark the position of the d-band flank.

Of special interest is the right flank of the cluster d-band onset. Measuring the position of the flank at half maximum a slight size dependent shift of its position can be observed. This is illustrated in figure **47**. The d-band onset shifts with increasing cluster size to higher energies. A similar behaviour was observed by DI NARDO [98] for evaporated clusters on polycrystalline graphite (figure **47**). There a shift of 1 eV occurs for copper clusters with 10-200 atoms per cluster. For clusters in the size range of the clusters used here (10 Å-16 Å average diameter → 40-180 atoms per cluster) the shift is

only 0.1 eV. This is a similar result as obtained in this measurement. Here the shift is 0.15 eV. Reasons for the discrepancy between this measurement and the results in ref. [98] of 0.05 eV can be found in the different substrates (HOPG to polycrystalline graphite) and the cluster sizes. The size of evaporated clusters could only be estimated in ref. [98] from the amount of material evaporated on the substrate and the clusters which form during this procedure show a broad size range. Therefore, only an average cluster height could be denoted.

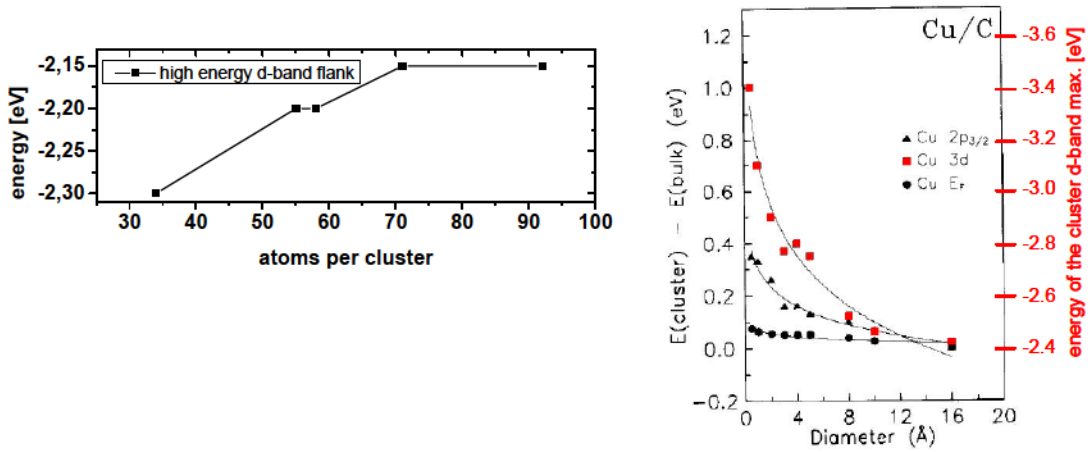

Figure 47: Left: position of the right d-band flank of the measured size selected copper clusters on HOPG. The observed shift is about 0.15 eV. Right: results of UPS measurements on evaporated copper clusters on polycrystalline graphite from ref. [98]. The red squares mark the position of the maximum of the cluster d-band.

In previous publications [99, 100] the cluster d-band shift of metal clusters on graphite was explained with the help of the final state effect. The positive charge left on the sample after the photoemission process, which was not replaced quickly enough by electrons from the substrate, results in a shift of all electronic structures observed in UPS spectra. For silver and gold clusters deposited on graphite this results in shifts of the Fermi edge of about 1 eV and 0.6 eV and a d-band shift of about 0.5 eV [100]. The shifts of the cluster d-band observed here are much smaller and in [98] it could be observed that the Fermi edge of the clusters did not shift at all on graphite (see figure **47**). Nevertheless for the measurements of copper clusters on HOPG in this thesis a reduced final state effect can not be excluded definitely because it was not possible to investigate the position of the cluster Fermi edge on HOPG.

To prove that the shift of the cluster d-band flank observed in the UPS measurements here is not a result of the final state effect, copper clusters were deposited on Ag(111). The metal substrate is highly conducting and should make sure that the final state effect did not occur because of the facilitated charge transfer between cluster and substrate. The results of this experiment are presented in the next chapter.

8.1.2. Copper clusters deposited on Ag(111)

In the previous chapters, UPS measurements of clusters deposited on a substrate which interacts weakly with the clusters (HOPG) were presented. This chapter presents UPS and STM measurements of copper clusters deposited directly on Ag(111), demonstrating a strong cluster surface interaction on a highly conducting surface.

8.1.2.1. UPS of copper clusters on Ag(111)

Copper clusters with 147 and 923 atoms were deposited on a pure Ag(111) substrate at 20 K and also measured at this temperature with the new argon discharge lamp with the attached heatable LiF window (see chapter 6.3). The low sample temperature is only possible because the pressure in the vacuum chamber is very low (10^{-11} mbar) due to the LiF window and, thus, the contamination of the sample can be minimized. As described in chapter 6.2, the sensibility of the discharge lamp for certain electronic states varies with the photon energy. In figure **48** two UPS spectra of bulk copper are shown, one taken with the helium gas discharge lamp and the other with the argon discharge lamp.

A clear difference between the spectra can be observed. The d-band has more structure if measured with the helium lamp but the s-p-band region near the Fermi edge shows more intensity and structure if measured with the argon lamp.

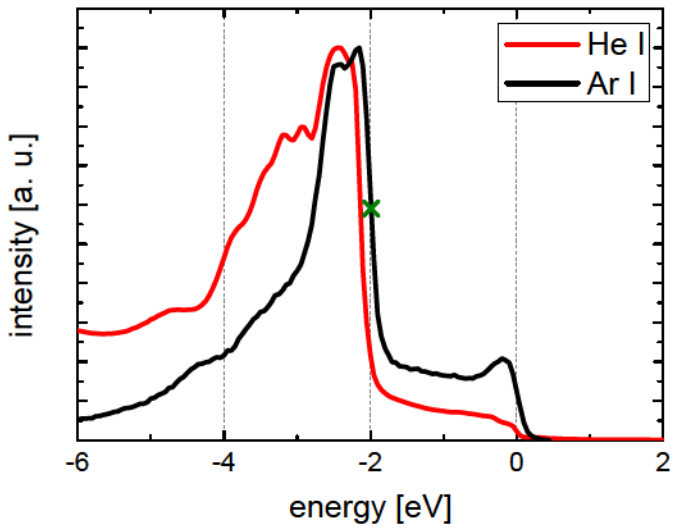

Figure 48: UPS spectra of polycrystalline copper measured with the helium (red) and the argon (black) gas discharge lamp. The spectra are normalized for a better comparability. The position of the d-band onset, measured at half its height, is -2 eV for bulk copper measured with the argon lamp (marked with a green cross). [89]

In figure **49** UPS spectra of Cu_{147} and Cu_{923} clusters deposited with different coverages on pure Ag(111) are shown. The coverages were chosen so that the surface is covered

with 5 % of a cluster ML[2] (for Cu_{147}: 66 pAmin; for Cu_{923}: 19 pAmin). The cluster coverage on Ag(111) can be higher than on HOPG because of the lower mobility of the clusters. The strong metallic bond between the clusters and the substrate prevents cluster diffusion even at a high coverage. However, the strong cluster surface interaction also leads to a deformation of the clusters as will be discussed in chapter 8.1.3.

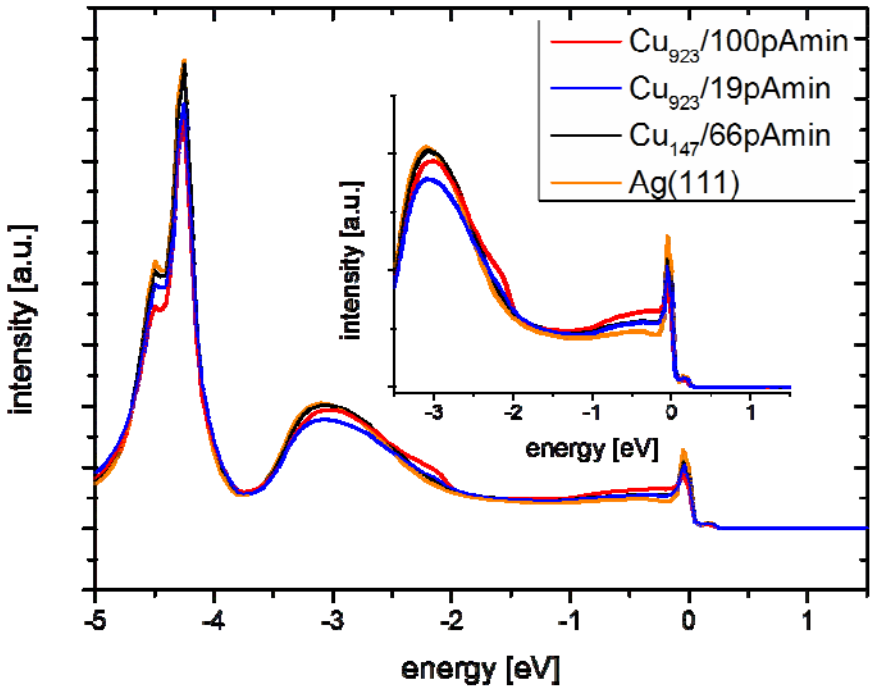

Figure 49: UPS spectra of Cu_{147} and Cu_{923} deposited with 66 pAmin, 19 pAmin and 100 pAmin on Ag(111). The inset magnifies the energy range -3.5 eV to 1.5 eV.

The inset magnifies the spectra in the energy region from -3.5 eV to 1.5 eV. It is clearly visible in the spectra that the surface state of Ag(111) changes with cluster coverage, i.e., its intensity decreases. This becomes even clearer after subtracting the Ag(111) background signal from the cluster signal (figure **50**). Because of the higher surface state signal of the pure Ag(111) surface the spectra have a negative peak at the Fermi edge after subtraction of the Ag(111) underground signal. The reason for this behaviour is that the surface state is quenched due to irregularities on the surface such as clusters or impurities, as described in [101] (see figure **9** & **10** in ref. [101]).

The d-band onset (measured at half the height of the d-band peak) of the subtracted spectra shifts only slightly from -2.13 eV for Cu_{147} to -2.06 eV for Cu_{923}. As mentioned in [98] the d-band shift gets smaller with increasing cluster size and approaches the value of bulk copper (d-band onset at -2 eV, see figure **48**). The shift of the d-band onset is of the same magnitude as the shift observed in the previous chapter for clusters deposited on HOPG. The shift of the cluster d-band flank occurring for clusters deposited on a conducting metal (Ag(111)) is a proof that here the shift is due to a size

[2] A cluster ML is the amount of clusters needed to cover an area completely with clusters.

related change of the electronic structure in the cluster and not due to the final state effect.

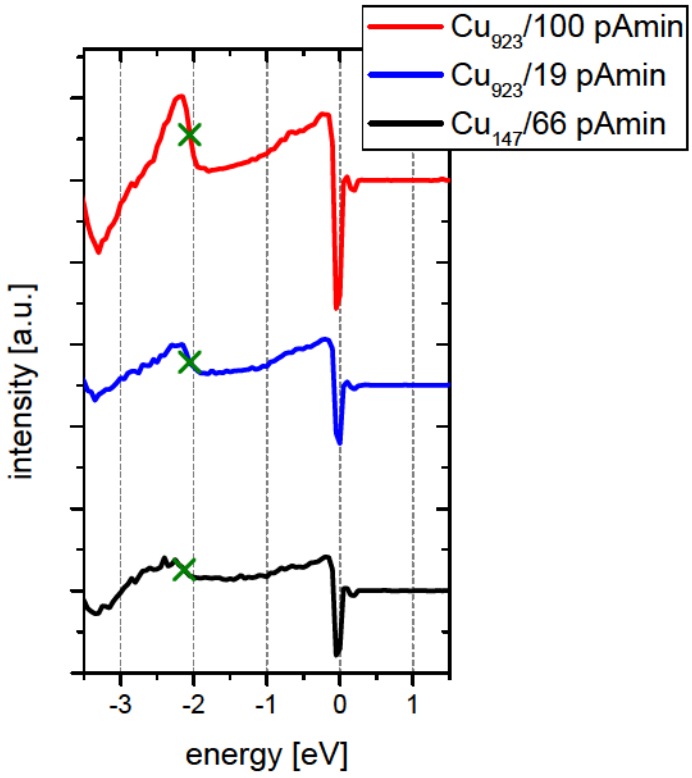

Figure 50: UPS spectra of Cu_{147} and Cu_{923} clusters after the subtraction of the Ag(111) substrate signal. For a better comparability the spectra are shifted relatively to each other. The green crosses mark the d-band onset.

8.1.2.2. STM of copper clusters on Ag(111)

Additionally to UPS measurements, the sample was measured with the STM at 5 K. STM images of the center of the deposition spots are presented in figure **51**.

For Cu_{147} and Cu_{923}/19 pAmin the clusters are pictured separately and seem to have the same size. For Cu_{923}/100 pAmin the clusters show different sizes and some bigger, coalesced clusters appear. Here the coverage is so high (25.7 % of a cluster ML) that the clusters already begin to land on each other during deposition and coalesce to bigger clusters (bright bumps in the STM image) on the sample.

Unfortunately, no height measurements were possible due to contamination of the sample. During measurements, impurities of 1-2 Å height were visible in the STM images. Clusters are way more reactive than bulk metal [102] so it is plausible that the impurities attach especially on clusters and change the height measurements.

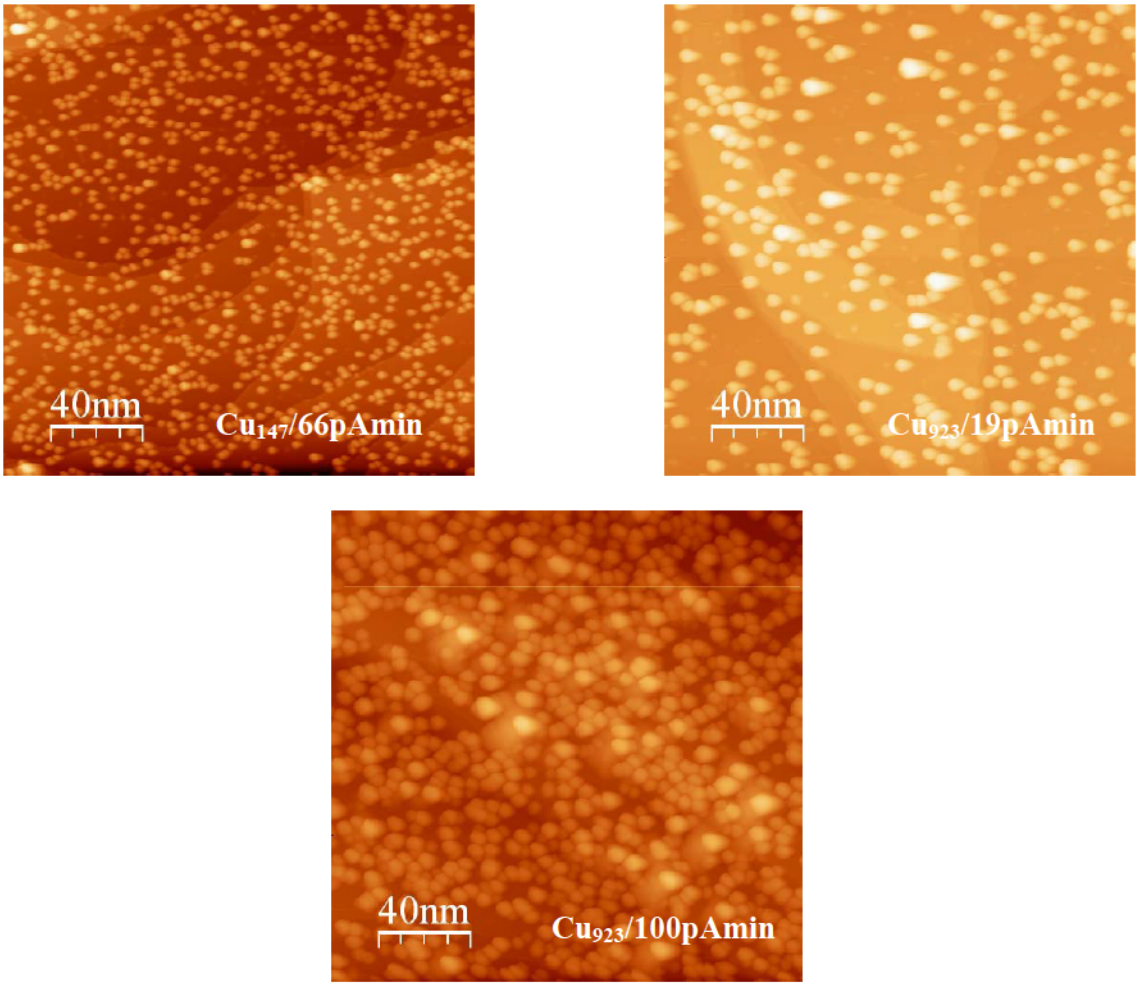

Figure 51: STM images of Cu_{147} and Cu_{923} clusters deposited with different coverages on Ag(111).

8.1.3. Silver clusters deposited on Au(111)/mica

This chapter presents STM measurements of silver clusters deposited directly on Au(111)/mica. Different cluster sizes were deposited with different deposition energies in two independent experiments at 77 K and 11 K, respectively, and measured at 77 K or 5 K. Additionally, annealing experiments were performed.

8.1.3.1. Ag_{55}-Ag_{147}/Au(111)/mica deposited at 77 K

The results for this experiment were already presented in [40, 59] and therefore will be treated here only briefly.

Ag_{86} clusters were deposited with a kinetic energy of 1, 3, 15, 34, 150 and 340 eV per cluster, respectively. Ag_{55}, Ag_{80}, Ag_{95} and Ag_{147} clusters were deposited with a kinetic energy of 3 eV. Here only the results for Ag_{86} at different deposition energies and Ag_{55} and Ag_{147} will be discussed. The results of the STM measurements are compared with results of molecular dynamic (MD) simulations, for further details see ref. [40].

Figure **52** shows height measurements and the appropriate MD simulations of the deposited clusters. An Ag(111) ML has a height of 0.236 nm. The peaks in the experimental and simulated data show multiples of that value. That is an evidence that the clusters become epitaxial at the given deposition energies. In addition, the number of Ag layers decreases with increasing deposition energy and decreasing cluster size.

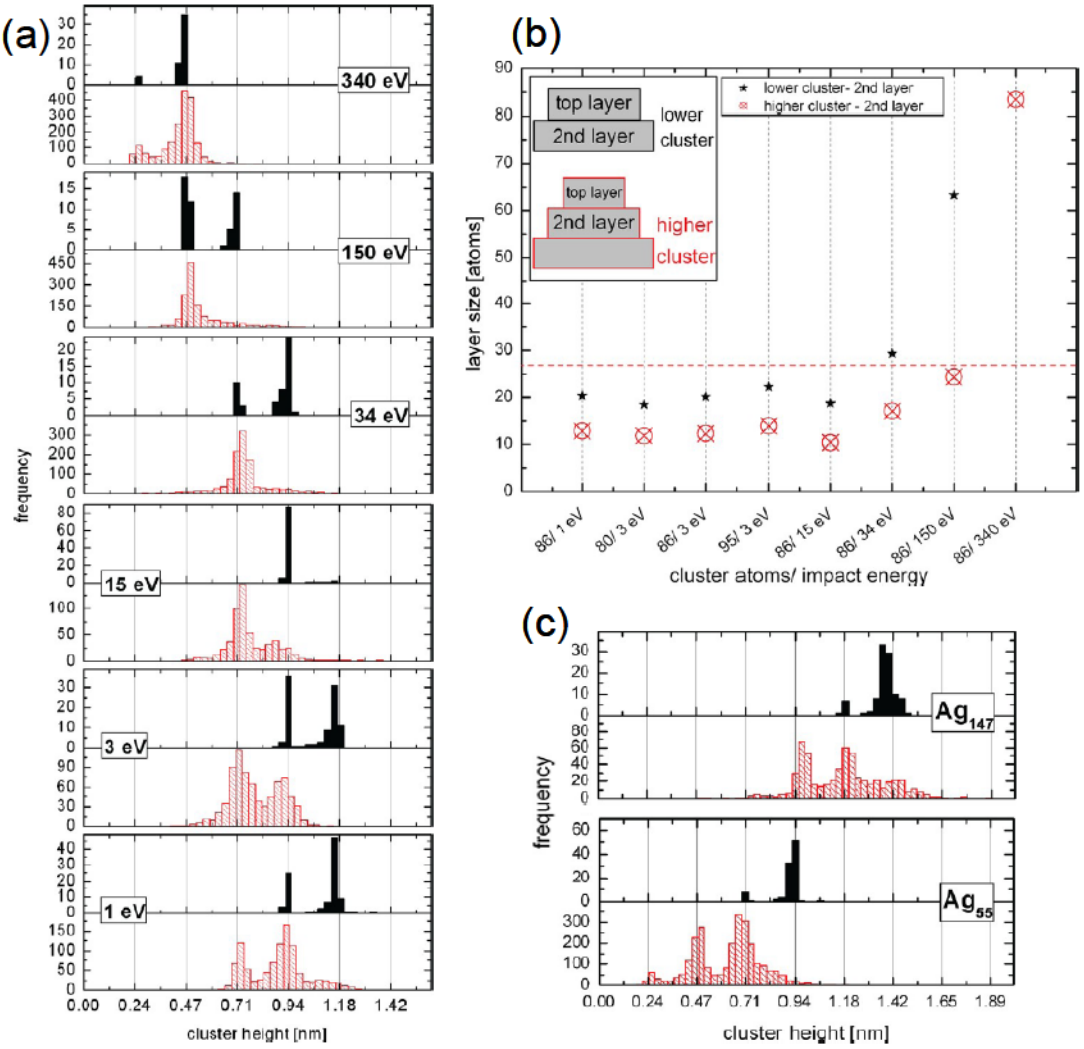

Figure 52: (a) Histograms of Ag_{86}/Au(111)/mica deposited with energies from 1-340 eV per cluster. Experimental data are displayed in red and data of the MD simulation in black. The increments of the x-axis correspond to single monolayers (0.236 nm). (b) Average sizes of the second layer from the top of a cluster for each deposition energy of Ag_{86}. The horizontal red dashed line marks a limiting layer size of 27 atoms. All clusters that have a second layer larger than that value exhibit no decay after deposition. The box schematically shows the profiles of the clusters with their respective layers. (c) Histograms of Ag_{55} and Ag_{147}/Au(111)/mica with a deposition energy of 3 eV. [40]

The histograms for a deposition energy of 1 and 3 eV (experiment and simulation) show only minor differences. This indicates that already for 3 eV the kinetic energy of the clusters can be neglected compared to the strong metallic interaction between the cluster and the surface. For this reason one can say that a kinetic energy of 3 eV per cluster is sufficient for soft landing conditions.

It is important to mention that the peak positions in figure **52** are shifted by 0.06 nm to match the heights of silver monolayers with fcc stacking (0.236 nm). This is explained in figure **53**. The measured peak positions show an offset regarding the theoretical height of one silver ML. The reason for this offset is the difference in the LDOS of the silver clusters and the Au(111) planes. That this electronic effects cause deviations in the height measurements was already shown in [103]. To determine the shift between the measured peak positions and the theoretical silver ML heights, the experimental peak positions are plotted versus the theoretical heights. The data points have only small error bars and the best-fit line shows a gradient of one. This behaviour shows that there is really only a constant shift between the experimental peak positions and the theoretical ML heights. The offset of the best-fit line marks the shift needed to compare experiment and simulation (0.06 nm). After the correction of 0.06 nm to lower values the peaks in the histograms show the right position of the silver monolayers.

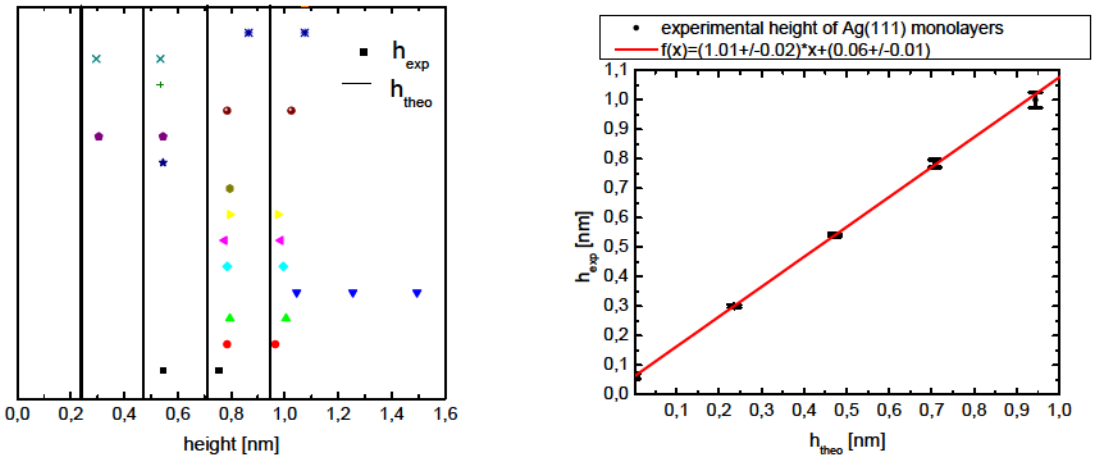

Figure 53: Left: Measured cluster height (dots, different colors mark different measurements) and theoretical cluster height (line), a clear offset is visible. Right: Experimental peak positions plotted versus theoretical ML height. The error bars show the scattering of individual heights.

The peak positions for Ag_{86} deposited with an energy of 340 eV are in good agreement with the simulation, but a discrepancy of about one silver monolayer between experiment and simulation can be found for energies ≤ 15 eV. For 34 eV and 150 eV only the lower cluster height of the simulation is seen in the experiment for Ag_{86}.

In order to explain the observed difference in cluster height between experiment and simulation it is important to keep in mind that at high deposition energies (150 eV and 340 eV), where the results of the measured data and the simulation are in agreement the clusters are almost completely flattened. For low deposition energies (1-15 eV), where a shift of about one ML can be observed, the clusters adopt a compact, roughly hemispherical shape. For low deposition energies the top layers of the simulated clusters are small (5-10 atoms). A proposition to explain the observed shift may be a post deposition decay process, even at 77 K, which takes places on a timescale of some hours, much longer than the possible time for MD simulations. Above a certain size of the second layer from the top of the cluster (red dashed horizontal line in figure **52** (b)) no shift of the cluster height is observed. All clusters that have a second layer larger than that value show no decay after deposition (e.g., 340 eV). In the cases of Ag_{86} at 34 eV and 150 eV the second layer of the higher clusters is smaller and that of the lower

is larger than the limiting size. From this follows that the higher clusters are shifted in the experiment and both kinds of clusters share the same peak, so that a single peak appears. This hints to a cluster shape dependent effect which enables a reduction of the energy barrier that has to be surpassed to allow the decay of the top layer within a timescale of hours at 77 K.

The energy barrier can be calculated with the help of MD simulations (figure **54**) this will be described shortly in the following. For more details see ref. [40].

In order to understand the discrepancy between the simulated and measured data an Ag_{86} cluster was deposited at 1 eV and annealed at 325-425 K within MD simulations. This as-deposited cluster had 4 atoms in the top ML and its evolution was followed until the top ML had vanished. Fitting the time to reduce the height by 1 ML vs. temperature to an Arrhenius equation yielded an activation barrier of ca. 0.4 eV. But this barrier would be still too high for any evolution at 77 K. For an accurate estimate of the barrier height nudged elastic band (NEB) calculations [104] within density functional theory (DFT) [105] were performed. Using the model including only the cluster the resulting barrier from DFT agreed perfectly with the one from MD simulations. But is the NEB calculation repeated with DFT including a 2 ML thick Au(111) surface under the cluster, the barrier decreases to 0.22 eV. The shift in binding because of the surface provides an additional driving force for the flattening of the clusters. At the Au and Ag layers directly at the interface, a charge transfer takes place and changes the energetics of the migration process. Thus, the charge transfer causes a lowering of the flattening barrier. As a conclusion, one can say that the fast decay of the top ML is responsible for the shift between the experimental and simulated height distributions. The clusters do not continue flattening after the top ML is gone because the driving force gets smaller as the cluster flattens.

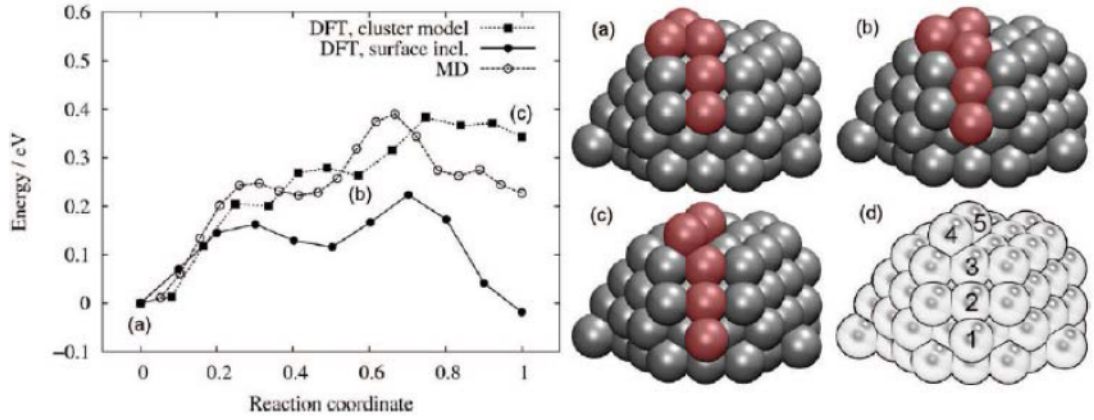

Figure 54: Flattening barrier with MD and DFT. For the two DFT cases are included: a cluster model and one with two Au(111) ML under the cluster. (a-c) Snapshots of the DFT cluster model along the transition path. Moving atoms are highlighted in red. (d) Atoms involved in the exchange process. [40]

8.1.3.2. Ag_{55}, Ag_{86} and Ag_{147}/Au(111)/mica deposited at 11 K

In order to investigate the decay of the top most cluster layer, the same cluster sizes as in the previous experiment were deposited with a deposition energy of 3 eV per cluster at 11 K and investigated with the STM at 5 K. The assumption was that at lower temperatures the decay slows down, or not happens at all. Additionally, the sample was annealed for one hour at 77 K and measured again at 5 K. The results and a comparison with the results of the previous chapter are presented in figure **55**.

The histograms measured at 5 K show a shift regarding the peak position, too, as can be observed in figure **55** comparing the results of the corrected measurements at 77 K and the new results. As explained in the previous chapter the reason for this offset is the difference in the LDOS of the silver clusters and the Au(111) planes which cause deviations in the height measurements [103]. But, in contrast to the measurements of the previous chapter, there are not enough data for a determination of the correct shift between the measured peak positions and the theoretical height of the silver monolayers. Therefore the peak positions of the experimental data measured at 5 K are shifted about the same value as the data of the previous chapter (0.06 nm to smaller cluster heights). The shifted results are presented in figure **56** and will be discussed in the following.

For Ag_{55} two peaks in the histograms may be visible before annealing with a height of two and three ML, respectively (figure **56**). But, this two peak structure is almost within the statistical errors of the histogram. Thus, this result has to be treated carefully. After annealing there are more clusters with a height of three ML than two. The peak at a height of two ML is weakened significantly in comparison with the peak at three ML, but has still the same amount of counts than before the annealing process. A similar result was obtained in the previous chapter for clusters deposited and measured at 77 K. There a two peak structure could be observed with a height of two and three ML.

At a height of 0.2 nm (0.3 nm without the shift), an additional peak appears in the histograms after annealing which could be identified as a sort of contamination, because it appears in all measurements after the annealing step. Due to the low temperature of the sample during deposition and the first measurements impurities adsorb on the surface. These impurities become mobile during the annealing process and agglomerate at step edges or surface defects to small particles which can be measured with the STM.

Ag_{86} clusters show only one peak at 5 K with a height between 4 and 5 ML. This unusual peak position may be a result of the contamination of the sample as can be seen after annealing. However, the clusters seem to be higher by at least one silver ML than at 77 K. This is a hint for a different or slower diffusion process of the top most atoms of the cluster. After annealing, the histogram looks like the one taken at 77 K in the previous experiment including the ratio of the two cluster heights (3 and 4 silver ML). Again, the peak resulting from a contamination of the sample is visible.

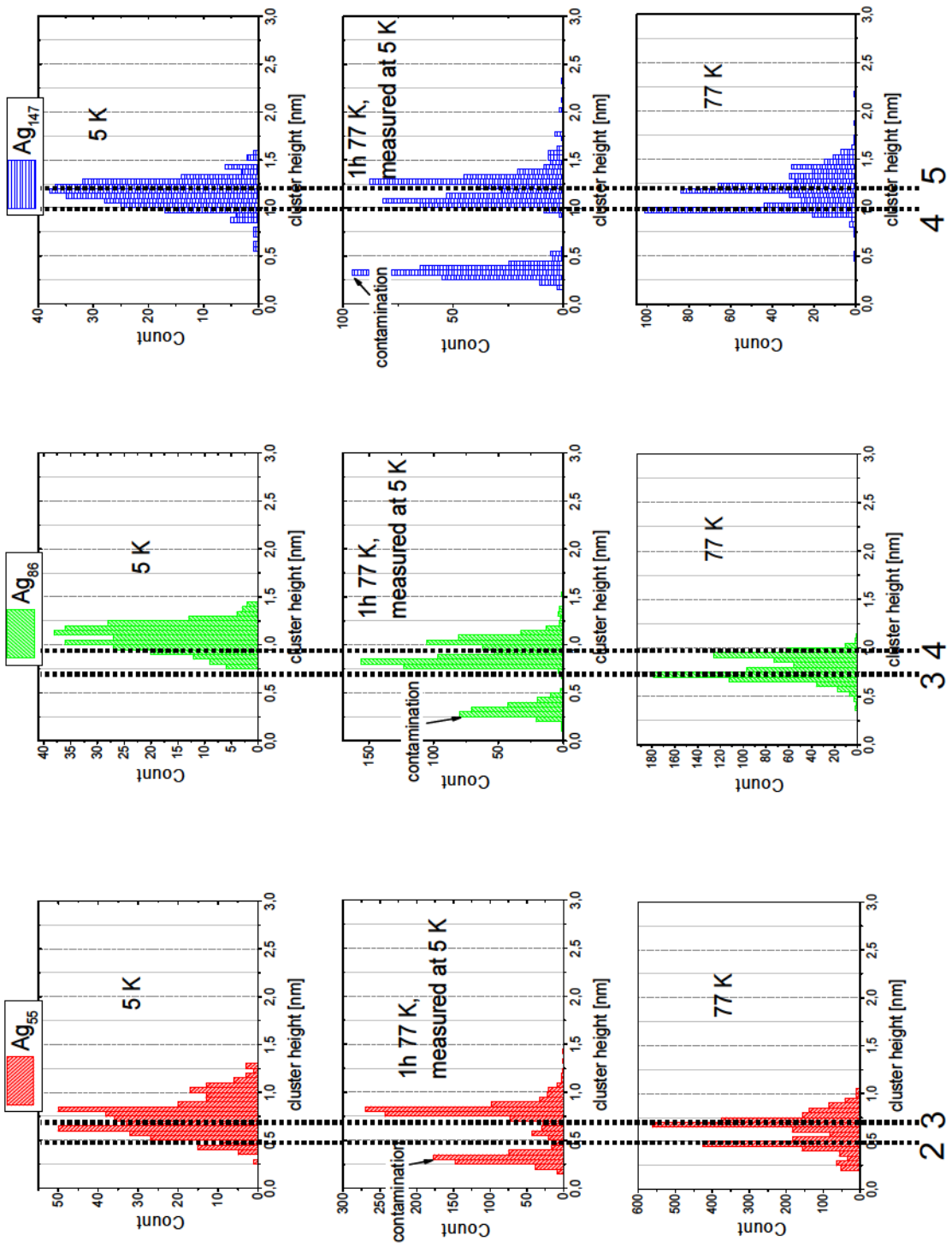

Figure 55: The histograms above show height measurements for Ag_{55} (red), Ag_{86} (green) and Ag_{147} (blue) clusters on Au(111). The upper histograms show the results for measurements at 5 K directly after deposition. The histograms in the middle show results after an annealing of 1 hour at 77 K and than cooled down to 5 K and measured at this temperature. The peak at 0.3 nm comes from a contamination which became mobile during annealing and agglomerated to small particles of 0.3 nm height. The histograms below show the results of the previous chapter for clusters deposited at 77 K and measured at this temperature. The dashed lines mark the position of the silver monolayers as measured in the previous chapter.

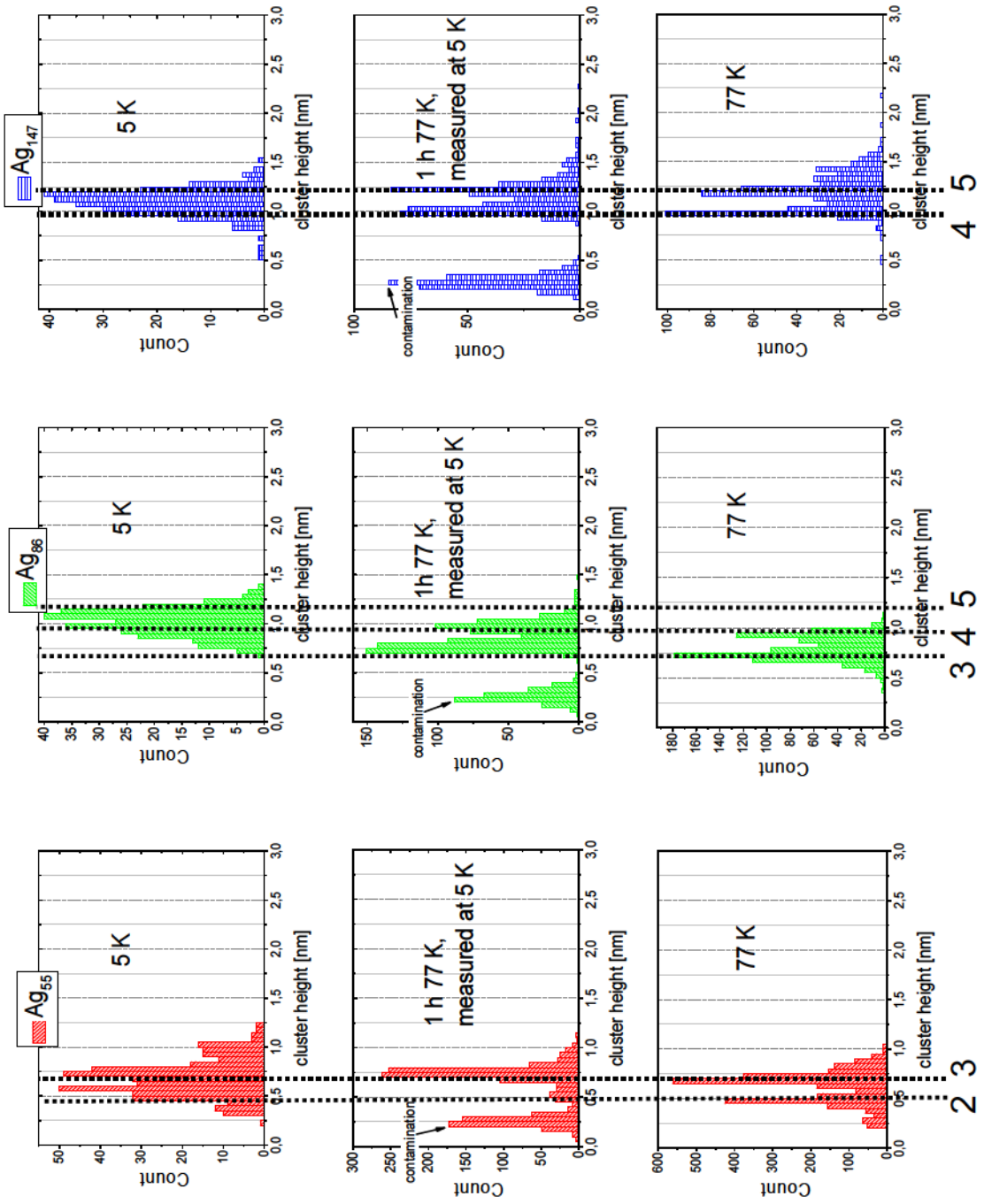

Figure 56: The histograms above show height measurements for Ag_{55} (red), Ag_{86} (green) and Ag_{147} (blue) clusters on Au(111). The upper histograms show the results for measurements at 5 K directly after deposition. The histograms in the middle show results after an annealing of 1 hour at 77 K and than cooled down to 5 K and measured at this temperature. The peak at 0.2 nm comes from a contamination which became mobile during annealing and agglomerated to small particles of 0.2 nm height. The histograms below show the results of the previous chapter for clusters deposited at 77 K and measured at this temperature. For a better comparability the histograms measured at 5 K are also shifted about 0.06 nm to smaller cluster heights like the histograms measured at 77 K. The dashed lines mark the position of the silver monolayers as measured in the previous chapter.

Ag_{147} clusters show similar results as Ag_{86} clusters. Again, only one peak is visible for the measurements at 5 K before annealing. Here it looks like the clusters have nearly a height of five silver ML, with a relatively broad size distribution. After annealing, the

situation of the previous experiment at 77 K could be established with an additional contamination peak.

Because of the poor statistics for the measurements at 5 K it is difficult to say, if the histograms show only one peak or would show two peaks in the case of a better statistic. Therefore, the mean value of the cluster height is investigated, even for the possible two peaks in the case of Ag_{55} at 5 K and also for the data of the previous chapter measured at 77 K from ref. [40]. The goal is to see if an overall change in the cluster heights appears. The mean value of the cluster heights before and after the correction with the shift of 0.06 nm to lower cluster heights is given in table **2**.

number of silver atoms in the cluster	measured cluster height at 5 K [nm]		measured cluster height after annealing for 1 h at 77 K and measured at 5 K [nm]		measured cluster height at 77 K [nm]	
	corr.	*uncorr.*	*corr.*	*uncorr.*	*corr.*	*uncorr.*
55	0.68±0.19	0.74±0.19	0.73±0.11	0.79±0.11	0.62±0.16	0.68±0.16
86	1.02±0.13	1.08±0.13	0.86±0.14	0.92±0.14	0.79±0.12	0.85±0.12
147	1.09±0.14	1.15±0.14	1.14±0.18	1.20±0.18	1.17±0.19	1.23±0.19

Table 2: Calculated mean values of the cluster heights for the measurements from figure 55 (without correction of 0.06 nm) and from figure 56 (including the correction of 0.06 nm) and the corresponding errors of the mean value.

It can be seen that in the case of Ag_{55} the average cluster height before and after the annealing process is the same, within the statistical error, and in good agreement with the measurements of the previous chapter at 77 K. This also applies for Ag_{147}. Ag_{86} show a height difference of about one half silver monolayer before and after annealing, which is higher than the statistical error. But, the cluster height of the measurements after the annealing process and the results for 77 K is equal within the statical error. So, only for Ag_{86} a real difference between the measurements at different temperatures can be observed.

The results obtained for the height measurements at 5 K were also studied using molecular dynamic (MD) simulations. A MD simulation of the used clusters deposited at a temperature of 15 K with the method described in [40] and a comparison with the actually measured and corrected spectra (shift of about 0.06 nm to smaller heights) is presented in figure **57**.

A comparison between measured (and shifted by 0.06 nm) and MD simulated height measurements shows some differences. The measured Ag_{55} clusters show two peaks in the histogram (or only one broad peak at a height of three silver ML, because the two peak structure is almost within the statistical error) whereas the simulated data show only one high peak at a height of four silver monolayers. Ag_{86} show one peak in the measurements but two peaks in the MD simulation. But it is possible that with more statistics also two peaks could occur in the measurements, as already indicated in the experimental histogram. In this case the results of the MD simulation would fit quite well with the measured and shifted data. For Ag_{147} MD simulation and experiment show

both only one main peak, but there is a shift of about one silver monolayer in the measured cluster height to smaller heights.

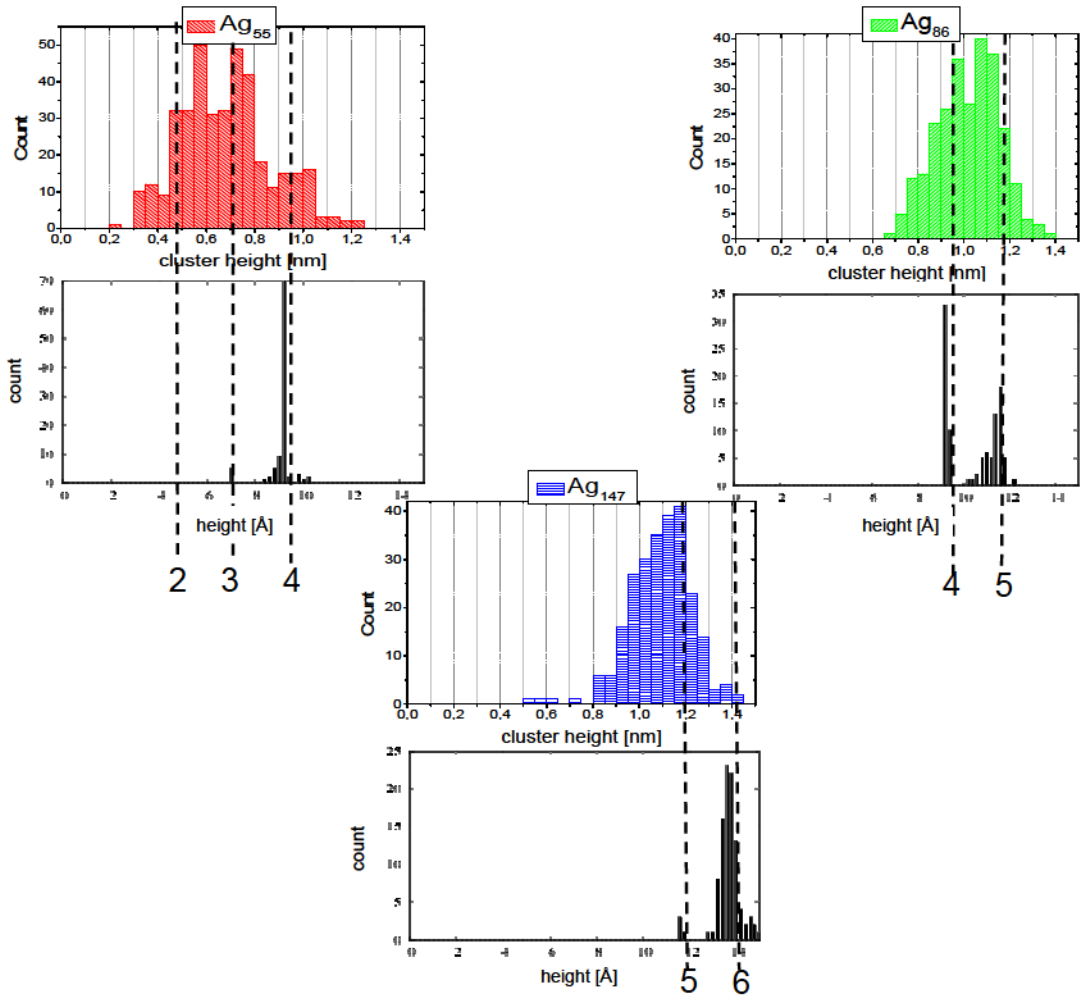

Figure 57: Comparison between measured and corrected height measurements (upper histograms; measured at 5 K) and MD simulated (histograms below; simulated at 15 K) height measurements. A clear difference is visible.

The differences in peak positions (cluster heights) between experiment and MD simulation and the missing of a two peak structure (Ag_{86}) in the measurements are surprising. It was expected that the low temperatures during the deposition of the clusters and during the measurements would prevent a decay of the top most cluster layer, which was assumed to be the main reason for the difference of one silver ML in cluster height in chapter 8.1.3.1 between simulation and experiment. But, it seems that other effects have to be taken into account to explain the appearing differences between experiment and MD simulation.

The reason for these differences is not quite clear and needs more investigation. But one possibility is the deposition of the clusters itself. The clusters have a certain temperature (several hundred K [106]) after they land on the surface. Due to this temperature the atoms are mobile in the cluster, i.e., the cluster is liquid. Maybe the cluster freezes out on the surface in a random orientation and due to the slow diffusion process it takes

some time to reach equilibrium and form silver monolayers. This could lead to the missing peaks in the experimental data or broad size distributions. Another possibility is that the cluster is so hot just after deposition that some atom monolayers already decay in the few picoseconds after deposition before the cluster cools down which would lead to a different height distribution than in the simulation.

Of special interest is that the results of Ag_{86} fit quite well with the MD simulated data (after applying the shift of 0.06nm to the measured data), but Ag_{55} and Ag_{147} show a shift of at least one silver ML between the measured and MD simulated data. In addition Ag_{86} is the only cluster size investigated, which shows an actual difference between the measurements at 5 K and 77 K. In [59] it could be shown that between Ag_{85} and Ag_{87} a transition to larger cluster heights occurs (from 1.4 nm to 1.5 nm). This height transition could influence the measurements. The reason why a cluster size which lies in the transition region between two heights shows a better agreement with the MD simulated data than geometric magic clusters (Ag_{55} and Ag_{147}) is not quite clear yet.

But, to get more insight additional experiments and detailed simulations are needed.

8.2. Clusters on rare gas layers

This chapter presents experimental results of UPS measurements of copper and silver clusters deposited on rare gas layers (mostly xenon). As substrates HOPG, Cu(111), Ag(111) and Au(111) single crystals were used.

The chapter is split into two parts. In the first part the experimental results are presented and in the second part these results are discussed and compared with spectra of free beam clusters.

8.2.1. Experimental results

The first part of this chapter presents the results for copper clusters and the second part the results for silver clusters.

8.2.1.1. Cu_N (N= 55, 92, 147, 309)/ 60 ML Xe/ HOPG

The HOPG sample was prepared as explained in chapter 5.1.1 and then 60 ML of xenon were adsorbed on the clean surface at 30 K. Afterwards the sample was cooled down to 25 K and Cu_{309} clusters were deposited on the sample with a coverage of 100 pAmin. This high amount of cluster material is clearly visible with UPS. When the center of the deposition spot was found, UPS spectra of the now empty positions of the later three deposition spots were taken as background spectra. Afterwards the other three cluster sizes were deposited with a coverage of 20 pAmin, respectively, and measured with the argon discharge lamp. This order of the measurements is a standard procedure for UPS measurements on rare gas layers as already mentioned in chapter 6.2. For all the

following experiments this order (deposition of a high coverage→ determining the position and measuring the empty deposition spots as background signal→ deposition of the other three cluster spots→ measuring of the deposition spots) is kept up. The results of these measurements are presented in figure **58**.

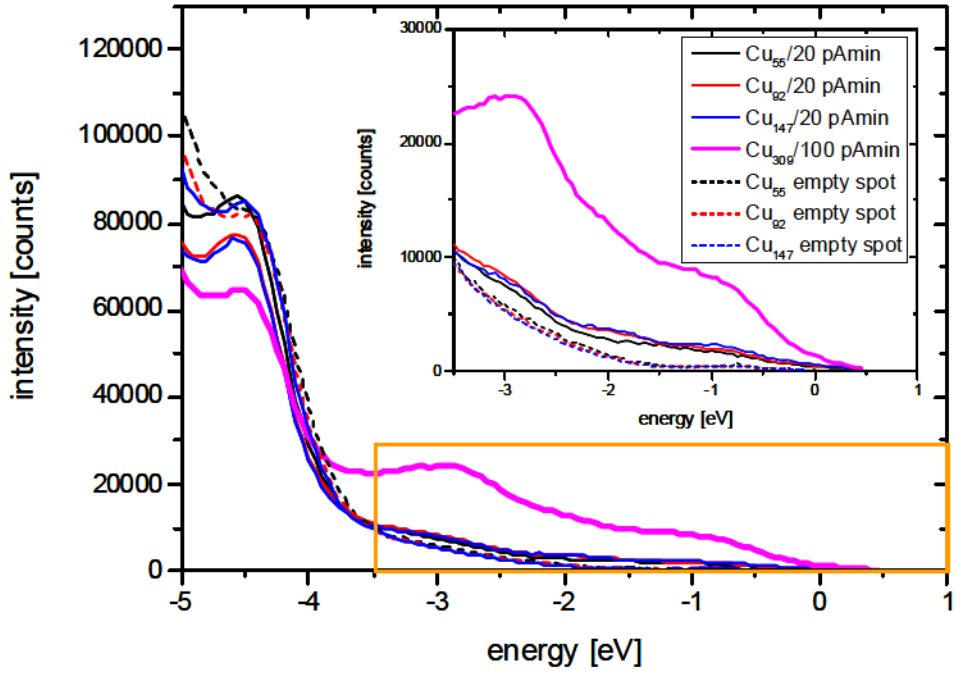

Figure 58: UPS spectra of Cu_{55}- Cu_{309} deposited with 20 pAmin and 100 pAmin on 60 ML xenon on HOPG and the corresponding background spectra. The inset magnifies the energy range from -3.5 eV to 1eV. 0 eV marks the position of the Fermi edge.

A clear difference between empty and covered spots is visible and in the energy region from -3.5 eV to 1 eV a size dependent structure in the s-p-band region is noticeable. At an energy of -4.5 eV a peak resulting from the xenon substrate is visible. The intensity of this peak changes and its position shifts with increasing metal coverage to higher energies. A similar behaviour was already observed in [107, 108] for copper and sodium clusters on Xe/HOPG. There the reason of this shift is explained with a charge transfer from the metal to the substrate which leads to a band filling and a shift of the Fermi energy towards higher energies. Due to the shift of the xenon peak the data from -5 eV to -3.5 eV are not evaluable after subtraction of the Xe/HOPG substrate signal. This energy region will not be discussed in the following.

Figure **59** shows the cluster spectra after the subtraction of the Xe/HOPG background signal. Additionally, the result of a second independent measurement of Cu_{147} clusters is shown. The same amount of clusters was deposited on a second sample on 60 ML xenon on HOPG under the same conditions to confirm the results obtained for Cu_{147} in the previous measurement. The two measurements show the same result. A clear size dependent structure is visible. The peak around -3 eV represents the cluster d-band. As already mentioned in chapter 8.1.1.2 the flank of the d-band (measured at half the height of the peak) shifts dependent on the size of the cluster. This behaviour can also be

observed for clusters on Xe/HOPG. The d-band flank shifts from -2.7 eV for Cu_{55} over -2.65 eV for Cu_{92} and -2.6 eV for Cu_{147} to -2.45 eV for Cu_{309}.

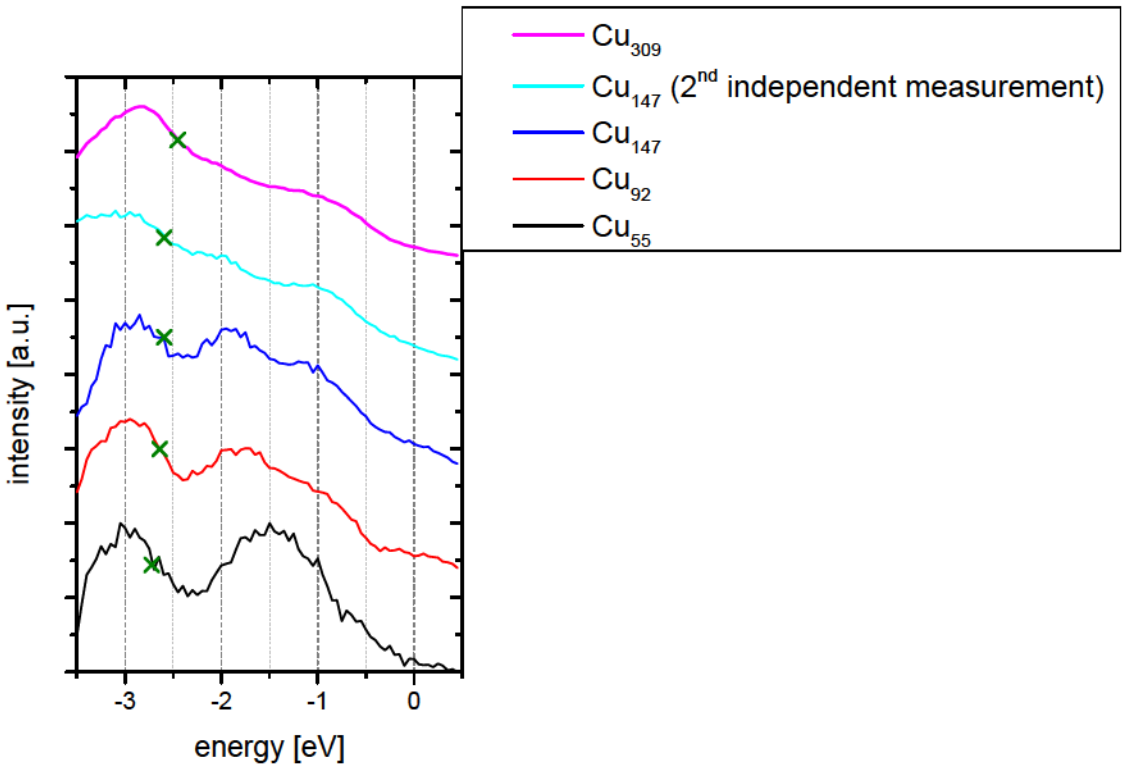

Figure 59: UPS spectra of Cu_{55} to Cu_{309} clusters after the subtraction of the Xe/HOPG substrate signal. Before subtraction the substrate signal was 10 point Savitzky-Golay (SG) smoothed via Origin [109]. For a better comparability the spectra are normalized on a scale from 0 to 1 and shifted relatively to each other. The green crosses mark the position of the d-band flank.

In the s-p-band region (below -2.5 eV) of the cluster signal a clear size dependence is visible. Cu_{55} clusters show one peak at -1.5 eV in the UPS spectra, whereas, Cu_{92} clusters have one peak at -1.75 eV and a shoulder at -0.9 eV. Cu_{147} clusters show two peaks in both measurements at -2 eV and -1 eV. But the peaks in the second measurement are not as prominent as in the first measurements. Overall the second measurement of Cu_{147} has a poorer statistic than the first measurement. The different peak positions and shapes of the spectra of the different cluster sizes are a hint that the deposited clusters show a differing electronic structure.

For Cu_{309} only two shoulders at -2 eV and -1 eV are visible but the d-band has a relatively strong signal. Due to the high coverage of the copper clusters (100 pAmin) it is probable that the clusters coalesced on the surface (see results of chapter 8.1.1.1).

8.2.1.2. Cu_N (N= 112, 147, 309, 923)/ 60 ML Xe/ Cu(111)

This chapter presents two experiments. In the first experiment Cu_{147}, Cu_{309} and Cu_{923} clusters were deposited at 60 ML xenon on a Cu(111) substrate at 20 K substrate

temperature and in the second experiment Cu_{112} and Cu_{147} clusters were deposited also at 20 K.

The Cu(111) sample was prepared as explained in chapter 5.1.2 and then 60 ML of xenon were adsorbed on the clean surface at 30 K in the first experiment and at 45 K in the second experiment. Afterwards the sample was cooled down to 20 K for cluster deposition.

The reason for the use of two different adsorption temperatures is the following: The temperature of the sample is measured at the helium cooled LT- sample holder and not directly on the sample. Therefore, it is possible that the sample has a slightly higher temperature than measured at the LT- sample holder if it is not attached properly. The Cu(111) sample is better attached to the sample plate than HOPG. Cu(111) is fixed with screws to the sample plate whereas HOPG is only fixed with welded tantalum stripes. Hence, HOPG has a worse thermal contact to the LT- sample holder and the real sample temperature is higher than measured. If xenon is adsorbed at a too low temperature the resulting layer can not heal during adsorption and a rough surface is the result [110]. Therefore the temperature of the xenon adsorption was increased in the second measurement to ensure a smoother xenon surface.

As in the measurement described in the previous chapter in a first step the biggest clusters (here Cu_{923}) were deposited with a coverage of 100 pAmin .Then measurements of the empty later cluster spots were taken as background signal. Afterwards the other three cluster sizes were deposited and measured with the argon gas discharge lamp. The measured data are presented in figure **60**.

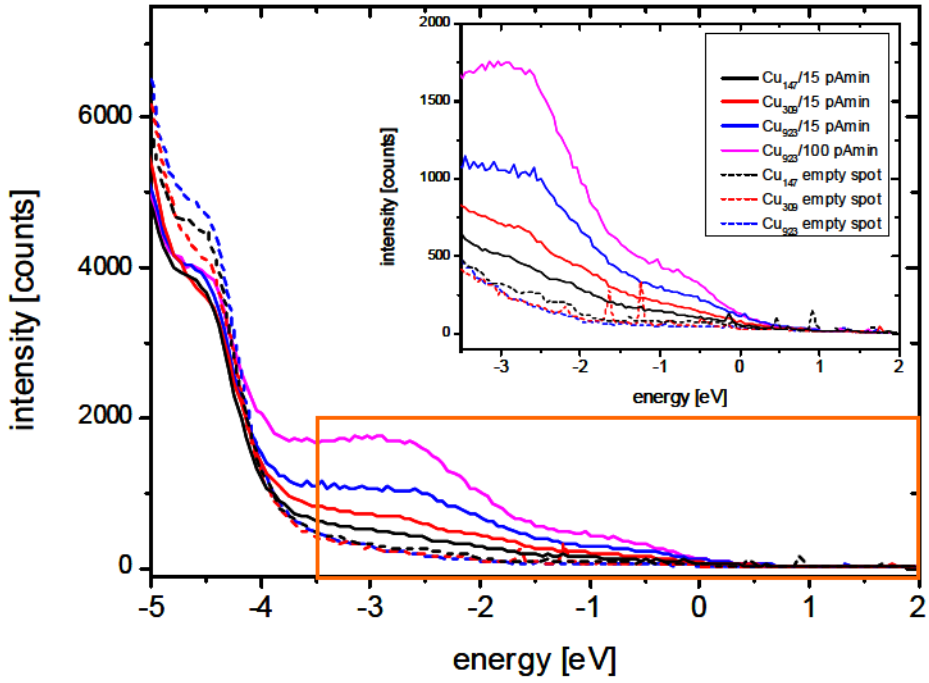

Figure 60: UPS spectra of Cu_{147}- Cu_{923} deposited with 15 pAmin and 100 pAmin on 60 ML xenon on Cu(111) and the corresponding background spectra. The inset magnifies the energy range from -3.5 eV to 2eV. 0 eV marks the position of the Fermi edge.

A change in the intensity of the xenon peak at -4.5 eV is visible as in the previous chapter. Due to this change the data below -3.5 eV are not useful and are not discussed in the following.

In the energy region from -3.5 eV to higher energies a clear size dependent cluster signal is visible. The large size range covered by this experiment is reflected in the intensities of the spectra in this region. As already discussed in chapter 6.2 the intensity of the UPS signal is dependent on the cluster size and coverage (equation (6.4) and (6.5)). In figure **61** the intensity of the cluster UPS signal at -2.74 eV and the calculated intensity with the help of equation (6.4) are plotted versus the cluster volume. The cluster volume is calculated by assuming a cylindrical cluster with $d = h$.

It is visible that the behaviour of the measured cluster intensity reflects the behaviour of equation (6.4). Cu_{147} lies in the size region where the intensity of the UPS signal can be described by a direct proportionality to the cluster volume just like Cu_{309}. Cu_{923} lies in the transition region between the two edge cases ($\propto V$ (red line) and $\propto V^{2/3}$ (green line in figure **61**)).

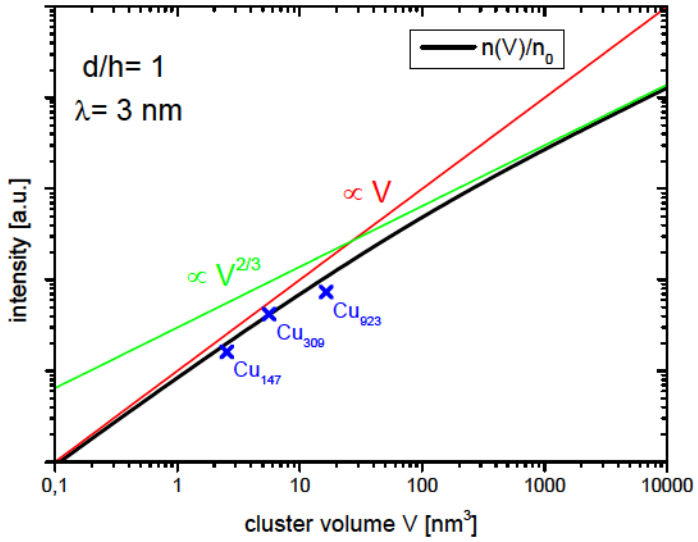

Figure 61: Calculated photoelectron intensity versus cluster volume for a cylindrical cluster with *d/h=1* (black line). The electron escape depth was calculated with the help of equation (6.6) (chapter 6.2) for copper clusters measured with ArI light (11.62 eV). The blue crosses mark the relative intensity of the UPS signal for copper clusters on Xe/Cu(111). The cluster volume was calculated by assuming a cylindrical cluster with $d = h$. The cluster height was calculated with $h = 0.282 \cdot N^{1/3}$ (N= # atoms per cluster).

Unfortunately, the empty Xe/Cu(111) spectra in figure **60** show some measuring errors resulting in sharp peaks in the energy region between -2 eV and +1 eV. These errors have their origin in the channeltrons of the electron energy analyzer. The channeltrons are very sensitive to electro-magnetic noise which can originate from e.g., flashing neon lamps in the laboratory. In the following these measuring errors are replaced by the mean value of the measuring points before and after the error. The cluster spectra subtracted from the revised Xe/Cu(111) are presented in figure **62**.

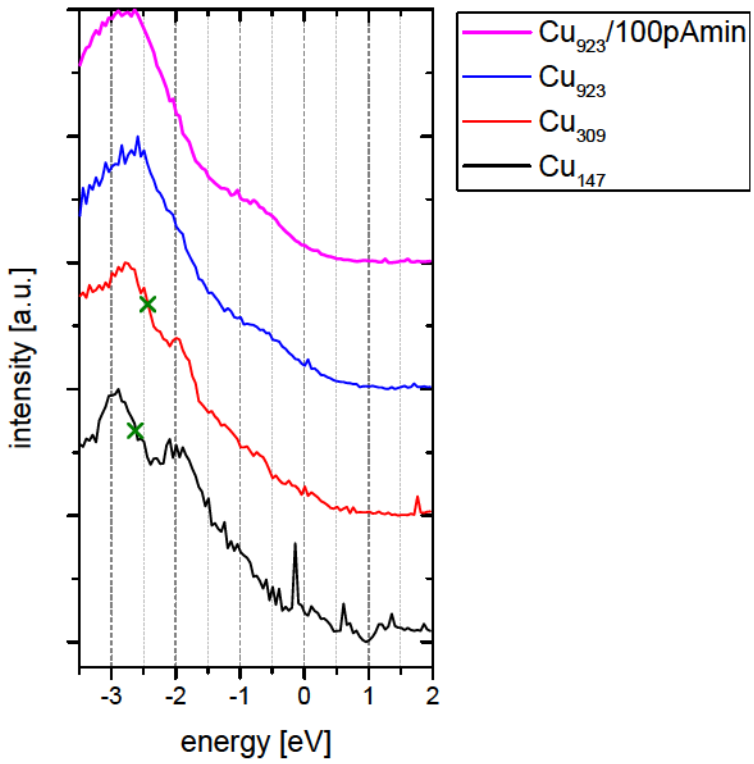

Figure 62: UPS spectra of Cu_{147} to Cu_{923} clusters after the subtraction of the Xe/Cu(111) substrate signal. Before subtraction the substrate signal was 10 point SG smoothed via Origin [109]. For a better comparability the spectra are normalized on a scale from 0 to 1 and shifted relatively to each other. The green crosses mark the position of the d-band flank.

After subtraction of the background signal size dependent cluster spectra are obtained. In all spectra the cluster d-band is visible in the energy region from -3.5 eV to approx. -2 eV. Additionally a shift of the d-band flank is detectable: The d-band flank shifts from -2.64 eV for Cu_{147} to -2.44 eV for Cu_{309}. The results of the position of the d-band flank are akin to the results for copper clusters on Xe/HOPG of the previous chapter. For Cu_{923} it is difficult to say where the cluster d-band begins therefore no position can be determined for the d-band flank.

The s-p-band region shows a size dependent structure. Cu_{147} has a peak at -2 eV and a flat shoulder at -1 eV on closer inspection. Cu_{309} has a relatively sharp peak at -2 eV and shows an even decrease in the energy region between -1.5 eV and the Fermi edge. Cu_{923} shows a similar structure at both coverages: A pronounced d-band and a shoulder at -0.8 eV. For Cu_{923} a similarity with the UPS spectrum of polycrystalline copper (figure **48**) can not be dismissed.

It is important to say that the measurements presented here have a quite poor statistic due to the low UPS signal (a factor 10 lower than for the measurements on Xe/HOPG). A reason for this is that the entering slit to the channeltrons in the electron energy analyser was smaller in this measurement (1 mm in diameter instead of 6 mm) [42]. The smaller entering slit increases the energy resolution of the UPS measurements but at the cost of intensity of the UPS signal. Unfortunately, this change leads to a worsening of the results presented here instead of an improvement.

In the second measurement Cu_{112} clusters and Cu_{147} clusters were deposited on 60 ML Xe on Cu(111) at 20 K substrate temperature. Additionally, Cu_{309} was deposited with a very high coverage as a reference point to find the later position of the deposition spots and to take the reference spectra. Unfortunately, the cluster current during the deposition of Cu_{309} was not stable and the deposition has to be repeated whereby the actual coverage could not be determined. Therefore, this deposition was only used to find the later deposition spots and of the Cu_{309} deposition spot no measurement was made. The results are shown in figure **63**.

The UPS spectrum of Cu_{112} shows a very low intensity, nearly in the range of the Xe/Cu(111) background spectra. Additionally, the spectra for Cu_{147} show the same intensity even though measurement (b) has twice the coverage of measurement (a). It is possible that in this case the center of the deposition spot of Cu_{147} (b) and probably Cu_{112} was not hit properly and the UPS measuring spot was only at the rim of the deposition spot where the cluster coverage is smaller.

In addition, the same measuring errors as in the previous experiment on Cu(111) occurred resulting in error peaks in the spectra. For subtraction of the Xe/Cu(111) underground spectra these errors are again replaced by the mean value of the data point before and after the error. Figure **64** shows the subtracted cluster spectra.

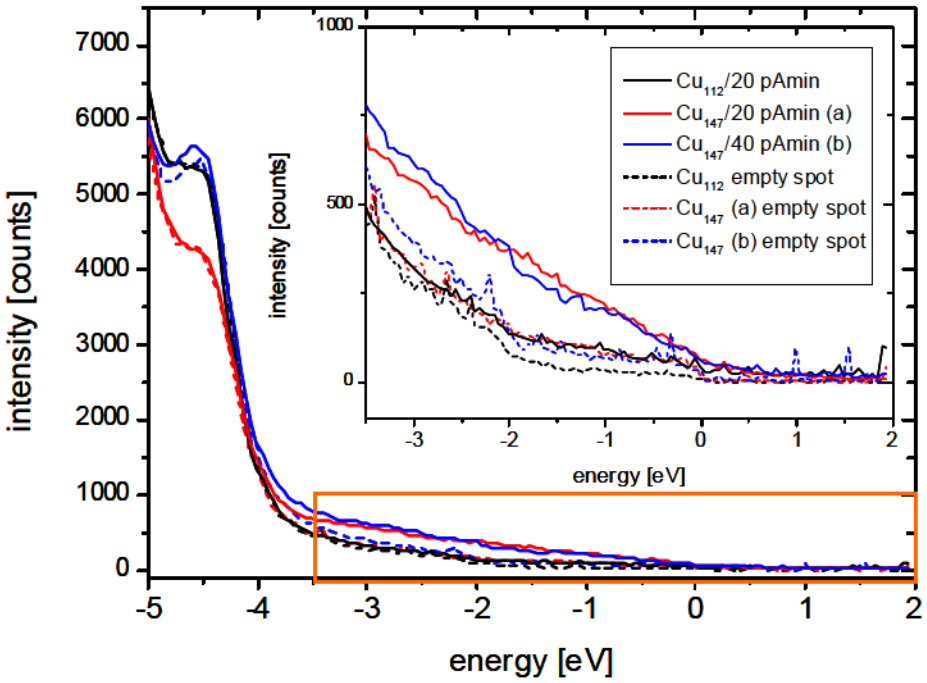

Figure 63: UPS spectra of Cu_{112} and Cu_{147} deposited with 20 pAmin and 40 pAmin on 60 ML xenon on Cu(111) and the corresponding background spectra. The inset magnifies the energy range from -3.5 eV to 2eV. 0 eV marks the position of the Fermi edge.

For Cu_{147} on Xe/Cu(111) a similar result as for Cu_{147} on Xe/HOPG and as for the previous measurement on Xe/Cu(111) (figure **62**) is obtained after subtraction of the Xe/Cu(111) background signal. In the s-p-band region there are two peaks at -2 eV and -1 eV, respectively, and the position of the d-band flank is -2.6 eV for a coverage of

40 pAmin and -2.64 eV for a coverage of 20 pAmin. The spectrum of Cu_{112} has a very bad signal to noise ratio and no significant d-band signal is visible. Apparently the deposition spot was missed during UPS measurements and only a small part of the rim was measured. Therefore this measurement has no significance and will not be discussed any further.

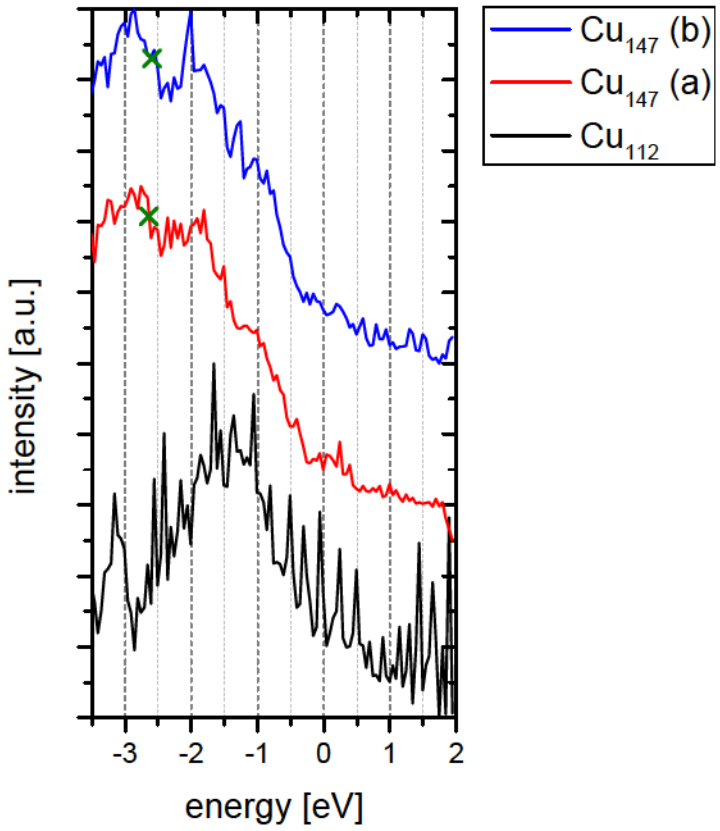

Figure 64: UPS spectra of Cu_{112} and Cu_{147} clusters after the subtraction of the Xe/Cu(111) substrate signal. Before subtraction the substrate signal was 10 point SG smoothed via Origin [109]. For a better comparability the spectra are normalized on a scale from 0 to 1 and shifted relatively to each other. The green crosses mark the position of the d-band flank.

8.2.1.3. Cu_N (N= 92, 112, 147, 309, 923)/ 60 ML Xe/ Au(111)

This chapter presents three experiments of clusters deposited on 60 ML xenon on a Au(111) substrate.

The Au(111) sample was prepared as explained in chapter 5.1.2 and then 60 ML of xenon were adsorbed on the clean surface at 45 K in the first and second experiment and at 54 K in the third experiment. Afterwards the sample was cooled down to 20 K and 23 K, respectively, for cluster deposition.

In the first experiment Cu_{92}, Cu_{112}, Cu_{147} and Cu_{923} were deposited at 20 K substrate temperature on Xe/Au(111). Cu_{923} was deposited first with the highest coverage (100 pAmin) to define the later deposition spots and take Xe/Au(111) background

spectra. Later the other three cluster sizes were deposited with a coverage of 20 pAmin, respectively. The measured data are presented in figure **65**.

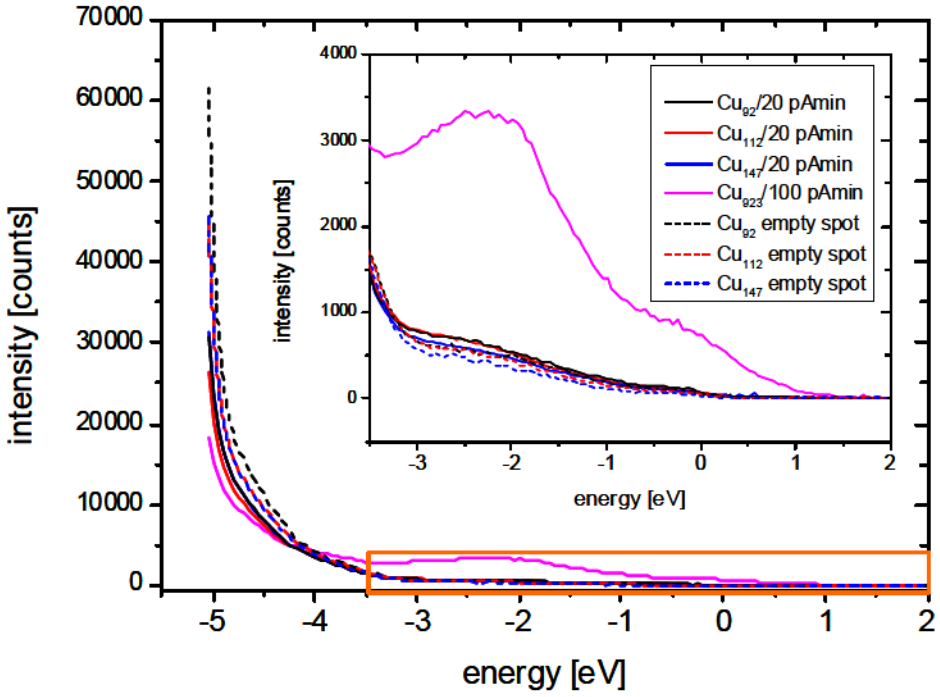

Figure 65: UPS spectra of Cu_{92} to Cu_{923} deposited with 20 pAmin and 100 pAmin on 60 ML xenon on Au(111) and the corresponding background spectra. The inset magnifies the energy range from -3.5 eV to 2eV. 0 eV marks the position of the Fermi edge.

The spectra look different than UPS spectra of copper clusters on Xe/HOPG or Xe/Cu(111). The typical shoulder of the xenon signal at -4.5 eV is not visible. This comes from a shift of the spectra to higher energies due to the Au(111) substrate as described in [41]. The xenon $5p_{1/2}$ peak, from which only the beginning is visible in the spectra presented here, shifts with about the difference of the surface work function. From this shifted peak results the massive increase in intensity at -5 eV (see figure **66**). Therefore, the typical xenon shoulder disappears due to the shift and the high intensity of the beginning xenon peak.

In the inset of figure **65** the signal resulting from Cu_{923} is clearly visible but the other three cluster sizes deposited with 20 pAmin coverage show only a poor intensity, maybe the center of the deposition spot was missed.

Clusters on rare gas layers are decoupled and referenced to the vacuum energy of the substrate [90]. Because of this the work function difference of the different cluster and substrate materials leads to a shift of the cluster spectra. Due to the shift of the spectra on Au(111) the spectrum of Cu_{923}/100 pAmin has still intensity above the Fermi edge. Similar results were observed in [90] for lead islands deposited on Xe/Au(111).

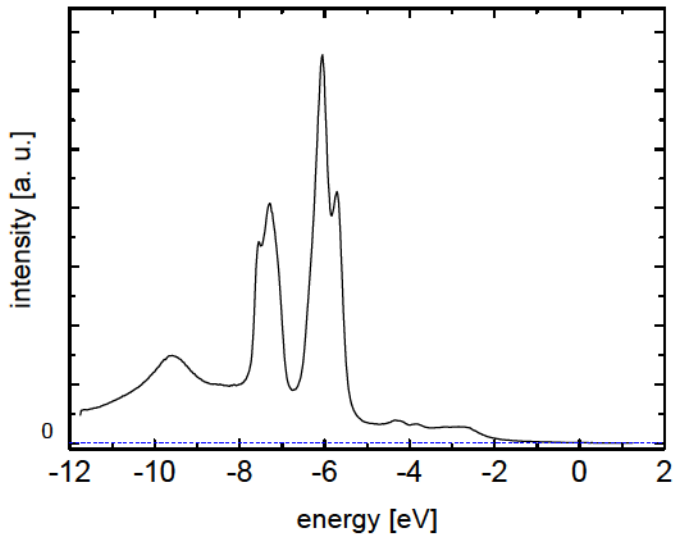

Figure 66: UPS spectrum of 1 ML xenon on HOPG measured with the helium gas discharge lamp. The peak at here -6 eV can also be found in the spectra measured with ArI radiation. The increase in intensity at -5 eV in the spectra presented here comes from this peak. [111]

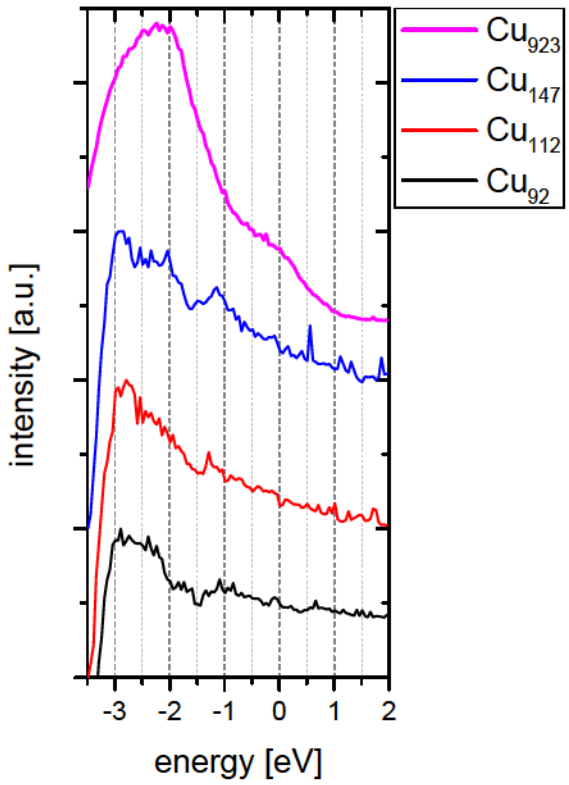

Figure 67: UPS spectra of Cu_{92} to Cu_{923} clusters after the subtraction of the Xe/Au(111) substrate signal. Before subtraction the substrate signal was 10 point SG smoothed via Origin [109]. For a better comparability the spectra are normalized on a scale from 0 to 1 and shifted relatively to each other.

The cluster spectra subtracted from the Xe/Au(111) background signal are presented in figure **67**. The spectrum of Cu_{923} has a signal up to 1 eV above the Fermi edge (E_F= 0 eV) and apart from the shift the spectrum looks like for Cu_{923} deposited on Xe/Cu(111) and similar to bulk Cu(111). The other spectra of this measurement show nearly no structure which confirms the assumption that the deposition spots were missed during measurement. Cu_{147} may have two peaks at -2 eV and -1 eV, but they are very small and can not really be considered as real. Due to the poor signal the position of the d-band flank can not be determined for Cu_{92}, Cu_{112} and Cu_{147}. Cu_{923} shows a clear cluster d-band but it is difficult to say where the d-band begins and therefore the position of its flank can not be determined.

In the second experiment Cu_{147} and Cu_{309} were deposited at 20 K substrate temperature. In a first step Cu_{309} was deposited with a coverage of 100 pAmin as reference point to find the later deposition spots and take spectra of the Xe/Au(111) background. Then Cu_{147} was deposited with a coverage of 40 pAmin and Cu_{309} was deposited with 30 pAmin on the same spots where the background spectra were taken. The results of this measurement are presented in figure **68**.

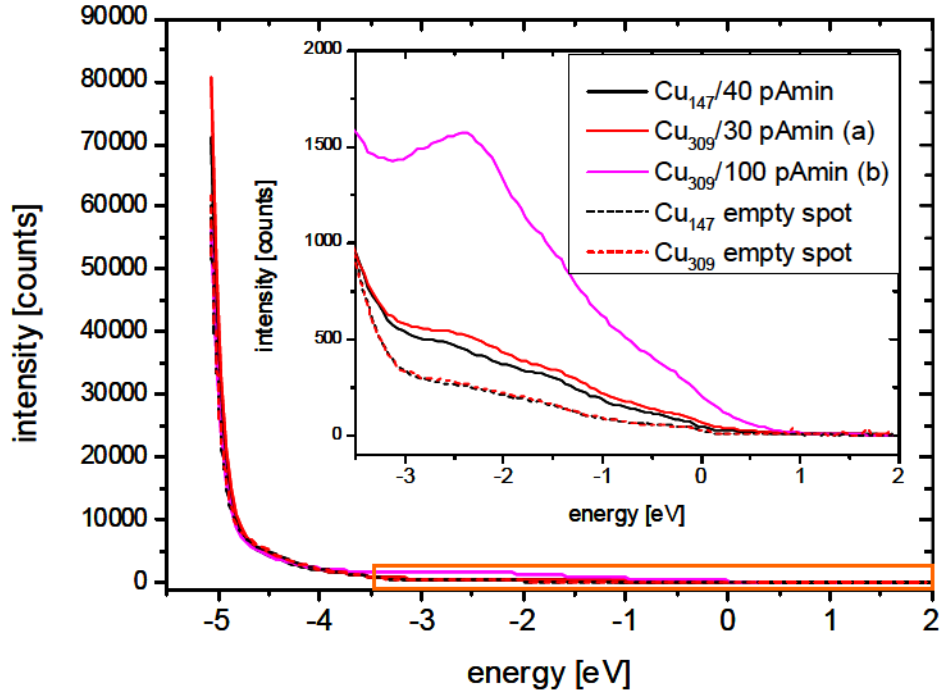

Figure 68: UPS spectra of Cu_{147} and Cu_{309} deposited with 40 pAmin, 30 pAmin and 100 pAmin on 60 ML xenon on Au(111) and the corresponding background spectra. The inset magnifies the energy range from -3.5 eV to 2eV. 0 eV marks the position of the Fermi edge.

A clear cluster signal is visible in the spectra. Again the cluster spectrum for the deposition spot with the highest coverage shows a UPS signal above the Fermi edge, but in contrast to the previous results there is no real Fermi edge visible in the cluster spectrum. The results after subtraction of the Xe/Au(111) signal are presented in figure **69**.

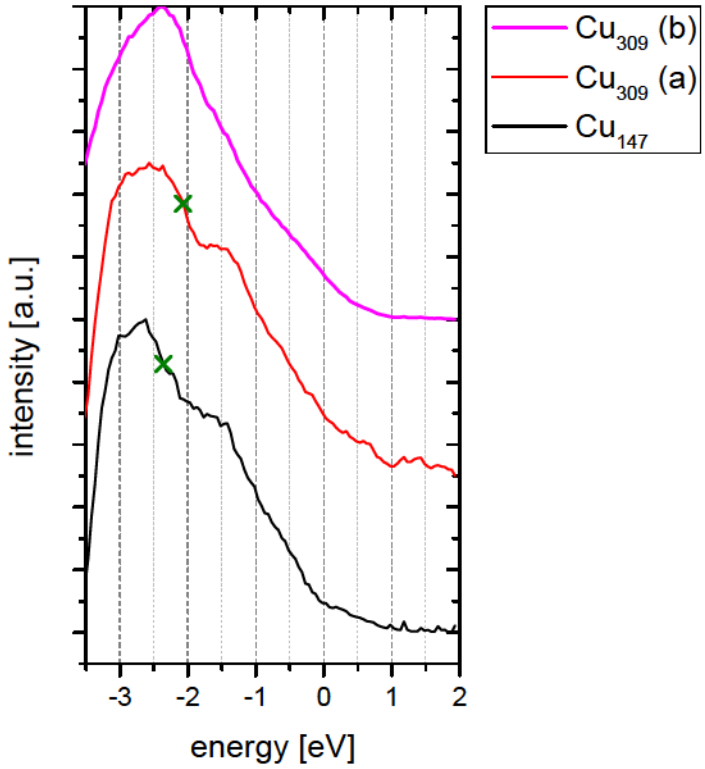

Figure 69: UPS spectra of Cu_{147} and Cu_{309} clusters after the subtraction of the Xe/Au(111) substrate signal. Before subtraction the substrate signal was 10 point SG smoothed via Origin [109]. For a better comparability the spectra are normalized on a scale from 0 to 1 and shifted relatively to each other. The green crosses mark the position of the d-band flank.

The spectra of Cu_{147} and Cu_{309} (a) are very similar to each other. Both have a shoulder at -1.5 eV and a clear cluster d-band. The d-band flank for Cu_{147} is at -2.37 eV and for Cu_{309} (a) at -2.07 eV. Additionally, both spectra show a small signal above the Fermi edge. The spectrum of Cu_{309} (b) has also a clear signal above the Fermi edge but no structure like for Cu_{309} deposited with a lower coverage in the s-p-band region. Here it is difficult to say where the cluster d-band begins therefore no position can be determined for the d-band flank.

In the third experiment the temperature for the xenon adsorption was higher than in the former two experiments (54 K instead of 45 K). Then the sample was cooled down to 23 K and Cu_{112}, Cu_{147} and Cu_{309} clusters were deposited. In a first step Cu_{309} clusters were deposited with a coverage of 100 pAmin, however, the mass selection for this deposition was not as accurate as for the other depositions. Here the waiting time t_W between the pulses of the acceleration plate and the deceleration plate (see chapter 4.1.3) was very small to get a higher cluster current and a shorter deposition time. Due to the short t_W the mass selection gets worse and other cluster masses except Cu_{309} were deposited. After the deposition spot with the highest coverage was found UPS spectra of the later deposition spots were taken as reference spectra and then the other cluster sizes were deposited. The results of these measurements are presented in figure 70.

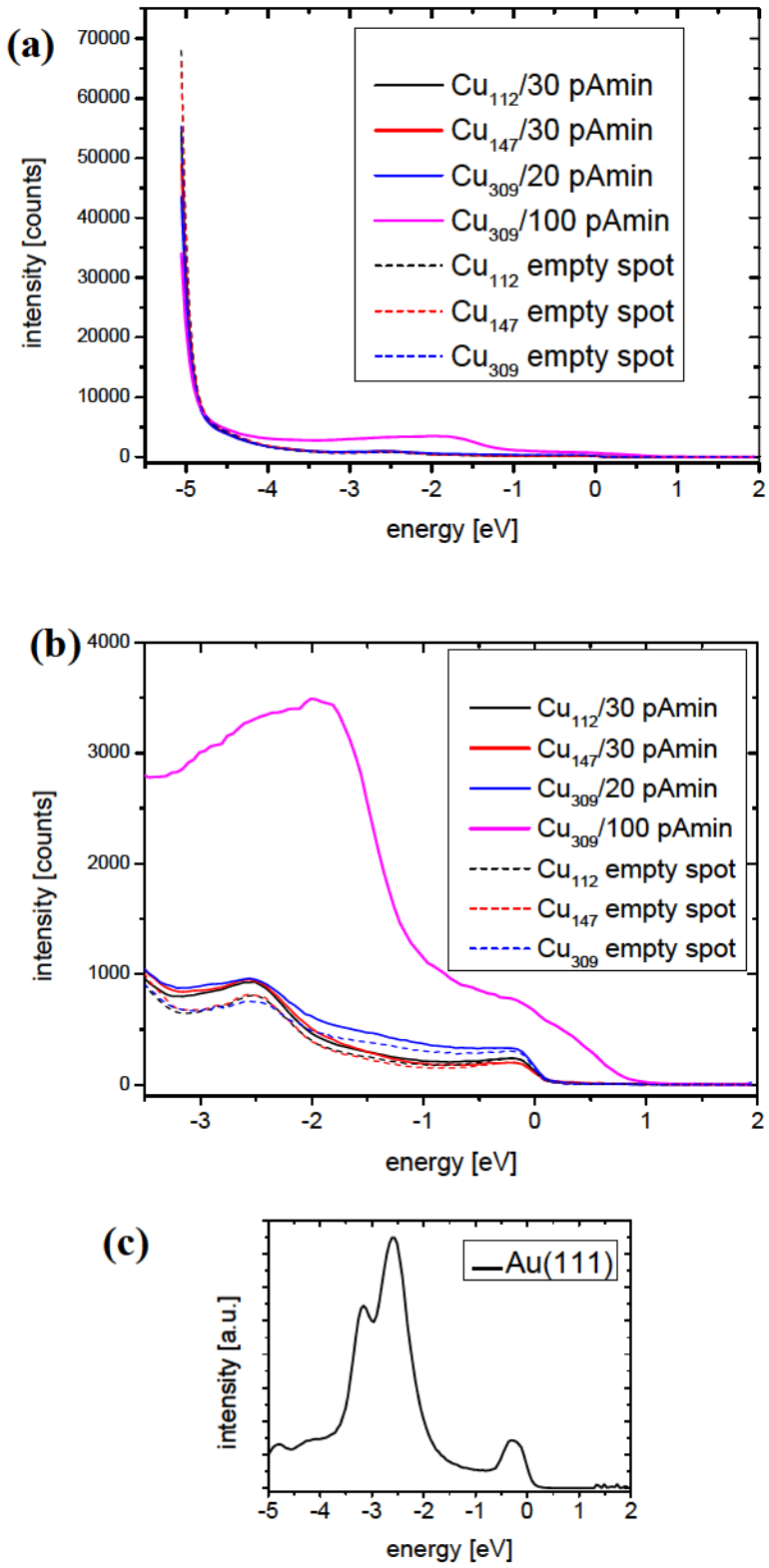

Figure 70: (a) UPS spectra of Cu_{112}, Cu_{147} and Cu_{309} deposited with 30 pAmin, 20 pAmin and 100 pAmin on 60 ML xenon on Au(111) and the corresponding background spectra. 0 eV marks the position of the Fermi edge. (b) Energy region between -3.5 eV and 2 eV, a Fermi edge at 0 eV and a peak at -2.5 eV, both resulting from the Au(111) substrate, are clearly visible. (c) Au(111) spectrum taken at room temperature.

In figure **70b** a clear Fermi edge is visible at 0 eV and at -2.5 eV a peak occurs in all spectra regardless if it is a cluster spectrum or a Xe/Au(111) spectrum. These features come from the Au(111) substrate below the xenon layer (see figure **70c**), i.e., the xenon layer is not thick enough to cover the Au(111) signal. Obviously the temperature for the adsorption of the xenon layer was too high to guarantee the growth of 60 ML of xenon on the Au(111) surface.

Due to the too thin xenon layer it is probable that the clusters were influenced by the gold substrate which would distort the results of the UPS measurements. Therefore, this measurement will not be investigated any further.

8.2.1.4. Cu_N (N= 55, 92, 147, 309)/10 ML Ar/60 ML Xe/ Ag(111)

This chapter presents two experiments of copper clusters deposited on 10 ML argon on 60 ML xenon on an Ag(111) surface. First the Ag(111) sample was prepared as described in chapter 5.1.2, then the sample was cooled down to 30 K for the adsorption of the xenon layers. Afterwards, the sample was cooled down to 15 K in the first experiment and 20 K in the second experiment for the adsorption of 10 ML argon on top of the 60 ML of xenon. It was decided to not go beyond 10 ML because static charging occurred for an argon film with more than 10 ML argon during measurements with a helium gas discharge lamp [90]. For the first experiment the temperature was kept 15 K, but for the second measurement the sample was cooled down to 11 K for cluster deposition and UPS measurements.

Cu_{309} clusters were deposited on the sample with a coverage of 100 pAmin, in both cases. From the position of this deposition spot the later deposition spots of the other clusters sizes were defined and spectra of the empty deposition spots were taken as background spectra. Then Cu_{55}, Cu_{92} and Cu_{147} were deposited on the same spots as those where the background spectra were made with a coverage of 10 pAmin, respectively. The results of both measurements are presented in figure **71**.

In the energy region of -5 eV to -4 eV a change in the spectra is visible. The shoulder at -4.5 eV, which could be observed for spectra where only xenon was absorbed, disappears during the experiment. This is also observable at an empty spot on the sample where no clusters were deposited (figure **72**).

The presence of the clusters can change the work function of the surface [90] and thus the UPS spectrum. However this cannot be the case for the empty spot in figure **72**. Another possible reason can be contamination of the sample over the time of the measurement due to the low sample temperature (15 K and 11 K, respectively). A combination of these two reasons is also imaginable.

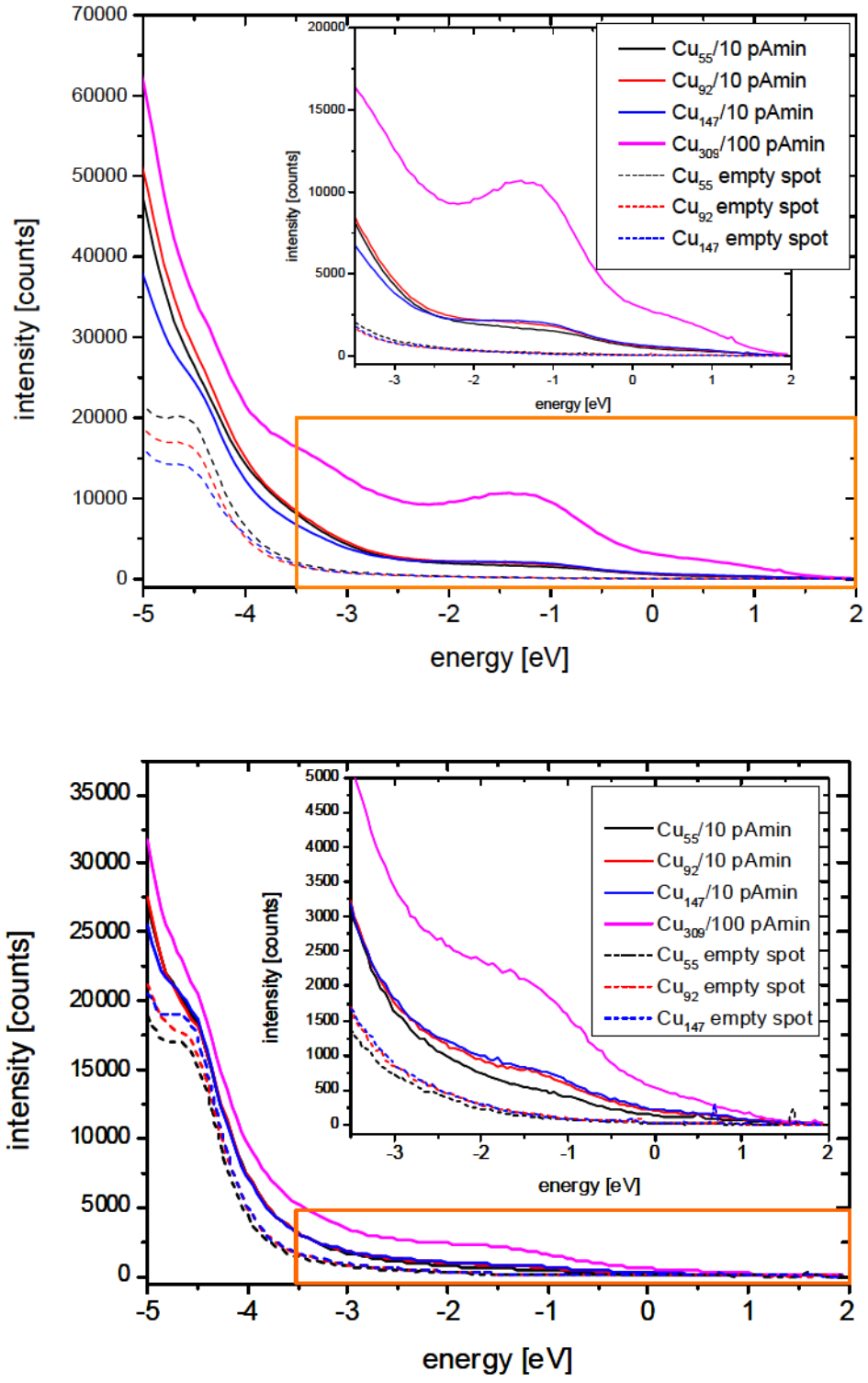

Figure 71: UPS spectra of Cu_{55}, Cu_{92}, Cu_{147} and Cu_{309} deposited with 10 pAmin and 100 pAmin on 10 ML argon on 60 ML xenon on Ag(111) and the corresponding background spectra. The inset magnifies the energy range from -3.5 eV to 2 eV. 0 eV marks the position of the Fermi edge. Top: First experiment at 15 K. Bottom: Second experiment at 11 K.

The LT-sample holder is cooled down for the adsorption of the rare gas and then even more for cluster deposition (in the case of the second experiment). As a result the other components of the sample manipulator are cooled down, too. On these components also rare gas, i.e. argon, is adsorbed. While moving the manipulator for measurements some

components become warmer and the argon layer can desorb. But, the sample is still at 15 K or 11 K and the desorbed argon can re-adsorb on the sample, especially on the clusters. This contamination leads to a change of the cluster signal.

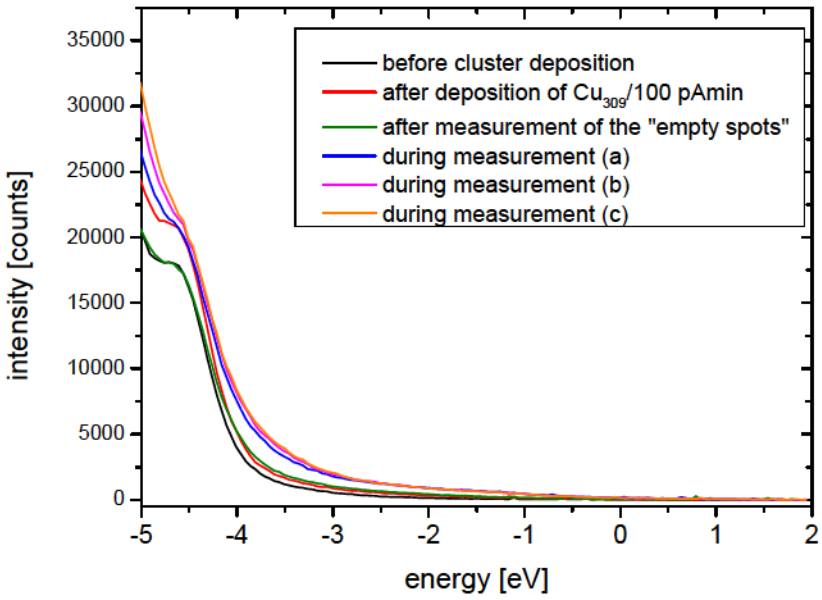

Figure 72: UPS measurements of an empty spot on the sample measured at different times of the second experiment. Even without the presence of clusters a clear change in the spectra is visible over time.

All spectra in figure **71** have a signal above the Fermi edge. In the case of Cu_{309} deposited with 100 pAmin this is explicitly visible. Comparing the spectrum of Cu_{309} in the upper UPS spectrum in figure **71** with the spectrum of Cu_{923} also deposited with a coverage of 100 pAmin on Xe/Cu(111) in figure **60** a clear similarity is observable. On Ar/Xe/Ag(111) the spectrum of the highest coverage and the other spectra are shifted about 1.4 eV to higher energies. So the main peak visible at 1.3 eV in the spectra represents the cluster d-band and the s-p-band region lies above the Fermi edge.

A possible reason for this shift could be the influence of the electron affinity of the rare gas layer. As already mentioned before clusters on rare gas layers are decoupled and referenced to the vacuum energy of the substrate [90], i.e. the highest occupied electronic states of the cluster do not align to the Fermi edge of the substrate. In [112, 113] it is described that within the phase accumulation model for a Shockley surface state the vacuum energy of a substrate shifts (if a rare gas is adsorbed) by the electron affinity *EA* of the rare gas (EA_{xenon}= 0.5 eV; EA_{argon}= -0.4 eV). So clusters deposited on several monolayers of xenon would be constantly shifted about -0.5 eV. In the case of several monolayers of argon on xenon an opposite shift of about 0.4 eV occurs, if the argon defines the electron affinity. In addition the adsorption of rare gas lowers the work function of the substrate (e.g., from 5.36 eV for Au(111) to 5.04 eV for Xe/Au(111) [113]). It is possible that an additional argon layer would lead to an additional decrease of the substrate work function, as in the case of a simple xenon layer. Additionally the different work function of the substrate and the clusters lead to a shift of the UPS spectra [90], as described above. In this context it has to be mentioned

that it is difficult to determine the exact shift resulting from the work function difference because it is difficult to say if the clusters have a rather polycrystalline structure or rather a fcc structure. But, depending on this the cluster work function may change (Φ_{Cu}(poly)= 4.65 eV; Φ_{Cu}(111)= 4.94 eV [114]). So the influence of the electron affinity of the rare gas layer, together with a work function decrease of the substrate and the shift due to the different work functions of the substrate and the clusters could be responsible for the shift of the UPS spectra on Ar/Xe/Ag(111) to higher energies.

The results after subtraction of the Ar/Xe/Ag(111) background are presented in figure **73** and **74**. Only one peak is visible in all spectra at -1.3 eV, representing the cluster d-band, although the intensity of the spectra in the second experiment has only half the value of the first experiment, also resulting in a poorer statistic regarding the cluster spectra. Especially for Cu_{55} the statistic in the second experiment is very poor. It is probable that in this case the cluster spot was not measured in the center but at its rim and the smaller amount of clusters leads to a poor cluster signal.

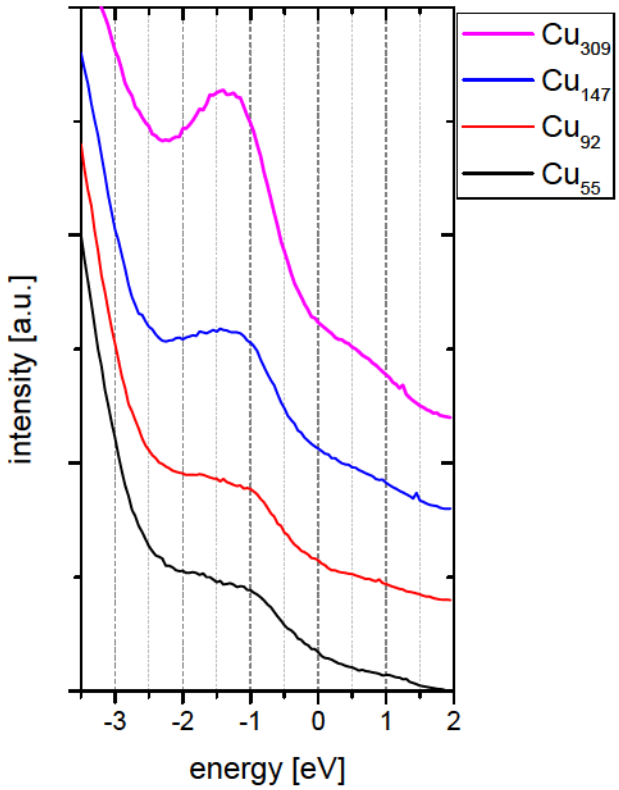

Figure 73: UPS spectra of Cu_{55} to Cu_{309} clusters after the subtraction of the Ar/Xe/Ag(111) substrate signal of the first measurement at 15 K sample temperature. Before subtraction the substrate signal was 10 point SG smoothed via Origin [109]. For a better comparability the spectra are normalized on a scale from 0 to 1 and shifted relatively to each other.

Nevertheless for each of the two experiments a size dependence of the spectra is visible, with increasing cluster size the intensity of the cluster d-band increases. The bigger the clusters are the more copper is on the sample and the bigger is the measured intensity in the UPS spectra. This explains the increase of the peak intensity at -1.3 eV for Cu_{55}/10 pAmin, Cu_{92}/10 pAmin and Cu_{147}/10 pAmin, respectively. Using the same argument for Cu_{309}/100 pAmin the coverage increased by more than a factor of 10

which does not correspond to the increase in peak intensity. Cluster coalescence and the effect of the electron mean free path (see chapter 6.2) for larger copper islands may be the reason for a lower intensity here.

The increase in intensity at -3 eV to lower energies in all spectra comes from the subtraction of the Ar/Xe/Ag(111) background due to the change of the signal after the deposition of the clusters (see figure **71**). The cluster spectra before subtraction have more intensity over the whole energy range than the empty Ar/Xe/Ag(111) spectra.

It is eye catching that the spectra of the Cu_{55}, Cu_{92} and Cu_{147} clusters deposited with 10 pAmin look very similar to the spectra of Cu_{309} deposited with 100 pAmin coverage on Ar/Xe/Ag(111) (for this coverage the clusters are already coalesced). It seems that the clusters coalesced on the argon substrate even at a low coverage of 10 pAmin. It is possible that at the temperatures used here the argon layer is still not completely frozen and the atoms in the layer are still very mobile. Due to the movement of the argon atoms in the rare gas layer the clusters are more mobile, too, and coalesce at much lower coverages than depicted in chapter 8.1.1.1.

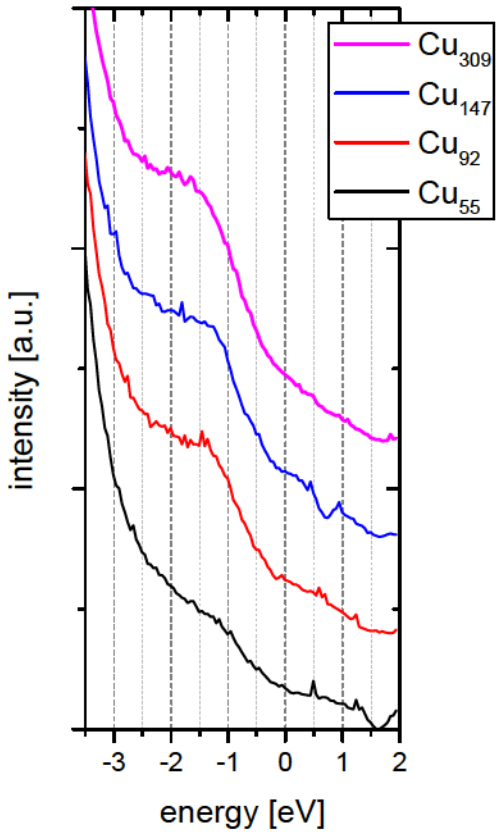

Figure 74: UPS spectra of Cu_{55} to Cu_{309} clusters after the subtraction of the Ar/Xe/Ag(111) substrate signal of the second measurement at 11 K sample temperature. Before subtraction the substrate signal was 10 point SG smoothed via Origin [109]. For a better comparability the spectra are normalized on a scale from 0 to 1 and shifted relatively to each other.

8.2.1.5. Ag_N /60 ML Xe/ HOPG

A HOPG sample was prepared as described in chapter 5.1.1. Then the sample was cooled down and 60 ML of xenon were adsorbed at 25 K substrate temperature. Afterwards silver clusters were deposited at this temperature.

Although the preparation steps and the cluster deposition were performed as in the former experiments it was not possible to detect a cluster signal with UPS measurements. Even big Ag_{309} clusters deposited with 100 pAmin on the sample could not be detected.

This behaviour suggests that the silver clusters sunk into the xenon layer. In fact such behaviour was already observed by OHNO et al. [115] for silver clusters deposited on several monolayers of xenon on gallium arsenide (GaAs) (figure **75**). First the clusters are covered with a xenon skin and then they are drawn through the xenon layer via van der Waals forces until they have contact with the substrate. This effect requires that the xenon layer is pliable enough to let the clusters travel through it. To avoid this, the xenon layer has to be cooled down sufficiently because xenon seems to be more plastic at higher temperatures.

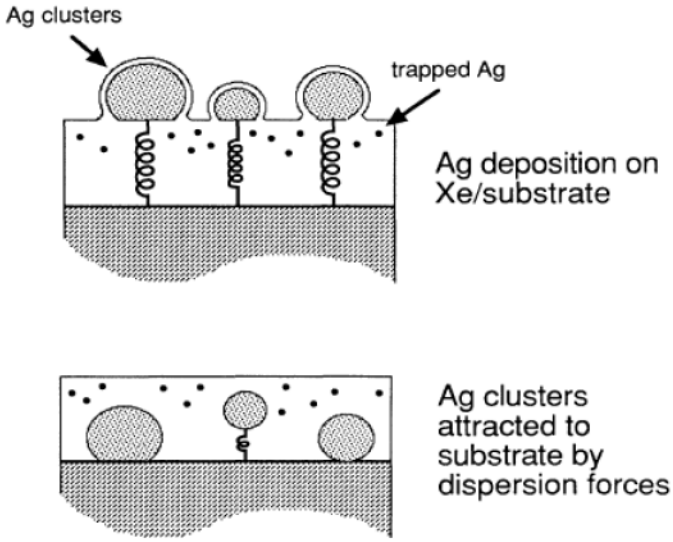

Figure 75: Schematic of Ag clusters deposited on a xenon layer on GaAs. A xenon skin covers the clusters, with time the clusters are drawn through the xenon layer until they contact the substrate. The springs represent the van der Waals force of attraction. [115]

In the following experiment this was achieved by changing the substrate from HOPG to Ag(111). As already explained in chapter 8.2.1.2 the Ag(111) sample is attached better to the sample holder than HOPG and the effective temperature of the sample is lower. Thus, the xenon layer becomes harder and it is more difficult for the clusters to travel through the xenon.

8.2.1.6. Ag_N (N=55, 92, 147, 309) /60 ML Xe/ Ag(111)

This chapter presents two experiments. In the first experiment Ag_{55}, Ag_{147} and Ag_{309} clusters were deposited on 60 ML xenon on Ag(111) at 17 K sample temperature and measured at this temperature. In the second experiment Ag_{55}, Ag_{92}, Ag_{147} and Ag_{309} clusters were deposited and measured on 60 ML xenon on Ag(111) at 15 K sample temperature.

For the first experiment Ag(111) was prepared as described in chapter 5.1.2 and then 60 ML of xenon were adsorbed at a sample temperature of 30 K. Afterwards, Ag_{309} clusters were deposited on the sample with a coverage of 100 pAmin and from the position of this deposition spot the other deposition spots were defined and background spectra were taken. Then Ag_{55}, Ag_{147} and Ag_{309} cluster were deposited with a coverage of 20 pAmin, respectively. The measured results are presented in figure **76**.

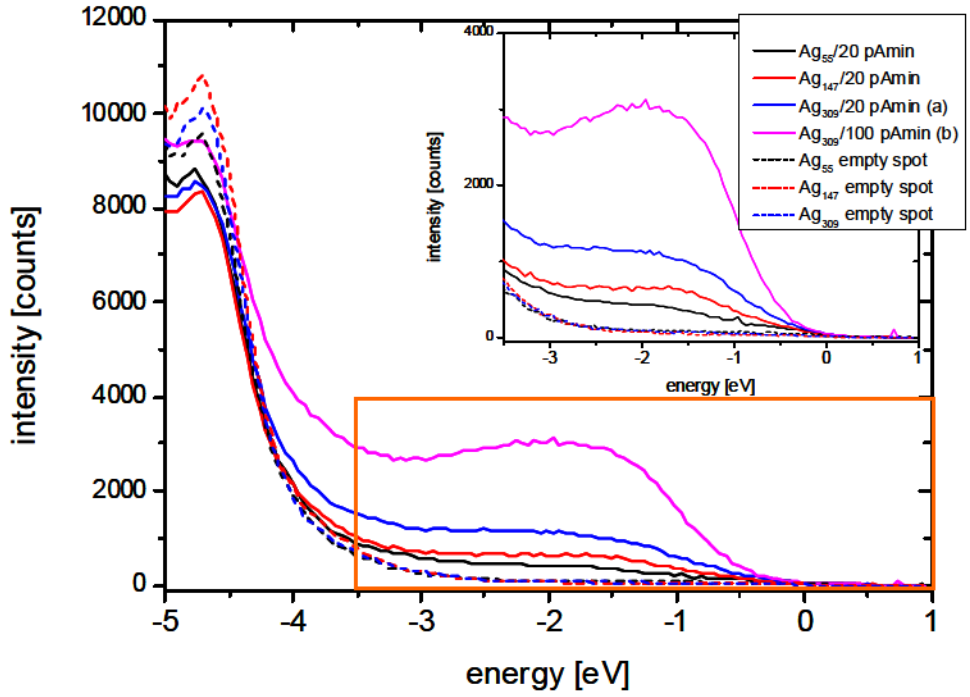

Figure 76: UPS spectra of Ag_{55}, Ag_{147} and Ag_{309} deposited with 20 pAmin and 100 pAmin on 60 ML xenon on Ag(111) and the corresponding background spectra. The inset magnifies the energy range from -3.5 eV to 2eV. 0 eV marks the position of the Fermi edge.

In the energy region from -3.5 eV to higher energies a clear size dependent cluster signal is visible which increases with increasing cluster size and coverage. Due to the better thermal contact of the sample to the cooled sample holder and the resulting lower temperature of the sample and the xenon layer, the clusters no longer travel through the xenon to the substrate.

As already discussed in chapter 6.2 and 8.2.1.2 for copper clusters on Xe/Cu(111) the intensity of the UPS signal is dependent on the cluster size and coverage. In figure **77** the intensity of the UPS signal at -2 eV and the calculated intensity (equation (6.4),

chapter 6.2) are plotted versus the cluster volume. For simplicity the cluster volume is calculated by assuming a cylindrical cluster with $d = h$.

The behaviour of the measured cluster intensity reflects the behaviour of equation (6.4), especially in the case of Ag_{147} and Ag_{309}. The intensity of Ag_{55} is higher than the calculated one. The reason for this could be the size of the cluster, which is much smaller than the electron escape depth λ (h_{Ag55}= 1.22 nm). Ag_{147} and Ag_{309} lie in the beginning of the transition region between the two edge cases of equation (6.4) where the intensity of the cluster signal is directly proportional to the cluster volume V and where it is proportional to $V^{2/3}$.

This result and the result for copper clusters on Xe/Cu(111) (figure **61**) are a good proof for the validity of equation (6.4).

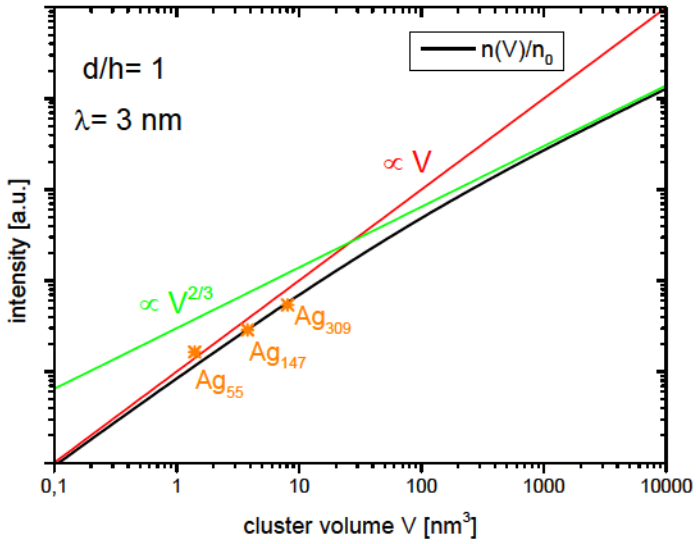

Figure 77: Calculated photoelectron intensity versus cluster volume for a cylindrical cluster with *d/h= 1* (black line). The electron escape depth was calculated with the help of equation (6.6) (chapter 6.2) for silver clusters measured with ArI light (11.62 eV). The orange stars mark the relative intensity of the UPS signal for silver clusters on Xe/Ag(111). The cluster volume was calculated by assuming a cylindrical cluster with *d= h*. The cluster height was calculated with *$h= 0.32 \cdot N^{1/3}$* (N= # atoms per cluster).

After subtraction of the Xe/Ag(111) background the size dependent s-p-band signal of the clusters is visible (figure **78**). The s-p-band onset gets steeper for larger clusters and higher coverage and a shift of the s-p-band flank (measured at half the height of the peak) is visible between Ag_{55} (-1.06 eV), Ag_{147} (-0.96 eV) and Ag_{309} (-0.91 eV). Apart from that no structure is visible in the s-p-band region. The cluster d-band is not visible because it has its onset -4 eV below the Fermi edge (figure **42**) but at this point the xenon signal is already so strong that the cluster d-band is covered by the xenon signal.

In the second experiment 60 ML of xenon were adsorbed on the clean Ag(111) surface at a temperature of 35 K. Than the sample was cooled down to 15 K and Ag_{309} clusters were deposited with a coverage of 100 pAmin. After the background spectra were

measured Ag_{55}, Ag_{92} and Ag_{147} clusters were deposited with a coverage of 10 pAmin, respectively. The results for these measurements are presented in figure **79**.

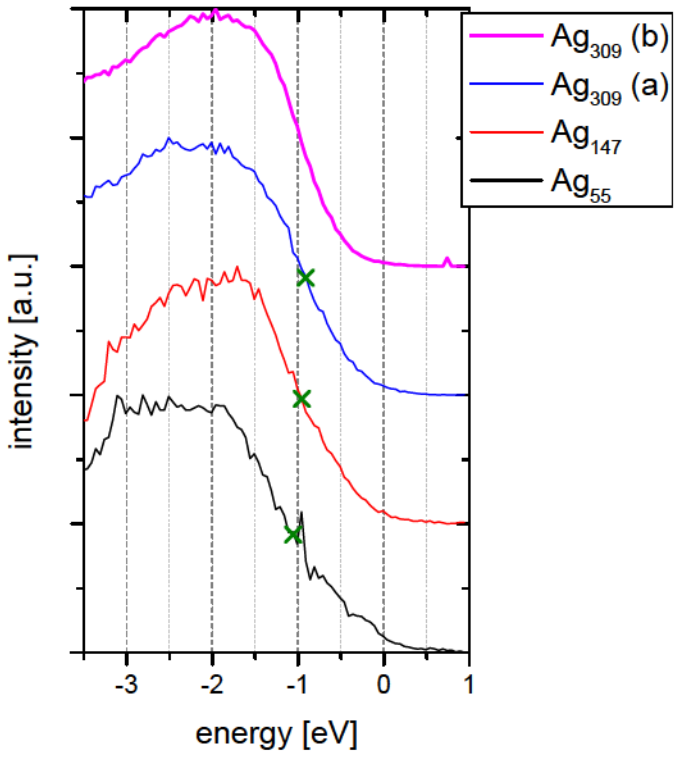

Figure 78: UPS spectra of Ag_{55}, Ag_{147} and Ag_{309} clusters after the subtraction of the Xe/Ag(111) substrate signal. Before subtraction the substrate signal was 10 point SG smoothed via Origin [109]. For a better comparability the spectra are normalized on a scale from 0 to 1 and shifted relatively to each other. The green crosses mark the position of the s-p-band flank measured at half the height of the peak.

A cluster signal is clearly visible. However, the intensity of the spectra of Ag_{55}, Ag_{92} and Ag_{147} is nearly the same despite the different cluster sizes. The results after subtraction of the Xe/Ag(111) background are shown in figure **80**.

Again a size dependent s-p-band is visible. The flank of the s-p-band shifts with cluster size (Ag_{55}: -0.96 eV, Ag_{92}: -0.86 eV, Ag_{147}: -0.83 eV). Additionally, the spectra show an internal structure, even though it is not so pronounced. Ag_{55} has a peak at -1.5 eV and two shoulders at -0.8 eV and -2.3 eV, respectively. Ag_{92} has only one peak at -1.5 eV, but Ag_{147} forms a plateau instead of a peak between -1.3 eV and -2 eV. Ag_{309} has only one broad peak. At the high coverage of 100 pAmin the clusters already coalesced.

The reason for the difference in the position of the s-p-band flank for Ag_{55} and Ag_{147} between this and the former measurement may come from the different coverage. Silver clusters seem to be more mobile on the xenon layer and as a result the clusters may coalesce at lower coverages than copper clusters. It seems possible that the clusters already coalesced at a coverage of 20 pAmin, which results among other things in an additional shift of the s-p-band flank.

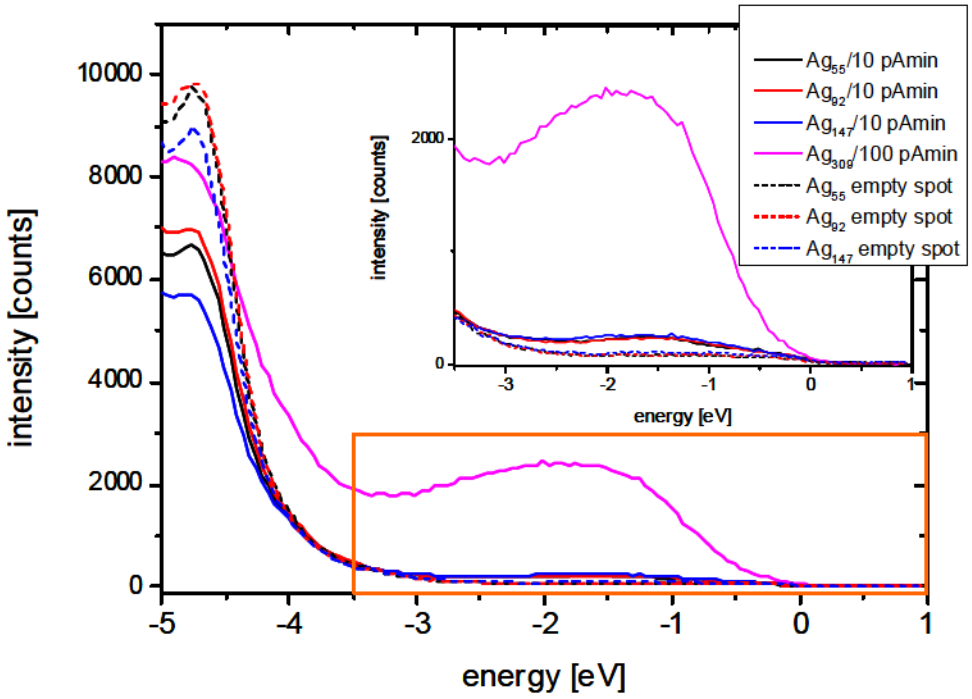

Figure 79: UPS spectra of Ag_{55}, Ag_{147} and Ag_{309} deposited with 10 pAmin and 100 pAmin on 60 ML xenon on Ag(111) and the corresponding background spectra. The inset magnifies the energy range -3.5 eV to 2eV. 0 eV marks the position of the Fermi edge.

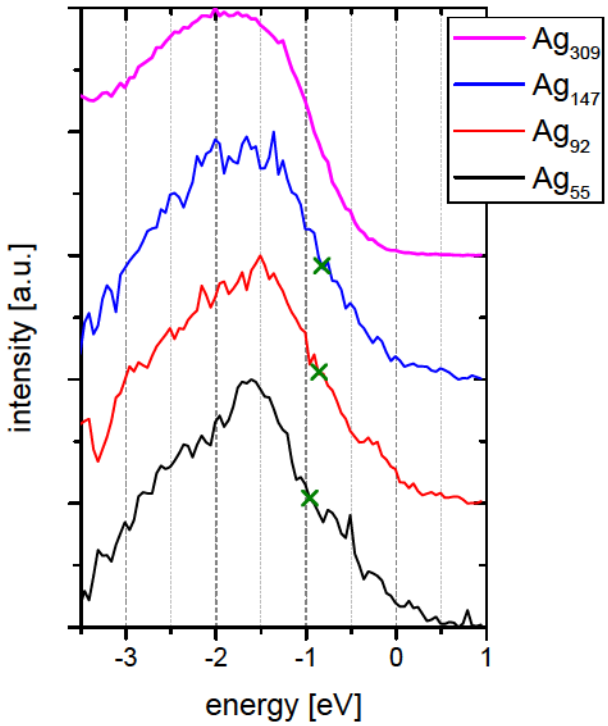

Figure 80: UPS spectra of Ag_{55}, Ag_{147} and Ag_{309} clusters after the subtraction of the Xe/Ag(111) substrate signal. Before subtraction the substrate signal was 5 point SG smoothed via Origin [109]. For a better comparability the spectra are normalized on a scale from 0 to 1 and shifted relatively to each other. The green crosses mark the position of the s-p-band flank.

8.2.2. Comparison with free beam spectra

In this chapter the experimental results are compared with free beam spectra, measured by the group of *Bernd von Issendorff* [8] in Freiburg and by CHESHNOVSKY et al. [84, 85]. For this purpose the results are discussed separately for copper and for silver clusters on different substrates.

8.2.2.1. Copper clusters

The results for copper clusters are discussed dependent on the used substrate. Depending on the substrate the shift needed to compare the deposited clusters with free beam clusters is different (see equ. (7.3) in chapter 7.2).

8.2.2.1.1. Cu_N (N= 55, 92, 147, 309)/ 60 ML Xe/ HOPG

A comparison between deposited copper clusters on Xe/HOPG (chapter 8.2.1.1) and free beam clusters is depicted in figure **81**.

The free beam spectra are shifted according to equation (7.3). The work function of HOPG is 4.5 eV [107, 108] and the charging energies are given in table **3**. The most striking similarity between the deposited spectra and free beam spectra can be found in the case of Cu_{147}. The cluster 2g and 3p band can be found in all four spectra, but the two peak structure of the 3p band is not visible for the deposited Cu_{147} clusters. Here only one peak occurs. In addition the 2f band is not visible in the spectra of the deposited clusters, it fused with the cluster d-band. For Cu_{55} the 2p and 1g band of the free beam spectra merged to one peak for the deposited clusters and the 1f peak is not visible. A similar behaviour shows Cu_{92}. The peaks of the free beam spectra merge to one peak in the s-p-band region of the deposited clusters.

copper cluster	cluster height for spherical clusters [nm]	charging energy [eV]	additional shift needed [eV]
55	1.07	2.26	0
90	1.26	1.97	0
92	1.27	1.96	0
147	1.49	1.71	0.35
152	1.50	1.69	0.25
342	1.97	1.33	-0.08

Table 3: Charging energy for negatively charged free beam clusters and additional shift needed to compare deposited clusters with free beam clusters in the case of copper clusters deposited on Xe/HOPG.

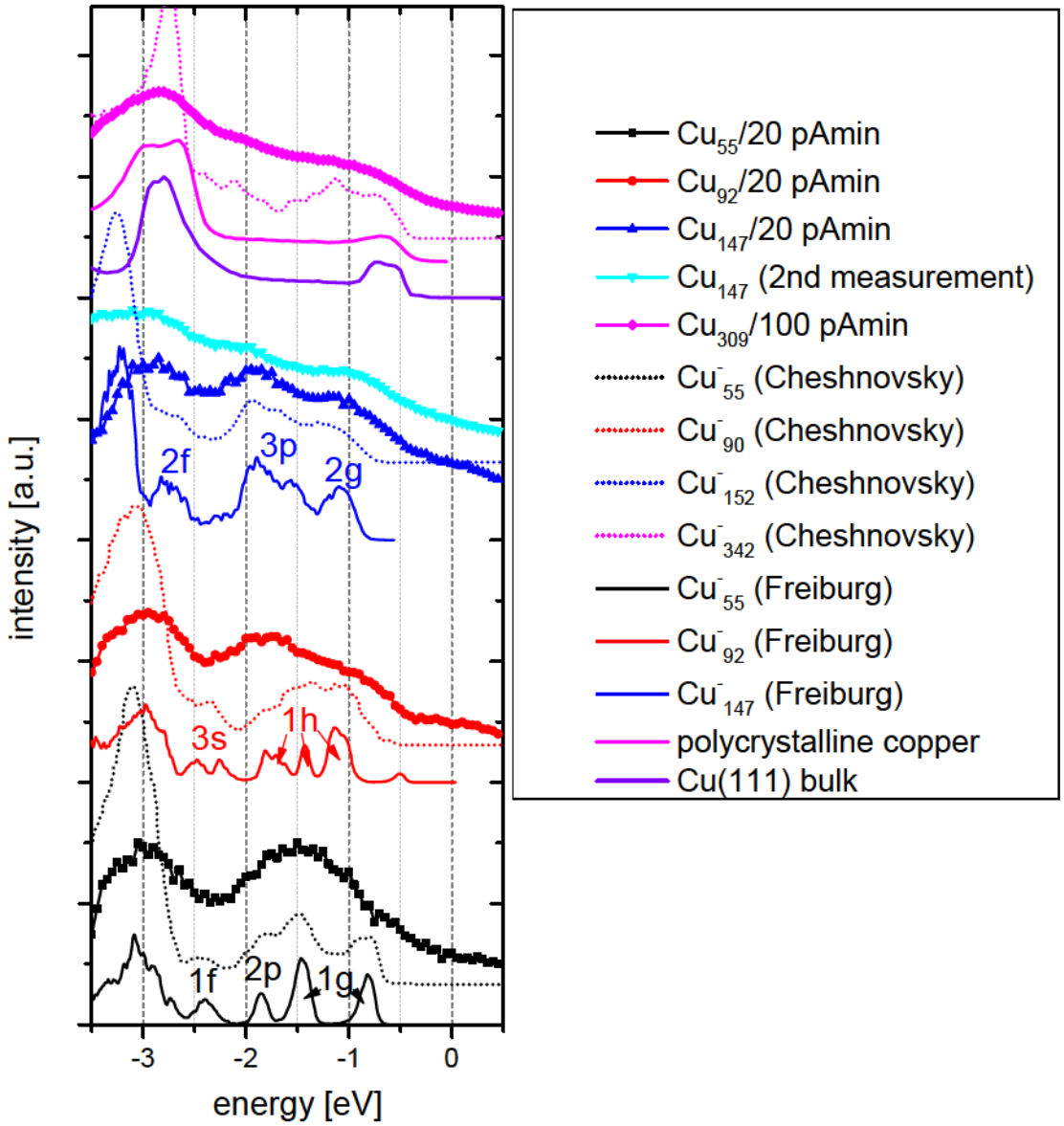

Figure 81: Comparison between free beam spectra and spectra of deposited clusters on 60 ML of xenon on HOPG measured in this thesis with the argon discharge lamp (11.62 eV). The spectra are shifted relatively to each other for a better comparability. The spectra of the deposited clusters are normalized. The energies used to measure the free beam spectra are 6.43 eV for the data from Freiburg [8] and 7.9 eV for the data from CHESHNOVSKY [84, 85]. The free beam spectra are shifted to compare them with deposited clusters. The bands of the free beam spectra are labeled by the quantum numbers of the corresponding states in the spherical free electron model [116].

The Cu_{309} clusters were deposited with a coverage of 100 pAmin. With regard to previous measurements (chapter 8.1.1.1) at this coverage the clusters already coalesced. But, a comparison with polycrystalline copper, bulk Cu(111)[3] and the free beam spectrum of Cu^-_{342} the deposited clusters show similarities with the free beam spectrum. Apart from the strong cluster d-band signal the structure in the s-p-band region of the free beam clusters is reflected in the shoulders around -2 eV and -1 eV in the spectrum of the deposited Cu_{309} clusters. The fact that the clusters here are compared with bigger

[3] The spectra for polycrystalline copper and Cu(111) are shifted so the position of the d-band signal fits the cluster spectra, i.e. the spectrum is shifted by the charging energy.

free beam clusters does not change this result. At this cluster size the difference in the UPS spectra is only small (see spectra of Cu^-_{410} and Cu^-_{256} in ref. [84]).

Comparing the two free beam spectra of Cu_{55}, Cu_{92} and Cu_{147} it is noticeable that they are slightly different from each other. The cluster d-band has a relatively higher intensity for the spectra from CHESHNOVSKY than in the spectra from Freiburg. Additionally, the peaks in the s-p-band region are sharper in the measurements from Freiburg than in the data from CHESHNOVSKY. Besides a lower cluster mass resolution and a lower photoelectron energy resolution one reason for these differences is the different photon energy used. Similarly differences between the free beam spectra and the spectra of the deposited clusters can be expected due to the different photon energy.

As already mentioned in chapter 6.2 the lower the photon energy, the better electronic states near the Fermi edge can be measured. The probability to excite an electron in a specific state is given by the dependence of the transition matrix elements on the photon energy. In the simplest case (harmonic oscillator) the dipole transition matrix element M is proportional to the overlap integral between initial state of an electron ψ_i and its final state (outgoing electron) ψ_f [71]:

$$M \propto \int \psi_f r \psi_i dV \quad . \tag{8.1}$$

This means that with a high probability low-energy radiation excites states with a low angular momentum, because of the large cross-section of the wave functions of the low-kinetic-energy final state electron and the low angular momentum initial state electron. Consequentially, the overlap for a high-kinetic-energy final state electron is also high for states with a high angular momentum initial state [71].

The photon energies used here are 6.43 eV (Freiburg), 7.9 eV (CHESHNOVSKY) and 11.62 eV (argon discharge lamp used in this thesis). The sensibility for the electron states with a low angular momentum decreases with increasing photon energy as can be observed in figure **81**. This context will be explained for the example of Cu_{92} and Cu_{147}.

Cu_{92} clusters show a 1h state with an angular momentum of $l=5$, which is split up into three main peaks and a 3s state ($l=0$) measured with a photon energy of 6.43 eV. For a higher photon energy (7.9 eV) the intensity of the 1h state increases whereas the intensity of the 3s state decreases. Additionally, the three peak structure of the 1h state gets lost. For the deposited clusters this trend goes on. The intensity of the 1h state becomes stronger whereas the 3s state is no longer visible, i.e., the sensibility for the electron states with a low angular momentum decreases with increasing photon energy.

The 3p state of the Cu_{147} clusters has an angular momentum of $l=1$, whereas the 2g state has $l=4$. In the free beam spectra measured with 6.43 eV the 3p state shows a good resolution and is split in two states which are both clearly visible. With higher photon energy this splitting becomes less visible. This is amongst others the reason that the two peak structure of the 3p band is not visible in the spectra of the deposited clusters. Additionally, the intensity of the 2g state becomes stronger, relatively to the 3p state with increasing photon energy. In addition the cluster 2f state ($l= 3$) becomes smaller with increasing photon energy until it is no longer visible in the spectra of the deposited clusters, which are measured with the highest photon energy.

Another possible reason which could lead to a broadening of the peaks in the UPS spectra of deposited clusters compared with free beam clusters could be the so called "dynamic final state effect" [73, 77] (see chapter 6.2, figure **29**). This effect was observed first for clusters grown in nanopits on HOPG [73], but recently also for mass selected gold clusters deposited on a thin silica layer, see e.g. ref. [117]. For free beam clusters the positive charge state just after the photoelectron emission stays constant over a time scale much larger than the time needed for the electron to escape. This results in well defined, sharp electron states in the spectra as can be observed in figure **81** for the free beam spectra. The kinetic energy of the emitting electron is lowered due to the positive hole, but this solely results in a constant energy shift. For deposited clusters the situation immediately after the excitation of the photoelectron is the same as for the free beam clusters, but after a certain time τ ($\approx fs$) the photohole is screened or a charge transfer from the substrate takes place and this change affects the kinetic energy of the emitting electron. This leads to a broadening of the UPS spectra for deposited clusters, if $v \cdot \tau$ is of the order of the cluster radius, with v as the velocity of the leaving photoelectron.

However, the thick xenon layer on the substrate should prevent a charge transfer between cluster and substrate on a timescale of femtoseconds. This should lead to sharper peaks in the UPS spectra than without the xenon layer. This is indeed the case if the results of copper clusters deposited directly on HOPG (chapter 8.1.1.2; figure **46**) and on Xe/HOPG are compared. The spectra on Xe/HOPG show more and sharper features than the results on HOPG due to the weaker interaction between the clusters and the Xe/HOPG.

Another reason for the differences between the spectra is their different energy resolution. The free beam spectra measured at Freiburg have an energy resolution of 60 meV [88] and the spectra measured by CHESHNOVSKY have an energy resolution of 150 meV [85]. The better resolution contributes to the spectra regarding the sharper peaks in the measurements from Freiburg. The energy resolution of the electron analyser used to investigate deposited clusters in this thesis can be determined with the help of the Fermi edge measured for every experiment. The energy resolution is, among others, dependent on the pass energy and the size of the entering and exit slits of the energy analyser [42]. The pass energy usually used in this work is 10 V, but the size of the slits can vary.

For the determination of the energy resolution from the Fermi edge the position of the Fermi edge has to be identified. Thereto the region before and after the Fermi edge are approximated by a straight line (figure **82**). The position where a perpendicular line crosses the Fermi edge at 50 % of the intensity between these lines marks the position of the Fermi edge. Then the energies at 84 % and 16 % of the Fermi edge are determined and the difference is the energy resolution. But, the thermal broadening of the Fermi edge has also to be taken into account. It is given by $\Delta E_T = 4k_BT$ [42] with k_B as the Boltzmann constant and T the temperature at which the Fermi edge was measured (in this case 50 meV for T= 150 K, as the Fermi edge was measured after xenon desorption). Therefore, the resulting energy resolution for the UPS measurements for deposited clusters on Xe/HOPG is slightly lowered from 160 meV to 150 meV.

The energy resolution is nearly the same as in the CHESHNOVSKY spectra, but worse than the one for the data from Freiburg. The worse energy resolution leads to a

broadening of the spectral features in both cases with the result that some features are smeared out and no longer visible.

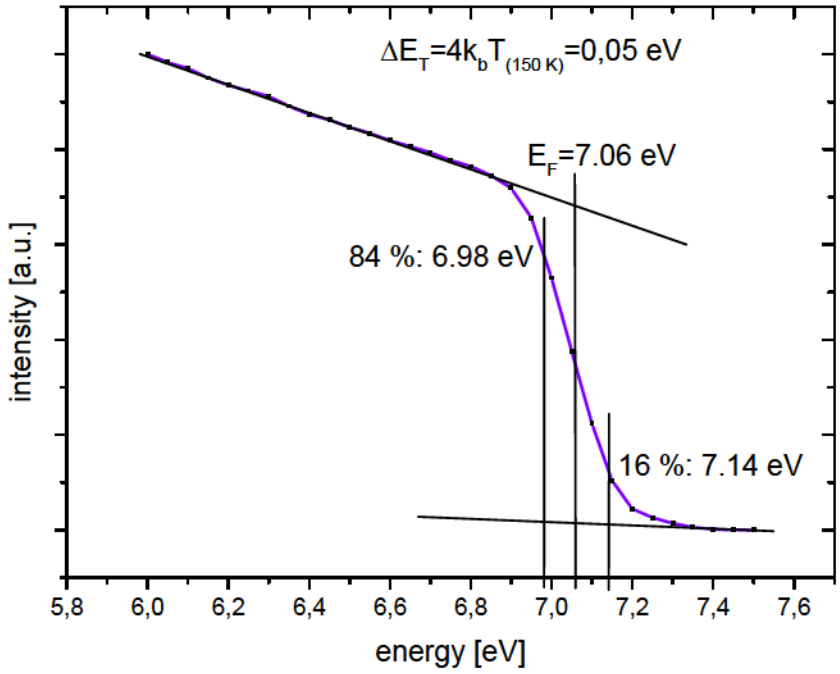

Figure 82: Fermi edge measured at the HB- holder of the manipulator at 150 K. The difference of 160 meV between the energies at 84 % and 16 % of the intensity of the Fermi edge under consideration of the thermal broadening of the Fermi edge yield the energy resolution for this UPS measurement (copper clusters on Xe/HOPG).

In addition, the mass resolution plays an important role. The mass resolution in the case of the spectra from Freiburg is m/dm~ 2000 [8], i.e. up to clusters with 2000 atoms can be resolved separately. CHESHNOVSKY can resolve copper clusters with up to 80 atoms [85], which is slightly better than the resolution of the mass selector used for this thesis (50- 70 atoms per cluster, see chapter 4.1.3). A worse mass resolution leads to a broadening of the UPS spectrum because other cluster sizes than the desired one can pass the mass selector and contribute to the measurement. In the case of Cu_{147} also a small amount of Cu_{146} and Cu_{148} could have passed the mass selector and landed on the sample. However, the small amount of the other cluster sizes does not change the overall shape of the spectra.

However, the fact that the clusters measured in this thesis are deposited on a surface can not be disregarded. This becomes clear looking at the shift needed to compare the results for free beam clusters with deposited clusters: an additional shift is needed (table 3). Especially in the case of Cu^-_{147} and Cu^-_{152} the charging energy must be increased to match the results of the deposited clusters. Even though the shift between the spectra from Freiburg and CHESHNOVSKY and of the deposited clusters should be the same, there is a difference between the shift needed for the spectra from Freiburg and the spectra of CHESHNOVKY of about 0.1 eV. The main reason for this shift is the different cluster size. As can be observed in ref. [84, 85] the shape of the cluster spectra

is similar for a certain size range (compare, e.g., the spectra of Cu^-_{193} and Cu^-_{256} in [85]), but the position of the spectra shifts to higher energies with increasing cluster size. Therefore, a shift between the two different cluster sizes appears, but the shape of the spectra is nearly the same and can be compared with the spectrum of the deposited Cu_{147} clusters.

One effect influencing the shift in table **3** could be the xenon layer. The charging energy of the free beam clusters is calculated with the help of equation (7.2) (chapter 7.2). In this equation ε contains information about the surrounding of the cluster. Here ε was set equal ε_0 what would be correct if the cluster would be surrounded by vacuum. But the clusters are deposited on xenon, where they can partially sink into. This would increase the value of ε. Hence, the charging energy would decrease.

Another contribution to the additional shift could be that the electron affinity and ionisation energy change between the free beam clusters and clusters deposited on a rare gas. As already mentioned in chapter 7.2 the deposited clusters are no longer referenced to the Fermi energy, but to the vacuum energy of the substrate. So the onset of the cluster spectrum lies about the difference of the work function between cluster and substrate and α times the charging energy (α is a quantum correction of the bulk work function for a spherical particle) under the Fermi energy (figure **37** and **38**, chapter 7.2) [90]. In the classic electrostatic drop model α equals 0.5 for a spherical particle [118]. But, it could be shown that for free cluster anions the value of α can differ from this number [8, 87, 119]. Especially for supported clusters this value becomes very small, see e.g., ref. [117] for supported gold clusters ($\alpha = 0.12$).

But, in equation (7.3), which is used to align the position of the free beam clusters with the deposited clusters, α does not appear. It is eliminated in the calculation of the shift between neutral and negatively charged clusters (equation (7.2)). In principle equation (7.3) transforms free beam cluster anions to neutral free beam clusters referenced to the vacuum energy of the system of the deposited clusters. As mentioned in [117] α can differ for free clusters and for deposited ones. This difference can be one reason for the additional shift needed for a comparison of the free beam clusters with the deposited ones.

In summary, reasons for the differences between the UPS spectra of free beam and deposited clusters are, in this case, the different photon energy, partially the dynamic final state effect, the different energy resolution and the different mass resolution. The additional shift needed, leading to an increasing of the charging energy, can be a combination of effects as the screening by the xenon layer and differences in the electron affinity/ionisation energy after deposition.

8.2.2.1.2. Cu_N (N= 147, 309, 923)/ 60 ML Xe/ Cu(111)

A comparison of free beam clusters with clusters deposited on 60 ML of xenon on Cu(111) (chapter 8.2.1.2) is presented in figure **83**.

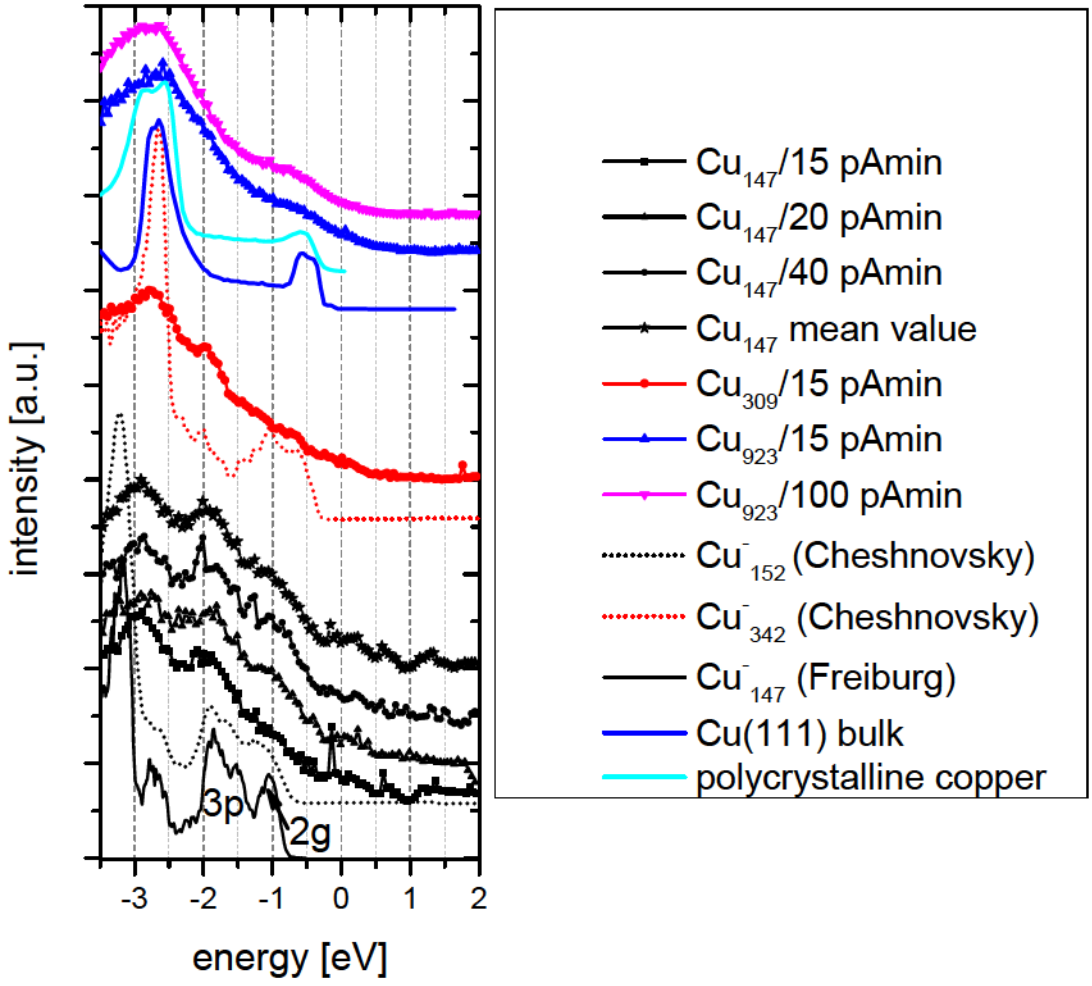

Figure 83: Comparison between free beam spectra and spectra of deposited clusters on 60 ML of xenon on Cu(111) measured in this thesis with the argon discharge lamp (11.62 eV). The spectra are shifted relatively to each other for a better comparability. The spectra of the deposited clusters are normalized. The energies used to measure the free beam spectra are 6.43 eV for the data from Freiburg [8] and 7.9 eV for the data from CHESHNOVSKY [84, 85]. The free beam spectra are shifted to compare them with deposited clusters. The results for Cu_{112} are not discussed here due to the low statistics of this measurement (see chapter 8.2.1.2).

The free beam spectra are shifted according to equation (7.3). The work function of Cu(111) is 4.94 eV [114] and the charging energies are given in table **4**. The most striking similarity between the deposited spectra and free beam spectra can be found again in the case of Cu_{147}. In all three measurements the 3p and the 2g state is visible. Because of the lower intensity of these measurements (see chapter 8.2.1.2) and the fact that all three spectra show the same result, it is justifiable to average over these three measurements. The resulting spectrum is also presented in figure **83**. Here, the similarities between the free beam spectra and the averaged Cu_{147} spectrum of the deposited clusters are even more eye-catching. The reason for the lower intensity and

the resulting poorer statistic is that the size of the exit slit of the energy analyser was reduced for these measurements. This increased the energy resolution (now 80 meV; calculated as described in the previous chapter) but at the cost of intensity, as explained in ref. [42]. For this case the increasing of the energy resolution did not lead to a better result concerning the UPS spectra of the deposited clusters.

copper cluster	cluster height for spherical clusters [nm]	charging energy [eV]	additional shift needed [eV]
147	1.49	1.71	0.75
152	1.50	1.69	0.65
342	1.97	1.33	0.27

Table 4: Charging energy for negatively charged free beam clusters and additional shift needed to compare deposited clusters with free beam clusters in the case of copper clusters deposited on Xe/Cu(111).

For Cu_{309} the resemblance between the free beam (indeed Cu^{-}_{342}) and the deposited spectra is not so clear. Apart from the cluster d-band the peak at -2 eV is visible in both spectra, but the structure in the free beam spectrum between -1.5 eV and -0.5 eV is not visible in the spectrum for the deposited clusters.

For Cu_{923} no free beam spectra exist so the deposited clusters are compared with spectra of bulk copper (both bulk spectra are again shifted slightly). The Cu_{923} clusters are in the transition region where first bulk properties begin to develop [2] (see chapter 2). The resemblance to the UPS spectrum of polycrystalline copper for a low coverage could be a proof for this assumption. For the high coverage (100 pAmin) the clusters probably already coalesced.

For a proper comparison of the free beam clusters with the deposited clusters the spectra of the free beam clusters again needed an additional shift (table **4**). For the cluster sizes in table **4** in comparison to the shifts needed on HOPG the difference of the shifts (0.4 eV) illustrates the influence of the substrate on the cluster spectra (this will be discussed in more detail in chapter 8.2.2.1.4). But in the previous chapter no additional shift was needed for Cu_{55}, Cu_{90} and Cu_{92}. It is possible that for these cases also an additional shift should occur, but the deposited clusters have only a poor structured s-p-band region, which could be used as a clear indication for an additional shift. Therefore, it is difficult to determine the right additional shift for the small free beam clusters.

Two possible origins of the additional shift are already described in the previous chapter. Another possible reason for the additional shift in table **4** could be the influence of the xenon layer on the work function of the substrate and the influence of the electron affinity of the rare gas, see ref. [113]. As already mentioned the adsorption of a xenon layer reduces the work function of the substrate (in the case of xenon on Au(111) the work function is reduced by 0.3 eV). Assuming that xenon reduces the work function of all metal substrates about the same value, the remaining shift of about 0.5 eV may be explained assuming an influence of the electron affinity of the xenon (EA_{xenon}= 0.5 eV). This is discussed in detail for copper clusters deposited on Ar/Xe/Ag(111) (see chapter 8.2.1.4). For Xe/HOPG the influence of the xenon layer on the work function of the substrate could be different which could result in a different shift.

The other differences between the UPS spectra of the free beam clusters and the deposited clusters come from the different photon energies used for the measurements, the different energy and mass resolutions and partially from the dynamic final state effect, as already discussed above.

8.2.2.1.3. Cu_N (N= 147, 309, 923)/ 60 ML Xe/ Au(111)

A comparison between UPS spectra of deposited clusters and free beam clusters is depicted in figure **84**.

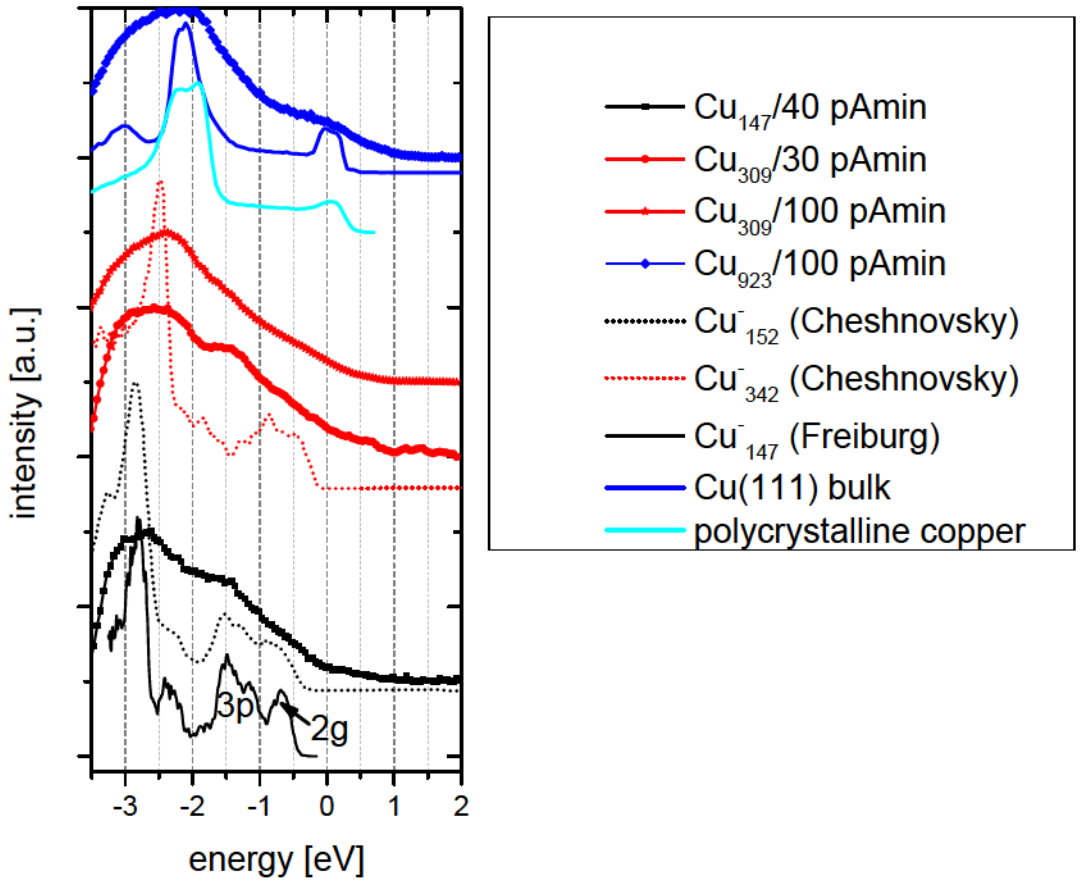

Figure 84: Comparison between free beam spectra and spectra of deposited clusters on 60 ML of xenon on Au(111) measured in this thesis with the argon discharge lamp (11.62 eV). The spectra are shifted relatively to each other for a better comparability. The spectra of the deposited clusters are normalized. The energies used to measure the free beam spectra are 6.43 eV for the data from Freiburg [8] and 7.9 eV for the data from CHESHNOVSKY [84, 85]. The free beam spectra are shifted to compare them with deposited clusters. Only the results of the second measurement and the Cu_{923} clusters from the first measurement from chapter 8.2.1.3 are discussed here.

The free beam spectra are shifted according to equation (7.3). The work function of Au(111) is 5.31 eV [114] and the charging energies are given in table **5**. As already described in chapter 8.2.1.3 the structure in the s-p-band region is not as pronounced as for the clusters on Xe/HOPG and Xe/Cu(111). In the case of the deposited Cu_{147} clusters only the 3p state can clearly be distinguished. The 2g state is only visible as a

slight shoulder around -0.5 eV. The reason for the differences to the previous measurements could be the higher coverage. Indeed for an experiment on Xe/Cu(111) Cu_{147} clusters were deposited with the same coverage, but as the intensity of the resulting spectrum was the same as for the clusters deposited with 20 pAmin the assumption was in this case that the cluster spot was not measured in the center but at its rim where the coverage was lower. Due to the higher coverage here some clusters may already be coalesced which would distort the result and lead to an additional broadening of the spectrum.

copper cluster	cluster height for spherical clusters [nm]	charging energy [eV]	additional shift needed [eV]
147	1.49	1.71	0.75
152	1.50	1.69	0.65
342	1.97	1.33	0.47

Table 5: Charging energy for negatively charged free beam clusters and additional shift needed to compare deposited clusters with free beam clusters in the case of copper clusters deposited on Xe/Au(111).

In the case of Cu_{309} deposited with 30 pAmin a shoulder at -1.5 eV appears which can not really be assigned to a structure in the free beam spectrum of Cu^-_{342}. Maybe in the case of the deposited clusters the structure in the s-p-band region broadened so that only one peak remains which results in the given shoulder. Cu_{309} deposited with 100 pAmin did not show any resemblance with the free beam spectrum differently than for Cu_{309} deposited on Xe/HOPG. It seems that only the cluster d-band is visible. It is possible that in the latter case the UPS spot was not in the center of the cluster spot so that the rim was measured where the cluster did not coalesced yet.

For Cu_{923} also deposited with 100 pAmin the spectrum equals Cu(111) bulk as in the previous chapter. The clusters are coalesced and may form islands with a Cu(111) structure.

Again an additional shift is needed to compare the free beam spectra with the spectra of the deposited clusters (table **5**). The shift is of the same magnitude as on Xe/Cu(111). But it is difficult to determine the shift in the case of Cu_{309} because of the missing structure in the s-p-band region due to the broadening of the spectrum.

A reason for the broadening of the UPS spectra of the deposited clusters is the energy resolution, here 120 meV. Hence the energy resolution is better than for the spectra of CHESHNOVSKY (150 meV) [85], but the spectra of the deposited clusters seem broader. One reason for this may be the higher coverage used for the deposition of the clusters than in the previous measurements (especially for Cu_{147}). Other reasons for the broadening were already discussed above.

8.2.2.1.4. Summary for copper clusters

In summary the comparison of the UPS spectra of deposited clusters with free beam clusters shows the best agreement for Cu_{147} [4]. Therefore, in figure **85** the measurements for Cu_{147} clusters on Xe/HOPG, Xe/Cu(111) and Xe/Au(111) are presented in one plot.

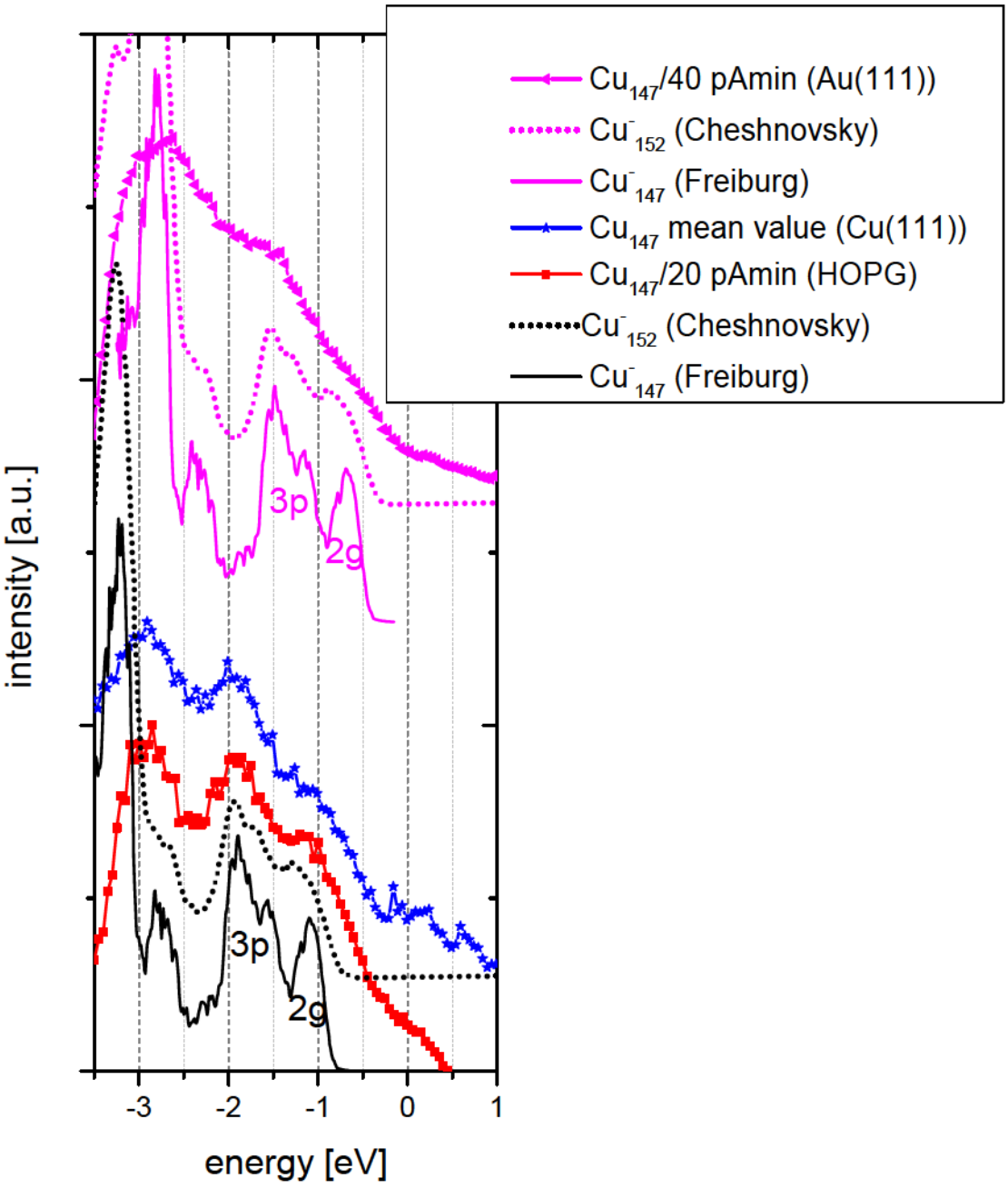

Figure 85: Comparison between UPS spectra of Cu_{147} clusters deposited on three different substrates and free beam spectra. For Cu_{147} on Xe/HOPG and Xe/Cu(111) the position of the 3p and 2g state is the same, whereas on Xe/Au(111) the whole spectrum is shifted about 0.4 eV to higher energies. For Cu_{147} on Xe/Cu(111) the mean value of the three measurements is depicted.

[4] The results for copper clusters on Ar/Xe/Ag(111) (chapter 8.2.1.4) are not discussed here because of the poor cluster signal.

On all three substrates the spectra show similar results for deposited Cu_{147} clusters which are in good agreement with the free beam spectra. But according to ref. [90] the cluster spectra should be shifted about the difference of the work function of the different substrates. Due to the xenon layer the clusters are decoupled and no longer referenced to the Fermi edge, but to the vacuum energy of the substrate. Dependent on the substrate the cluster spectrum is shifted to higher or lower energies. However, the spectra on Xe/HOPG and Xe/Cu(111) show no shift relative to each other, so the peaks are at the same positions in spite of a work function difference of 0.4 eV. In contrast, the Cu_{147} cluster spectrum on Xe/Au(111) shows a shift of about 0.4 eV relating to the spectra on Xe/Cu(111), which corresponds to the work function difference between Cu(111) (4.94 eV) and Au(111) (5.31 eV) [114].

The missing shift between the experimental results of HOPG and Cu(111) can be identified in the additional shift needed to compare the free beam spectra with spectra of deposited clusters (table **3** (0.35 eV for HOPG) & **4** (0.75 eV for Cu(111))). The difference between the additional shifts is 0.4 eV and cancels the difference between the work function of HOPG (4.5 eV) and Cu(111) (4.94 eV) [114]. The xenon layer can change the work function of the substrate, as observed in [90], and lead to an additional shift in the cluster spectra. This effect can be different for HOPG and the metals copper and gold.

In figure **86** the position of the copper cluster d-band flank is plotted versus the cluster size. It is observable that in all experiments (independent of the substrate) the position of the d-band flank shifts to higher energies with increasing cluster size. But, for clusters deposited on substrates without a xenon layer the overall shift is smaller than for clusters deposited on xenon. The reason for this behaviour is that for the clusters deposited directly on HOPG or Ag(111) the highest occupied state of the clusters aligns to the Fermi edge of the substrate due to the stronger cluster surface interaction. On HOPG the shift of the cluster d-band includes the dynamic final state effect on HOPG, as already observed in [73, 77]. This effect is stronger for smaller clusters which results in a higher shift with decreasing cluster size, as observed here. On Ag(111) this effect did not occur possibly because of the high conductivity of the substrate. Therefore the shift observed on Ag(111) can be directly related to a size dependent change in the electronic structure of the clusters.

For clusters deposited on xenon the main shift of the cluster d-band flank comes from the charging energy ΔE_i of the cluster. The charging energy becomes smaller with increasing cluster size ($\Delta E_i \propto 1/R$, with the cluster radius R; see equation (7.2) in chapter 7.2) which results in a smaller shift of the cluster spectrum for bigger clusters. In addition the position of the cluster spectrum, and therewith the position of the cluster d-band, is dependent on the work function difference between the cluster material and the substrate (as discussed above). The influence of the charging energy and the work function difference superimpose with the shift of the cluster d-band resulting from a cluster size dependent change of the electronic structure.

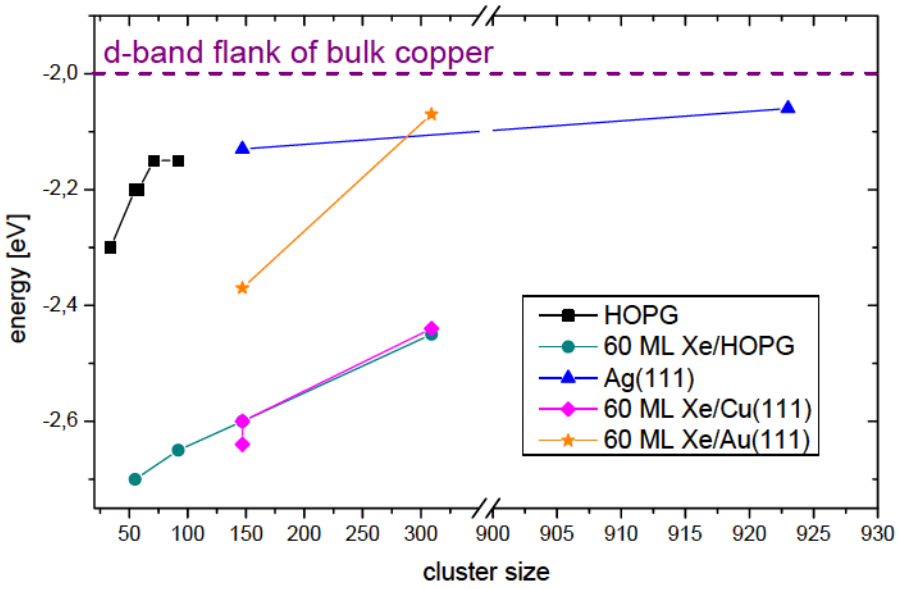

Figure 86: Position of the copper cluster d-band flank for different cluster sizes on different substrates. The results on HOPG were measured with the helium discharge lamp and the other results with the argon discharge lamp.

8.2.2.2. Silver clusters

A comparison of UPS spectra of deposited silver clusters on 60 ML xenon on Ag(111) is depicted in figure **87**. Only the cluster s-p-band region is visible. Comparing the spectra deposited with 20 pAmin coverage with the spectra of Ag_{309} deposited with 100 pAmin a strong similarity is visible in contrast to the spectra of the clusters deposited with 10 pAmin. It seems that at a coverage of 20 pAmin the silver clusters already coalesced on the surface. Therefore, only the spectra of clusters deposited with 10 pAmin coverage are compared with the free beam spectra and used for the discussion.

The free beam spectra are shifted according to equation (7.3). The work function of Ag(111) is 4.74 eV [114] and the charging energies are given in table **6**. The best agreement between the free beam spectrum and the spectrum of deposited clusters shows Ag_{92}. The three peaks of the 1h state are broadened and fused to one peak. One reason for the broad spectrum of the deposited clusters is the worse energy resolution (160 meV, calculated as described above) in comparison with the energy resolution of the spectra from Freiburg (60 meV) [88]. But, more important are other broadening mechanisms, which are discussed above.

Ag_{55} deposited with a coverage of 10 pAmin shows a similar structure like Ag_{92}. Here the single peaks which are visible in the free beam spectra also fused to one broad peak. The same happens in the case of Ag_{147}. But, here the resulting peak is broader and looks more like a plateau.

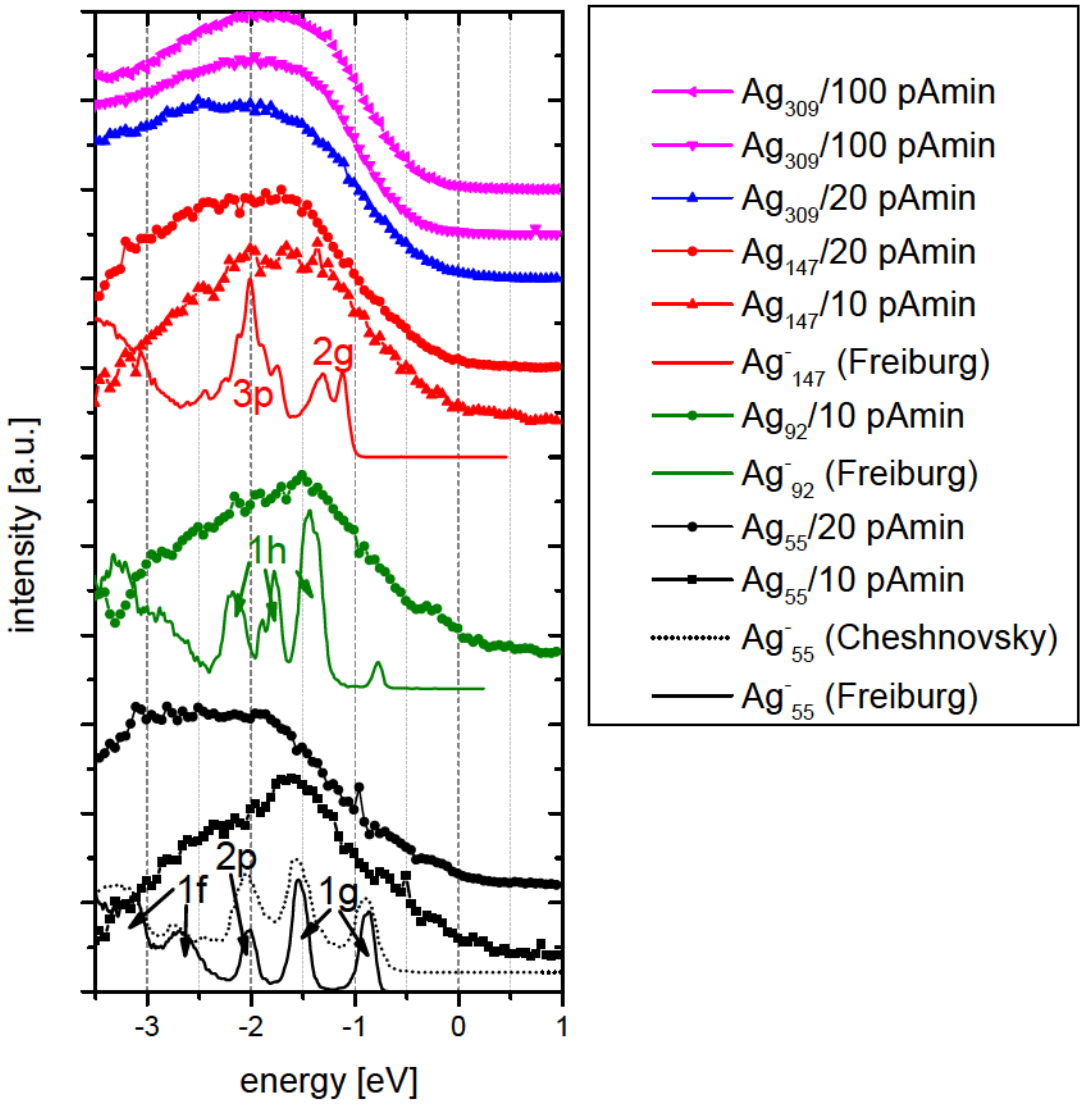

Figure 87: Comparison between free beam spectra and spectra of deposited clusters on 60 ML of xenon on Ag(111) measured in this thesis with the argon discharge lamp (11.62 eV). The spectra are shifted relatively to each other for a better comparability. The spectra of the deposited clusters and the spectra from Freiburg are normalized. The energies used to measure the free beam spectra are 6.43 eV for the data from Freiburg [8] and 7.9 eV for the data from CHESHNOVSKY [84, 85]. The free beam spectra are shifted to compare them with deposited clusters. The bands of the free beam spectra are labeled by the quantum numbers of the corresponding states in the spherical free electron model [116]. The small peak in the Ag^-_{92} free beam spectrum at -0.8 eV comes from the negative charge of the free beam cluster. The extra electron begins to fill up a new electronic state (2f). For Ag_{309} no free beam spectra exist.

For best agreement between the free beam spectra and the spectra of the deposited clusters again an additional shift to equation (7.3) is needed (table 6). The shift needed in the case of Ag_{92} and Ag_{147} is the same as for copper clusters on Xe/Cu(111) and Xe/Au(111) which is in agreement with the results from ref. [90] (see chapter 8.2.2.1.2 & 8.2.2.1.3).

silver cluster	cluster height for spherical clusters [nm]	charging energy [eV]	additional shift needed [eV]
55	1.22	2.03	0.50
92	1.44	1.75	0.75
147	1.69	1.53	0.75

Table 6: Charging energy for negatively charged free beam clusters and additional shift needed to compare deposited clusters with free beam clusters in the case of silver clusters deposited on Xe/Ag(111).

With the argon gas discharge lamp it is not possible to measure the silver cluster d-band. Therefore, the position of the cluster s-p-band is investigated for the clusters deposited with 10 pAmin coverage (figure **88**). The s-p-band flank was measured at half the height of the s-p-band peak. With increasing cluster size the position of the s-p-band flank shifts to higher energies. This is a similar result as for the position of the cluster d-band for copper clusters in the previous chapter. It can be assumed that the reasons for the shift of the cluster s-p-band are the same as for the cluster d-band in the previous chapter.

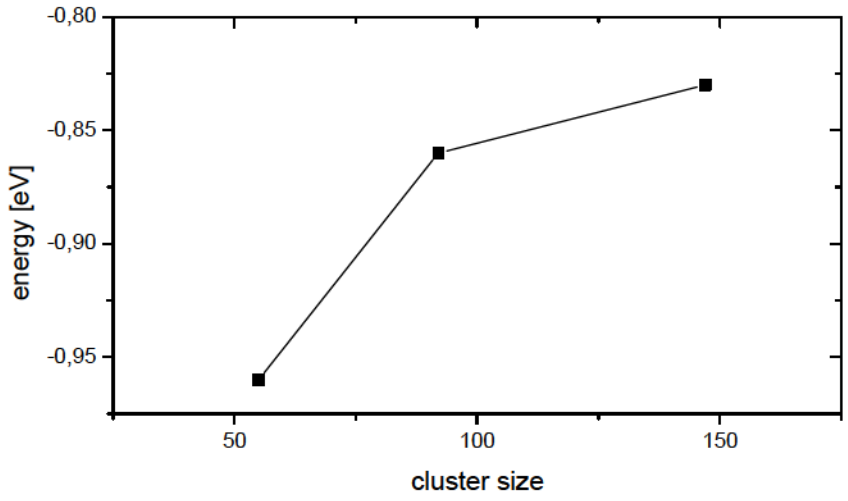

Figure 88: Position of the cluster s-p-band flank for silver clusters deposited on 60 ML xenon on Ag(111).

9 Summary and Outlook

This chapter summarizes the results obtained within this thesis and gives a brief outlook on future trends and experiments.

9.1. Summary

Clusters on pure substrates:
In the first part of the experimental results cluster were deposited on pure substrates (HOPG and fcc metal) without any rare gas adsorbed on the substrate. Compared to clusters deposited on rare gas layers this leads to a stronger cluster- surface interaction.

Silver clusters (Ag_{55}-Ag_{923}) were deposited on HOPG at a sample temperature of 125 K with different coverages (10 pAmin-129 pAmin) and measured with UPS with the helium gas discharge lamp. It could be observed that UPS spectra of small clusters (Ag_{55}-Ag_{147}) deposited with a low coverage ($\leq$ 20 pAmin) resemble the UPS spectrum of polycrystalline silver. Spectra of small clusters deposited with a high coverage and big clusters (Ag_{309}-Ag_{923}), independent of their coverage, look like the UPS spectrum of Ag(111). After annealing of the sample with the big clusters up to room temperature the spectra changed from Ag(111) like to polycrystalline silver, except for the clusters deposited with the highest coverage (Ag_{561}/63 pAmin). Here the spectrum still resembles Ag(111). From these measurements the best cluster coverage for silver clusters on HOPG at 125 K sample temperature could be determined. The resemblance of the spectra to polycrystalline silver for coverages $\leq$ 20 pAmin (in the case of big clusters, after annealing) is a hint, that the clusters are not coalesced at this coverage and lie randomly on the surface for T= 125 K. For higher coverages the clusters already coalesced and build Ag(111) oriented silver islands. Hence, for clusters deposited on HOPG at 125 K sample temperature the best cluster coverage is $\leq$ 20 pAmin. But, for lower sample temperatures and/or other sample materials this value can vary, according to the mobility of the clusters on the substrate material.

In a second experiment on HOPG copper clusters (Cu_{34}-Cu_{92}) were deposited at T= 125 K with different coverages (15 pAmin-70 pAmin) and investigated via UPS with the helium gas discharge lamp. Due to a high similarity between the UPS spectrum of polycrystalline copper and Cu(111) it was more difficult to compare the UPS spectra of the copper clusters with bulk copper. But, despite this limitation and problems occurring during the cluster deposition (see chapter 8.1.1.2) an overall agreement with the results of silver clusters on HOPG could be reached. In addition the position of the cluster d-band flank was investigated. In agreement with previous measurements [98] of evaporated copper clusters on amorphous graphite the position of the cluster d-band flank shifts with increasing cluster size to higher energies. In contradiction to previous publications of metal clusters on HOPG [99, 100] where mainly a charge related final

state effect was discussed this energy shift comes from a size related change in the electronic structure of the clusters.

In order to prove size effects without charge related final state effects copper clusters were deposited on Ag(111) at 20 K substrate temperature. Due to the high conductivity of the metal substrate a possibly occurring final state effect can be excluded. Again a size dependent shift of the onset of the cluster d-band could be observed. But, here the shift is smaller than for copper clusters on HOPG (0.07 eV instead of 0.15 eV) this could be a hint that on HOPG possibly a reduced dynamic final state effect [77] appears which is responsible for a higher shift.

Compared to clusters on fcc metals, clusters deposited on HOPG experience a relatively weak cluster surface interaction. The strong interaction between cluster and fcc metal substrate, changing also the cluster geometry, was investigated with STM for deposited silver clusters at 77 K and 5 K substrate temperature. It could be observed that silver clusters deposited and measured at 77 K substrate temperature on Au(111)/mica develop a structure consisting of several silver monolayers [40], whereupon clusters deposited with $\leq$ 15 eV deposition energy per cluster show two heights in a histogram differing by one silver monolayer. The height of this layered structure varies with the amount of silver atoms in the clusters and the deposition energy per cluster. Additionally molecular dynamic (MD) simulations were performed which could reproduce the experimental data, but lead to clusters constantly higher of about one silver monolayer than the experimental data for deposition energies $\leq$ 15 eV. The assumption was that even at 77 K a post-deposition decay process occurs which takes place on a timescale of some hours, much longer than the possible time for MD simulations.

In an additional experiment Ag_{55}, Ag_{86} and Ag_{147} were deposited at much lower temperatures (11 K) on Au(111)/mica and investigated with the STM at T= 5 K. Here the clusters show only one peak in the histograms with a height in between two silver monolayer heights. Then the sample was annealed for 1 h at 77 K and again measured with the STM at 5 K. The results obtained here reproduce the results of the silver clusters deposited and measured at 77 K. But, because of a poor statistics for the measurements it is difficult to say if a two peak structure in the measurements before the annealing process would be visible with more statistics. Therefore the mean height of the clusters was investigated. For Ag_{55} and Ag_{147} the average cluster height before and after annealing is the same, within the statistical error. But for Ag_{86} a height difference of about one half silver monolayer before and after annealing is visible, indicating a real difference between the measurements at 5 K and at 77 K. The results obtained for the height measurements at 5 K were also studied using MD simulations. Again some differences were visible regarding the cluster height. The reason for these differences is not quite clear and needs more investigation. But one possible reason could be that the clusters are too hot during deposition and freeze on the surface in a random orientation which would explain the missing peaks in the experimental data or the broad size distributions. Another possibility is that the cluster is so hot just after deposition that some atom monolayers already decay in the few picoseconds after deposition before the cluster cools down which would lead to a different height distribution than in the simulation.

Clusters on rare gas layers:
In the second part of the experimental results copper and silver clusters deposited on rare gas layers (mostly xenon) on different substrates were investigated. Clusters on rare gas layers show a very weak cluster-surface interaction and can be considered as "quasi free".

Copper clusters were deposited on 60 ML xenon on HOPG, Cu(111) and Au(111) with different sizes and coverages and investigated via UPS with the argon gas discharge lamp. On all substrates a size dependent cluster signal of the s-p-band region of the clusters was visible. The different shapes of the spectra are a hint that the deposited clusters show a differing, cluster size dependent electronic structure. The obtained spectra were compared with results from clusters measured in the free beam [8, 84, 85] and some similarities between the UPS spectra of free beam clusters and deposited clusters could be found. Especially in the case of Cu_{147} a good agreement between the spectra was observable. But, to compare the UPS spectra properly the free beam spectra had to be shifted according to equation (7.3) (chapter 7.2). The shift is necessary because of the different reference energies of the spectra (free beam clusters: E_{vac}= 0 eV; deposited clusters E_F= 0 eV) and the different charging of the clusters (free beam clusters: negatively charged; deposited clusters: neutral). After this the free beam spectra are also referenced to the Fermi energy and can be compared with UPS spectra of deposited clusters. But, an additional shift was needed for a good agreement between the cluster spectra (in the case of Cu_{147}: on HOPG: 0.35 eV; on Cu(111): 0.75 eV; on Au(111): 0.75 eV). There are different possible reasons for the necessity of the additional shift. One reason could be that the clusters partially sink into the xenon layer. This changes the surroundings of the clusters and the value of ε in equation (7.2) for the cluster charging energy. However this would reduce the charging energy and therefore it can contribute only in combination with other reasons for the shift. The value of α influencing the absolute position of the electron affinity and the ionisation potential [8] varies for free beam clusters and deposited ones [117] and can be a reason for a different position of the UPS spectra of free beam clusters and deposited clusters. A third possible reason could be the influence of the electron affinity of xenon and the reduction of the work function of the substrate due to the xenon layer [113]. A combination of all these possible reasons is imaginable. But further investigations are necessary.

The position of the cluster d-band flank for clusters deposited on xenon was investigated. The position of the cluster d-band flank shifts with increasing cluster size to higher energies. For clusters on xenon the shift was bigger than for clusters on HOPG and Ag(111). The main reason for this is the contribution of the cluster size dependent charging energy of the clusters deposited on xenon (see, e.g., figure **37** & **38**).

Because the results for Cu_{147} were the best obtained for these measurements their results on different substrates were compared with each other. An overall good agreement regarding the shape of the cluster spectra could be observed on the different substrates demonstrating that the obtained results are independent of the underlying substrate. In addition a shift of the energy position of the cluster spectrum could be observed dependent on the work function of the substrate as already observed for big clusters and metal islands in [90]. The cluster spectra on Xe/Au(111) are shifted about 0.4 eV to higher energies related to the spectra on Xe/Cu(111), which is the difference of the work function of Cu(111) (4.94 eV) and Au(111) (5.31 eV) [114] and confirms the

results from ref. [90]. The Cu_{147} spectra on Xe/HOPG and Xe/Cu(111) lie at the same energy position in the UPS spectrum. The missing shift can be identified in the additional shift needed to compare the free beam spectra with the spectra of deposited clusters (on HOPG: 0.35 eV; on Cu(111): 0.75 eV). The difference between the additional shifts cancels the difference between the work function of HOPG (4.5 eV [107, 108]) and Cu(111). As already mentioned the xenon layer can change the work function of the substrate, but this change can be different for HOPG and the metals copper and gold.

In addition to xenon, copper clusters (Cu_{55}- Cu_{309}) were deposited on 10 ML argon on top of 60 ML xenon on Ag(111). Comparing the obtained UPS spectra with spectra of copper clusters on Xe/Cu(111) it becomes clear that the spectra on argon are shifted to higher energies. The cluster d-band is clearly visible and the s-p-band is shifted above the Fermi edge. A possible reason for this shift could be the influence of the electron affinity of the rare gas layer. It was described in ref. [112] that the electron affinity shifts the vacuum energy of the substrate in the phase accumulation model of the surface state and with this the energy of the surface state. Similarly the electron affinity can also influence the energies here. In addition the adsorption of xenon decreases the work function of the substrate and it is possible that an additional layer of argon would lead to an additional decrease of the substrate work function, as in the case of a simple xenon layer. Additionally the work function difference between the cluster material (copper) and the substrate (Ag(111)) leads to an extra shift in the UPS spectrum, as for copper clusters on Au(111). So the influence of the electron affinity of the rare gas layer, the work function decrease and the work function difference between cluster and substrate could be responsible for the shift of the cluster spectra on Ar/Xe/Ag(111). But to prove this assumption further investigations are necessary.

In addition to copper, silver clusters were deposited on 60 ML xenon on HOPG and Ag(111). On HOPG it was not possible to detect a cluster signal with UPS. This behaviour suggests that the silver clusters sunk into the xenon layer. This behaviour was already observed for silver clusters deposited on Xe/GaAs [115]. The clusters are covered with a xenon skin and than drawn through the xenon layer via van der Waals forces until they reach the substrate. To avoid this experiments of silver clusters deposited on Xe/Ag(111) at lower temperatures were performed.

Silver clusters (Ag_{55}- Ag_{309}) were deposited on 60 ML xenon on Ag(111) and investigated with UPS. A size dependent s-p-band signal could be detected, but it was not possible to measure the cluster d-band because of the used photon energy ($h\upsilon$= 11.62 eV). Therefore the flank of the cluster s-p-band was investigated which shows a similar behaviour as the cluster d-band in the case of deposited copper clusters: With increasing cluster size the position of the s-p-band shifts to higher energies. This is in agreement with former investigations (see ref. [85]). The obtained spectra were compared with cluster spectra measured in the free beam [8] and again some similarities could be found regarding the shape of the cluster spectra, especially in the case of Ag_{92}. For a proper comparison of the free beam spectra with the spectra of deposited clusters the free beam spectra were shifted according to equation (7.3) (chapter 7.2). As for the copper clusters again an additional shift is needed for a good agreement between the spectra. The shift is of the same dimension as for copper clusters on Xe/Cu(111) and Xe/Au(111) which confirms the results from ref. [90] (see above).

Concluding one can say that it was possible to compare results of deposited clusters on a xenon layer on different substrates with UPS results of free beam clusters measured with different photon energies successfully. The shift needed to compare UPS spectra of charged free beam clusters with spectra of neural clusters deposited on rare gas layers could be calculated successfully up to some tenth eV. Furthermore the obtained results could be proved to be reproducible on the same and on different substrates. Occurring differences between different sample systems could be described correctly. But, it became apparent that the models used need further refinement.

9.2. Outlook

The reasons for the shift of copper clusters deposited on Ar/Xe/Ag(111) versus copper clusters deposited on, e.g., Xe/Cu(111) and the reasons for the additional shift necessary for the comparison of free beam clusters and deposited ones need more detailed investigation. Thereto current UPS experiments are running to investigate the behaviour of C_{60} molecules, which represent a well known model system, evaporated on different substrates and different adsorbed rare gas layers.

For future experiments another substrate will be used than rare gas layers adsorbed on surfaces, namely alumina (Al_2O_3). For this purpose thin Al_2O_3 films are grown on a $Ni_3Al(111)$ single crystal by surface oxidation [120]. The goal is to deposit size selected metal clusters on this oxide surface and investigate them with UPS, STM and STS. Therefore a collaboration with *Conrad Becker* from the "Université de la Méditerranée" and "Université Paul Cézanne" is started.

Alumina films on $Ni_3Al(111)$ show a superstructure due to the superposition of the hexagonal $Ni_3Al(111)$ substrate lattice and the hexagonal oxygen layers. As a result a "network structure" develops with an internal so-called "dot structure" [120]. The dot structure comes from special electronic states of the alumina film and presents a good template for the nucleation and growth of clusters. After evaporation of metal onto this surface this results in a well ordered cluster arrangement with a $(\sqrt{3}\times\sqrt{3})R30°$ symmetry of the clusters which represents a perfect model of a supported catalyst. In addition evaporated metal clusters on alumina show a high temperature stability. For further information see ref. [120].

The results in the literature refer only to clusters grown on alumina which results in a broad size distribution of the clusters. Therefore the investigation of size selected clusters deposited under controlled conditions represents an interesting new point of view. The question is if the deposited clusters are mobile on the surface and also arrange themselves in a $(\sqrt{3}\times\sqrt{3})R30°$ symmetry as in the case of the grown clusters or lie randomly on the surface.

In addition the change of the electronic structure of the clusters due to the stronger interaction with the surface will be investigated in comparison to the electronic structure of free beam clusters.

To enable the preparation of the desired thin alumina films a heating station [42] will be put in operation in the preparation chamber of the surface science facility in the near future.

10 Appendix

10.1. Transmission electron microscopy

This chapter presents results received during a collaboration with the "Max Planck Institut" (MPI) in Stuttgart. First the working principle of a transmission electron microscope (TEM) is described and then sample preparation and experimental results are presented.

For TEM a sample is illuminated with an electron beam and the electrons are transmitted through the sample where they interact with its atoms. A part of the electrons pass through the sample without interaction and the other part is scattered elastically and inelastically. The energy loss of the inelastically scattered electrons can be used for spectroscopic measurements (electron energy loss spectroscopy (EELS)) and allows an investigation of, e.g., the chemical composition of the sample.

An image of the sample is formed by measuring the electrons that are not scattered but go right through the sample. The scattered electrons are suppressed with the help of a slit. At thicker structures the electrons are scattered more than at thinner ones so the intensity of the transmitted electrons is higher the thinner an object is. In this way an image of the structure of the sample is achieved.

The MPI in Stuttgart uses a special type of TEM, a scanning transmission electron microscope (STEM). Here, a focussed electron beam is scanned over a specific area in a raster. With a STEM high-resolution images are possible by measuring the incoherent elastically scattered electrons from the sample, which exit in a high angle. This method is called high-angle annular dark field (HAADF) [121] imaging and was used here to measure clusters deposited on thin surfaces. The intensity of the HAADF signal is dependent on the atomic number of the sample material and for thin samples also on its thickness.

A schematic of a typical TEM is presented in figure I. For a detailed description of the working principle and set-up of a transmission electron microscope see, e.g. ref. [121, 122].

For TEM measurements special samples are needed (figure II) which do not fit in the sample manipulator used here. Therefore, a special sample holder was build by *Christoph Schröder* for cluster deposition (figure II). The samples are placed in the holes in a way they are not damaged and the grid prevents the samples from falling down.

Silver clusters with 923, 1100, 1200 and 2493 atoms were deposited on the TEM samples at room temperature with 20 pAmin coverage, respectively. The deposition

procedure was the same as described in chapter 5.2, including a soft landing of the clusters.

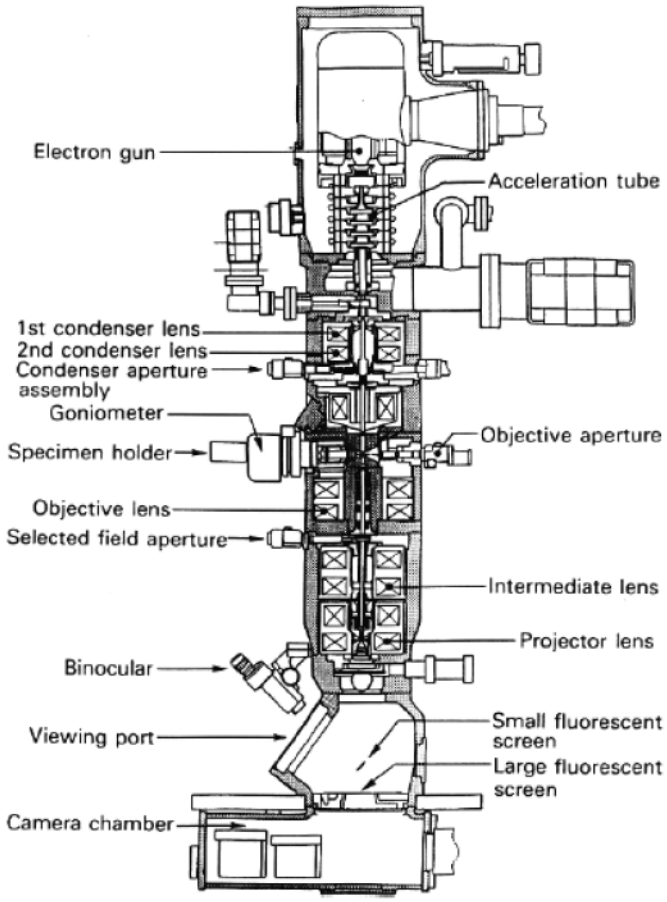

Figure I: Typical set-up of a transmission electron microscope. [121]

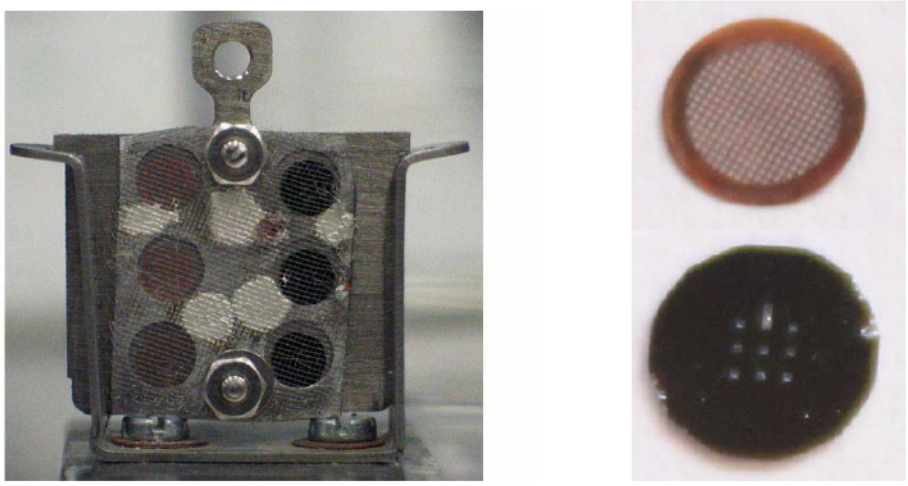

Figure II: Left: Sample holder for the TEM samples build by *Christoph Schröder*. Right: The two TEM samples used. Top: 2 nm amorphous carbon on a copper grid. Bottom: 5 nm silica in nine 100µm x 100 µm openings. Diameter: 3 mm.

After deposition the clusters were exported from the vacuum chamber and send in a bottle filled up with argon to the MPI in Stuttgart for TEM measurements. A selection of the resulting TEM images is presented in figure III.

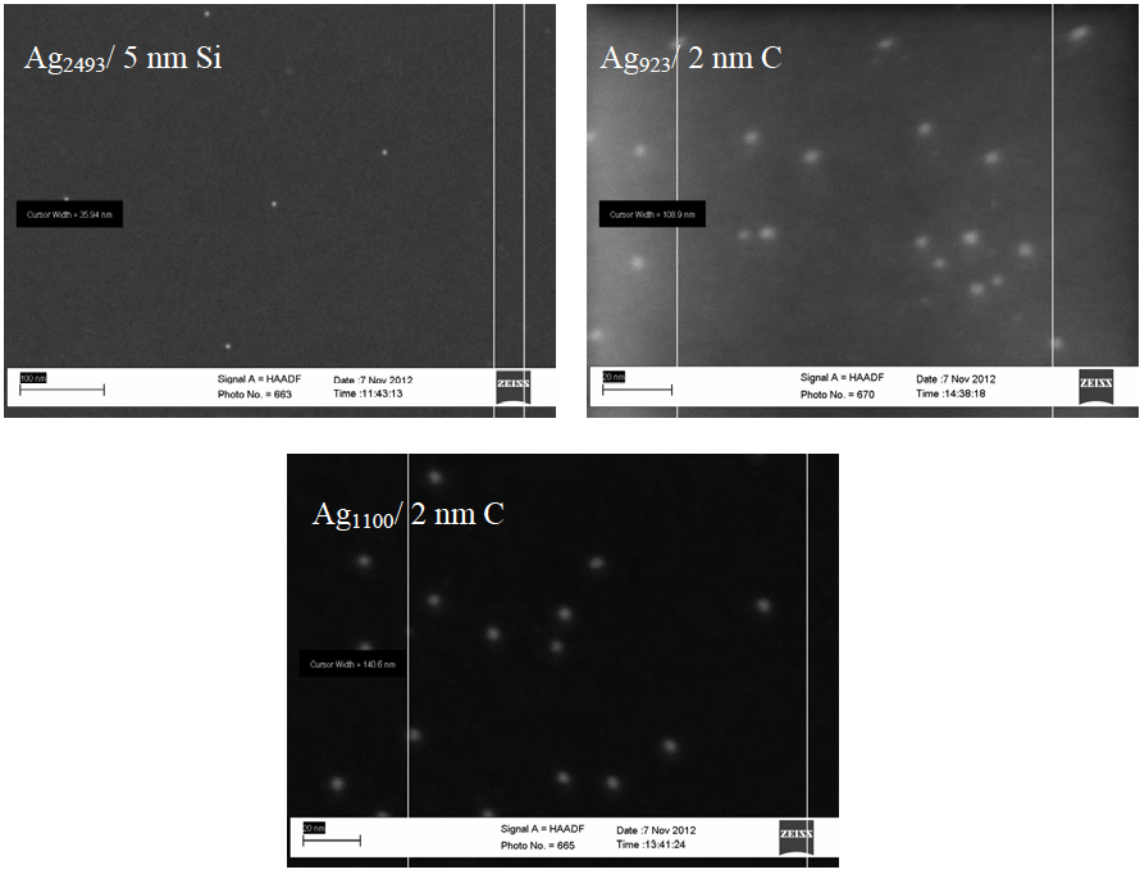

Figure III: STEM images of silver clusters deposited on a 5 nm silica or a 2 nm amorphous carbon substrate. The images were made in the HAADF mode.

From the TEM images the width of the clusters can be determined. The width of the clusters was measured as the full width half maximum in the greyscale images by visual inspection. The measured width and calculated cluster heights for spherical clusters are given in table A.

cluster	number of counted clusters	width measured with TEM [nm]	cluster height for spherical clusters [nm]
923	31	3.03 ± 0.27	3.12
1100	40	3.34 ± 0.30	3.30
2493	7	5.59 ± 0.76	4.34

Table A: Measured cluster width and calculated cluster heights for the deposited clusters. The error of the measured width is the error of the standard deviation. Ag_{923} and Ag_{1100} were deposited on 2 nm amorphous carbon and Ag_{2493} was deposited on 5 nm silica.

The results for Ag_{923} and Ag_{1100} are of the same magnitude as the calculated height. Ag_{923} was already measured with the STM by *Stefanie Duffe* during her dissertation on one and two monolayers C_{60} on HOPG at 77 K with similar results for the cluster height as in the TEM measurements [47][5]. The reason for the big difference in the case of Ag_{2493} could be the poor statistics combined with the worse image quality on the silica substrate as can already be seen in the big error of the standard deviation. In addition silver clusters deposited on silica show a strong cluster-surface interaction, see, e.g., ref. [123], which leads to a deformation of the clusters. In [123] an axial ratio of $c/a = 0.86$ was determined for the clusters, with a as the major axis parallel and c as the minor axis perpendicular to the substrate, i.e. the clusters become "flatter" but also "broader". This could also be a possible reason for the difference between the measured and the calculated cluster height in the case of Ag_{2493}.

[5] On one ML C_{60}: 2.98±0.18 nm; on two ML C_{60}: 3.06±0.22 nm [47].

10.2. Parameter for cluster deposition

Ag/HOPG

cluster	mass [amu]	coverage [pAmin]	deposition time	τ_w	bias [V]	position of the manipulator
55	5901	15	1 min 21 sec	40	-3.4	X= 23.5 mm Y=15 mm Z=176.5 mm Φ= 74°
55	5901	30	2 min 42 sec	40	-3.4	X= 23.5 mm Y=12.5 mm Z=176.5 mm Φ= 74°
71	7613	15	2 min	40	-3.3	X= 23.5 mm Y=10.2 mm Z=176.5 mm Φ= 74°
71	7613	30	4 min	40	-3.3	X= 23.5 mm Y=10 mm Z=179 mm Φ= 74°
92	9859	15	2 min 30 sec	40	-2	X= 23.5 mm Y=10 mm Z=181.5 mm Φ= 74°
147	15742	10	2 min 38 sec	40	-0.3	X= 23.5 mm Y=15 mm Z=179 mm Φ= 74°
147	15742	20	5 min 16 sec	40	-0.3	X= 23.5 mm Y=15 mm Z=181.5 mm Φ= 74°
55	5901	129	15 min	40	-3.4	X= 23.5 mm Y=12.5 mm Z=181.5 mm Φ= 74°

Substrate temperature during deposition: 70 K

cluster	mass [amu]	coverage [pAmin]	deposition time	τ_w	bias [V]	position of the manipulator
147	15710	10	2 min 34 sec	40	7	X= 22.5 mm Y=15 mm Z=180 mm Φ= 74°
309	33001	10	2 min 52 sec	40	12	X= 22.5 mm Y=15 mm Z=182.5 mm Φ= 74°
309	33001	20	5 min 43 sec	40	12	X= 22.5 mm Y=10 mm Z=182.5 mm Φ= 74°
561	59897	10	2 min 23 sec	40	20	X= 22.5 mm Y=10 mm Z=177.5 mm Φ= 74°
561	59897	20	4 min 47 sec	40	20	X= 22.5 mm Y=10 mm Z=180 mm Φ= 74°
923	98534	10	4 min 10 sec	40	23	X= 22.5 mm Y=12.5 mm Z=177.5 mm Φ= 74°
923	98534	20	8 min 20 sec	40	23	X= 22.5 mm Y=15 mm Z=177.5 mm Φ= 74°
561	59897	63	15 min	40	20	X= 22.5 mm Y=12.5 mm Z=182.5 mm Φ= 74°

Substrate temperature during deposition: 125 K

Cu/HOPG

cluster	mass [amu]	coverage [pAmin]	deposition time	τ_W	bias [V]	position of the manipulator
34	2165	40	10 min 31 sec	40	-10	X= 24 mm Y=15 mm Z=180 mm Φ= 74°
55	3494	15	3 min 16 sec	40	-10	X= 24 mm Y=10 mm Z=177.5 mm Φ= 74°
55	3494	30	7 min 24 sec	40	-10	X= 24 mm Y=12.5 mm Z=177.5 mm Φ= 74°
58	3683	15	3 min 16 sec	40	-10	X= 24 mm Y=12.5 mm Z=180 mm Φ= 74°
58	3683	30	6 min 34 sec	40	-10	X= 24 mm Y=10 mm Z=180 mm Φ= 74°
71	4505	15	3 min 29 sec	40	-8	X= 24 mm Y=15 mm Z=182.5 mm Φ= 74°
71	4505	30	6 min 59 sec	40	-8	X= 24 mm Y=10 mm Z=182.5 mm Φ= 74°
92	5834	20	5 min 53 sec	40	-8	X= 24 mm Y=15 mm Z=177.5 mm Φ= 74°
58	3683	70	15 min 55 sec	40	-10	X= 24 mm Y=12.5 mm Z=182.5 mm Φ= 74°

Substrate temperature during deposition: 125 K

Cu/Ag(111)

cluster	mass [amu]	coverage [pAmin]	deposition time	τ_W	bias [V]	position of the manipulator
147	9579	66	22 min	40	-6	X= 23.5 mm Y=11 mm Z=183.33 mm Φ= 74°
923	60049	19	10 min 33 sec	40	12	X= 23.5 mm Y=11 mm Z=180.33 mm Φ= 74°
923	60049	100	41 min 40 sec	40	14	X= 23.5 mm Y=13 mm Z=181.83 mm Φ= 74°

Substrate temperature during deposition: 20 K

Ag/Au(111)

cluster	mass [amu]	coverage [pAmin]	deposition time	τ_W	bias [V]	position of the manipulator
55	5892	9	1 min 17 sec	40	-8	X= 26.2 mm Y=9.7 mm Z=179.5 mm Φ= 74°
80	8559	9	1 min 13 sec	40	-8	X= 26.2 mm Y=13.7 mm Z=179.5 mm Φ= 74°
95	10160	9	1 min 19 sec	40	-8	X= 26.2 mm Y=11.7 mm Z=179.5 mm Φ= 74°
147	15709	9	3 min 55 sec	40	-6	X= 26.2 mm Y=7.7 mm Z=189.5 mm Φ= 74°
86	9200	9	4 min 46 sec	40	-2.5 (1 eV per cluster)	X= 26.2 mm Y=11.7 mm Z=181.5 mm Φ= 74°
86	9200	9	1 min 5 sec	40	-20 (15 eV per cluster)	X= 26.2 mm Y=13.7 mm Z=181.5 mm Φ= 74°
86	9200	9	1 min 3 sec	40	-40 (34 eV per cluster)	X= 26.2 mm Y=13.7 mm Z=183.5 mm Φ= 74°
86	9200	9	1 min	40	-155 (150 eV per cluster)	X= 26.2 mm Y=11.7 mm Z=183.5 mm Φ= 74°
86	9200	9	1 min	40	-345 (340 eV per cluster)	X= 26.2 mm Y=9.7 mm Z=189.5 mm Φ= 74°

Substrate temperature during deposition: 77 K

The deposition parameters for Ag_{86} deposited with 3 eV per cluster can be found in [80]. This deposition was preformed during my diploma thesis.

cluster	mass [amu]	coverage [pAmin]	deposition time	τ_w	bias [V]	position of the manipulator
55	6016	9	2 min	40	-8	X= 23.5 mm Y=12 mm Z=182.5 mm Φ= 74°
86	9391	9	2 min 54 sec	40	-8	X= 23.5 mm Y=10 mm Z=182.5 mm Φ= 74°
147	16033	9	3 min 6 sec	40	-9	X= 23.5 mm Y=11 mm Z=181 mm Φ= 74°

Substrate temperature during deposition: 11 K

Cu/60 ML Xe/HOPG

cluster	mass [amu]	coverage [pAmin]	deposition time	τ_w	bias [V]	position of the manipulator
55	3547	20	16 min 40 sec	40	-2	X= 23.5 mm Y=12 mm Z=179.46 mm Φ= 74°
92	5921	20	12 min 30 sec	40	-2	X= 23.5 mm Y=14.5 mm Z=181.96 mm Φ= 74°
147	9449	20	10 min 32 sec	40	0	X= 23.5 mm Y=9.5 mm Z=181.96 mm Φ= 74°
309	19843	100	33 min 20 sec	40	0	X= 23.5 mm Y=12 mm Z=184.46 mm Φ= 74°

Substrate temperature during deposition: 25 K

Cu/60 ML Xe/Cu(111)

cluster	mass [amu]	coverage [pAmin]	deposition time	τ_W	bias [V]	position of the manipulator
147	9448	15	16 min 40 sec	40	-1	X= 23.5 mm Y=12 mm Z=179.96 mm Φ= 74°
309	19848	15	10 min	40	1.5	X= 23.5 mm Y=12 mm Z=183.96 mm Φ= 74°
923	59268	15	6 min 49 sec	40	10	X= 23.5 mm Y=10 mm Z=181.96 mm Φ= 74°
923	59268	100	55 min 33 sec	40	10	X= 23.5 mm Y=14 mm Z=181.96 mm Φ= 74°

Substrate temperature during deposition: 20 K

cluster	mass [amu]	coverage [pAmin]	deposition time	τ_W	bias [V]	position of the manipulator
112	7253	20	20 min	40	0	X= 23.5 mm Y=10 mm Z=181.96 mm Φ= 74°
147	9515	20	15 min 23 sec	40	-1	X= 23.5 mm Y=12 mm Z=183.46 mm Φ= 74°
147	9515	40	30 min 46 sec	40	-1	X= 23.5 mm Y=12 mm Z=180.46 mm Φ= 74°
309	19989	100	71 min 26 sec + 30 min at 0 V bias	40	2	X= 23.5 mm Y=14 mm Z=181.96 mm Φ= 74°

Substrate temperature during deposition: 20 K

Cu/60 ML Xe/Au(111)

cluster	mass [amu]	coverage [pAmin]	deposition time	τ_W	bias [V]	position of the manipulator
92	6050	20	10 min 32 sec	40	-5	X= 23.5 mm Y=10.5 mm Z=181.53 mm Φ= 74°
112	7363	20	7 min 8 sec	40	-7	X= 23.5 mm Y=12 mm Z=180.03 mm Φ= 74°
147	9660	20	6 min 40 sec	40	-6	X= 23.5 mm Y=12 mm Z=183.03 mm Φ= 74°
923	59904	100	45 min 27 sec	40	12.5	X= 23.5 mm Y=13.5 mm Z=181.53 mm Φ= 74°

Substrate temperature during deposition: 20 K

cluster	mass [amu]	coverage [pAmin]	deposition time	τ_W	bias [V]	position of the manipulator
147	9466	40	66 min 40 sec	40	-7.5	X= 23.5 mm Y=10.5 mm Z=181.53 mm Φ= 74°
309	19879	30	34 min 20 sec	40	0	X= 23.5 mm Y=12 mm Z=180.03 mm Φ= 74°
309	19879	100	66 min 40 sec	40	-8	X= 23.5 mm Y=13.5 mm Z=181.53 mm Φ= 74°

Substrate temperature during deposition: 20 K

cluster	mass [amu]	coverage [pAmin]	deposition time	τ_W	bias [V]	position of the manipulator
112	7281	30	23 min 5 sec	40	-7	X= 23.5 mm Y=12 mm Z=183.03 mm Φ= 74°
147	9553	30	30 min	40	-4	X= 23.5 mm Y=12.25 mm Z=181.28 mm Φ= 74°
309	20067	20	28 min 34 sec	40	-1	X= 23.5 mm Y=10.5 mm Z=181.53 mm Φ= 74°
309	20067	100 + 60	11 min 45 sec + 7 min 4 sec	10	-10	X= 23.5 mm Y=13.5 mm Z=181.53 mm Φ= 74°

Substrate temperature during deposition: 23 K

Cu/10 ML Ar/60 ML Xe/Ag(111)

cluster	mass [amu]	coverage [pAmin]	deposition time	τ_W	bias [V]	position of the manipulator
55	3528	10	9 min 5 sec	40	-3	X= 23.5 mm Y=9 mm Z=181.83 mm Φ= 74°
92	5893	10	7 min 42 sec	40	-2.5	X= 23.5 mm Y=11 mm Z=183.33 mm Φ= 74°
147	9409	10	7 min 9 sec	40	-2	X= 23.5 mm Y=11 mm Z=180.33 mm Φ= 74°
309	19763	100	62 min 30 sec	40	-1	X= 23.5 mm Y=13 mm Z=181.83 mm Φ= 74°

Substrate temperature during deposition: 11 K

Ag /60 ML Xe/Ag(111)

cluster	mass [amu]	coverage [pAmin]	deposition time	τ_W	bias [V]	position of the manipulator
55	6066	20	14 min 17 sec	40	-12	X= 23.5 mm Y=12 mm Z=180.33 mm Φ= 74°
147	16180	20	10 min 32 sec	40	-12	X= 23.5 mm Y=10 mm Z=181.83 mm Φ= 74°
309	33989	20	10 min 32 sec	40	-8	X= 23.5 mm Y=12 mm Z=183.33 mm Φ= 74°
309	33989	100	45 min 27 sec	40	-10	X= 23.5 mm Y=14 mm Z=181.83 mm Φ= 74°

Substrate temperature during deposition: 17 K

cluster	mass [amu]	coverage [pAmin]	deposition time	τ_W	bias [V]	position of the manipulator
55	6035	10	2 min	40	-3	X= 23.5 mm Y=9 mm Z=181.83 mm Φ= 74°
92	10080	10	2 min 24 sec	40	-2	X= 23.5 mm Y=11 mm Z=183.33 mm Φ= 74°
147	16093	10	3 min 42 sec	40	0	X= 23.5 mm Y=11 mm Z=180.33 mm Φ= 74°
309	33805	100	23 min 16 sec	40	0	X= 23.5 mm Y=13 mm Z=181.83 mm Φ= 74°

Substrate temperature during deposition: 15 K

TEM

Ag/2 nm C

cluster	mass [amu]	coverage [pAmin]	deposition time	τ_w	bias [V]	position of the manipulator
923	100003	20	16 min 40 sec	40	7	X= 23 mm Y=15.84 mm Z=175.36mm Φ= 74°
1100	119174	20	22 min 13 sec	40	8	X= 23 mm Y=11.69 mm Z=175.76 mm Φ= 74°
1200	130004	20	28 min 34 sec	40	10	X= 23 mm Y=7.60 mm Z=175.95 mm Φ= 74°

Substrate temperature during deposition: room temperature

Ag/5 nm Si

cluster	mass [amu]	coverage [pAmin]	deposition time	τ_w	bias [V]	position of the manipulator
923	100003	20	12 min 30 sec	40	7	X= 23 mm Y=15.84 mm Z=175.36mm Φ= 74°
1200	130004	20	22 min 13 sec	40	10	X= 23 mm Y=11.69 mm Z=175.76 mm Φ= 74°
2493	270004	20	28 min 34 sec	40	6	X= 23 mm Y=7.60 mm Z=175.95 mm Φ= 74°

Substrate temperature during deposition: room temperature

11 Reference

[1] U. Kreibig, M. Vollmer,
Optical properties of metal clusters,
Springer (1995)

[2] H. Haberland, K. Kleinermanns, F. Träger,
Cluster,
Lehrbuch der Experimentalphysik edited by W.Raith, de Gruynter (2005)

[3] T. Ahmad, I.A. Wani, N. Manzoor, J. Ahmed, A.M. Asiri,
Biosynthesis, structural characterization and antimicrobical activity of gold and silver nanoparticles,
Coll. Surf. B **107**, 227 (2013)

[4] S. Singamaneni, V.N. Bliznyuk, C. Binek, E.Y. Tsymbal,
Magnetic nanoparticles: Recent advances in synthesis, self-assembly and applications,
J. Mater. Chem. **21**, 16819 (2011)

[5] A. Sanchez et al,
When gold is not noble: Nanoscale gold catalysts,
J. Phys. Chem. **103**, 9573 (1999)

[6] F. Baletto, R. Ferrando,
Structural properties of nanoclusters: Energetic, thermodynamic and kinetic effects,
Rev. Modern Phys. **77**, 371 (2005)

[7] V.N. Popok, I. Barke, E.E.B. Cambell, K.-H. Meiwes-Broer,
Cluster-surface interaction: From soft landing to implantation,
Surf. Sci. Rep. **66**, 347 (2011)

[8] O. Kostko,
Photoelectron spectroscopy of mass-selected sodium, coinage metal and divalent metal cluster anions,
Dissertation, Albert-Ludwig-Universität Freiburg (2007)

[9] D.E. Beck,
Self-consistent calculation of the polarizability of small jellium spheres,
Phys. Rev. B **30**, 6935 (1984)

[10] D.E. Beck,
Self-consistent calculation of the electronic structure of small jellium spheres,
Solid State Commun. **49**, 381 (1984)

[11] W. Ekardt,
Work function of small metal particles: Self-consistent spherical jellium-background model,
Phys. Rev. B **29**, 1558 (1984)

[12] W. Ekardt,
Dynamical polarizability of small metal particles: Self-consistent spherical jellium model,
Phys. Rev. Let. **52**, 1925 (1984)

[13] W.A. de Heer,
The physics of simple metal clusters: Experimental aspects and simple models,
Rev. Modern Phys. **65**, 611 (1993)

[14] M.M. Kappes, R.W. Kunz, E. Schumacher,
Production of large sodium clusters (Na_x, $x \leq 65$) by seeded beam expansions,
Chem. Phys. Lett. **91**, 413 (1982)

[15] W.D. Knight et al,
Electronic shell structure and abundances of sodium clusters,
Phys. Rev. Lett. **52**, 2141 (1984)

[16] W.D. Knight. W.A. de Heer, K. Klemenger, W.A. Saunders,
Electronic shell structure in potassium clusters,
Solid State Commun. **53**, 445 (1985)

[17] B. von Issendorff,
The electronic structure of alkali and noble metal clusters,
Handbook of nanophysics 2, Clusters and Fullerens, 1st edition, edited by K.D. Sattler, CRC Press (2011)

[18] W.A. de Heer, W.D. Knight, M.Y. Chou, M.L. Cohen,
Electronic shell structure and metal clusters,
Solid States Physics **40**, edited by H. Ehrenreich and D. Turnbull, 93 (1987)

[19] M.L. Cohen, M.Y. Chou, W.D. Knight, W.A. de Heer,
Physics of metal clusters,
J. Phys. Chem. **91**, 3141 (1987)

[20] H.A. Jahn, E. Teller,
Stability of polyatomic molecules in degenerate electronic states. I. Orbital degeneracy,
Proc. R. Soc. London Ser. A **161**, 220 (1937)

[21] K. Clemenger,
Ellipsoidal shell structure in free-electron metal clusters,
Phys. Rev B **32**, 1359 (1985)

[22] B.R. Mottelson, S.G. Nilsson,
Classification of the nucleonic states in deformed nulei,
Phys. Rev. **99**, 1615 (1955)

[23] G. Alameddin, J. Hunter, D. Cameron, M.M. Kappes
Electronic and geometric structure in silver clusters,
Chem. Phys. Let. **192**, 122 (1992)

[24] O. Echt, K. Sattler, E. Recknagel,
Magic numbers for spherer packings: Experimental verification in free xenon clusters,
Phys. Rev. Let. **47**, 1121 (1981)

[25] T.P. Martin, T. Bergmann, H. Göhlich, T. Lange,
Observation of electronic shells and shells of atoms in large Na clusters,
Chem. Phys. Let. **172**, 209 (1990)

[26] P. Stampfli et al,
Unified model for the shell structure in the cohesive energy, ionization potential and photoyield of metallic clusters,
Phys. Rev. Let. **69**, 3471 (1992)

[27] A.L. Mackay,
A dense non-crystallographic packing of equal spheres,
Acta Cryst. **15**, 916 (1962)

[28] T.P. Martin,
From atoms to solids,
Solid State Ion. **131**, 3 (2000)

[29] I.A. Harris, R.S. Kidwell, J.A. Northby,
Structure of charged argon clusters formed in a free jet expansion,
Phys. Rev. Let. **53**, 2390 (1984)

[30] O. Kostko, B. Huber, M. Moseler, B. von Issendorff,
Structure determination of medium-sized sodium clusters,
Phys. Rev. Let. **98**, 043401 (2007)

[31] M. Moseler et al,
Thermal effects in the photoelectron spectra of Na-N clusters (N= 4-19),
Phys. Rev. B **68**, 165413 (2003)

[32] R. Wiesendanger, D. Anselmetti,
STM on Layered Materials,
Scanning tunnelling microscopy 1 edited by H. J. Güntherodt, Springer Verlag (1994)

[33] C.E. Mortimer, U. Müller
Chemie,
Thieme-Verlag, 8th edition (2003)

[34] Ch. Kittel,
Einführung in die Festkörperphysik,
Oldenburg Verlag, 14th edition (2006)

[35] Ch. Wöll, S. Chiang, R.J. Wilson, P.H. Lippel,
Determinetion of atom positions at stacking-fault dislocations on Au(111) by scanning tunnelling microscopy,
Phys. Rev. B **39**, 7988 (1989)

[36] J.V. Barth, H. Brune, G. Ertl, R.J. Behm,
Scanning tunnelling microscopy observations on the reconstructed Au(111) surface: Atomic structure, long-range superstructure, rotational domains, and surface defects
Phys. Rev. B **42**, 9307 (1990)

[37] W. Shockley,
On the surface states associated with periodic potential,
Phys. Rev. **56**, 317 (1939)

[38] F. Reinert, G. Nicolay, S. Schmidt, D. Ehm, S. Hüfner,
Direct measurments of the L-gap surface states on the (111) face of noble metals by photoelectron spectroscopy,
Phys. Rev. B **63**, 115415 (2001)

[39] A. Zangwill,
Physics at surfaces,
Cambridge University Press, 4th edition (1992)

[40] N. Grönhagen, T.T. Järvi, N. Miroslawski, H. Hövel, M. Moseler,
Decay kinetics of cluster-beam-deposited metal particles,
J. Phys. Chem. C **116**, 19327 (2012)

[41] A. Jablonski, K. Wandelt,
Quantitative aspects of ultraviolet photoemission of adsorbed xenon- A review,
Surf. Inter. Anal. **17**, 611 (1991)

[42] D. Boeker,
Wachstum von Metallclusters auf Edelgasschichten und Analyse der elektronischen Wechselwirkung mit Hilfe von Ultravioletter Photoelectronen Spektroskopie,
Diploma thesis, Technische Universität Dortmund (2004)

[43] R.J. Behm, C.R. Brunndle, K. Wandelt,
The underlayer influence on photoemission and thermal desorption of xenon adsorbed on Ag(111),
J. Chem. Phys. **85**, 1061 (1986)

[44] H.Haberland et al,
Filling of micron-sized-contact holes with copper by energetic cluster impact,
J. Vac. Sci. Technol. A **12**, 2925 (1994)

[45] B. von Issendorff, R.E. Palmer,
A new transmission infinite range mass selector for clusters nanoparticle beams,
Rev. Sci. Instr. **70**, 4497 (1999)

[46] S. Duffe (former Krause),
Massenselektierte Cluster deponiert auf Oberflächen,
Diploma thesis, Technische Universität Dortmund (2006)

[47] S. Duffe,
Thermally activated processes and electronic properties of size selected Ag clusters and grown metal islands on C_{60} functionalized surfaces,
Dissertation, Technische Universität Dortmund (2009)

[48] M. Wutz, H. Adam, W. Walcher,
Theorie und Praxis der Vakuumtechnik,
Vieweg Verlag, 5th edition (1992)

[49] H. Hövel et al,
High-resolution photoemission combined with low-temperature STM,
J. Electr. Spectros. **88-91**, 1015 (1998)

[50] T. Becker, H. Hövel, M. Tschudy, B. Reihl,
Applications with a new low-temperature UHV STM at 5 K,
Appl. Phys. A **66**, 27 (1998)

[51] I. Barke,
Edelgasschichten auf der Au(111)-Oberfläche: Präparation und lokale Tunnelspektroskopie,
Diploma thesis, Technische Universität Dortmund (2001)

[52] O. Albrektsen, H.W.M. Salemink, K.A. Morch, A.R. Tholen,
Reliable tip preparation for high-resolution scanning-tunneling-microscopy,
J. Vac. Sci. Tech. B **12**, 3187 (1994)

[53] E. Taglauer,
Surface cleaning using sputtering,
Appl. Phys. A **51**, 238 (1990)

[54] K. Reichelt, H.O. Lutz,
Hetero-epitaxial growth of vacuum evaporated silver and gold,
J. Cryst. Gro. **10**, 103 (1971)

[55] Ch. Yin,
Depostion and characterizationof size-selected metal clusters,
Dissertation, Albert Ludwig Universität Freiburg (2007)

[56] D. Engemann,
Anwendung und Weiterentwicklung von Photoemission und Rastertunnelmikroskopie zur Untersuchung von massenselektierten Ag und Cu clustern deponiert auf Oberflächen,
Diploma thesis, Technische Universität Dortmund (2011)

[57] S. Abbet, K. Judai, L. Kger, U. Heiz,
Synthesis of monodispersed model catalysts using softlanding cluster deposition,
Pure Appl. Chem. **74**, 1572 (2002)

[58] S. Duffe et al,
Softlanding and STM imaging of Ag561 clusters on a C60 monolayer,
Eur. Phys. J. D **45**, 401 (2007)

[59] N. Grönhagen,
Cluster-surface interaction of mass selected Ag clusters with graphite, gold and C_{60} functionalized surfaces,
Dissertation, Technische Universität Dortmund (2011)

[60] H. Lüth,
Surfaces and interfaces of solids,
Sringer Series in Surface Science **15** (1993)

[61] G. Binning, H. Rohrer, C. Gerber, E. Weibel,
Tunneling through a controllable vacuum gap,
Appl. Phys. Lett. **40**, 57 (1981)

[62] G. Binning, H. Rohrer, C. Gerber, E. Weibel,
Surface studies by scanning tunneling microscopy,
Phys. Rev. Lett. **49**, 57 (1982)

[63] F. Schwabl,
Quantenmechanik I,
6th edition, Springer Verlag (2005)

[64] J. Simmons,
Gereralized formula for the electric tunnel effect between similar electrodes separated by a thin insulating film,
J. Appl. Phys. **34**, 1793 (1963)

[65] J. Tersoff, D.R. Hamann,
Theory of the scanning tunneling microscope,
Phys. Rev. B **31**, 805 (1985)

[66] R. Howland, L. Benatar,
A practical guide to scanning probe microscopy,
Park Scientific Instruments (1993-96)

[67] I.S. Tilinin, M.K. Rose, J.C. Dunphy, M. Salmeron, M.A. Van Hove,
Identification of adatoms on metal surfaces by STM: experiment and theory,
Surf. Sci. **418**, 511 (1998)

[68] H. J. Güntherodt,
Scanning tunneling microscopy I&II,
Springer Ser. Surf. Sci. **20, 28** (1992)

[69] H.R. Hertz,
Über den Einfluss des ultravioletten Lichtes auf die elektrische Entladung,
Ann. Phys. u. Chem. **31**, 983 (1887)

[70] A. Einstein,
Über die Erzeugung und Verwandlung des Lichtes betreffenden heuristischen Gesichtspunkt,
Ann. Phys. **17**, 132 (1905)

[71] S. Hüfner,
Photoelectron spectroscopy,
Springer Series in Sol. Stat. Sci. **82,** 1st edition (1995)

[72] L. Ley, M. Cardona,
Photoemission in solids II, Case studies,
Topics in Appl. Phys. **27**, Springer-Verlag (1979)

[73] H. Hövel, I. Barke,
Morphology and electronic structure of gold clusters on graphite: scanning tunneling techniques and photoemission,
Progr. Sur. Sci. **81**, 53 (2006)

[74] A. Goldmann, J. Tejeda, N. J. Shevchik, M. Cardona,
Density of valence states of CuCl, CuBr, CuI, and AgI,
Phys. Rev. B **10**, 4388 (1974)

[75] I. Barke,
Morphology and electronic structure of gold clusters on graphite,
Dissertation, Technische Universität Dortmund (2004)

[76] M.P. Seah, W.A. Dench,
Quantitative electron spectroscopy of surfaces: A standard data base for electron inelastic mean free paths in solids,
Surf. Int. Anal. **1**, 2 (1979)

[77] H. Hövel, B. Grimm, M. Pollmann, B. Reihl,
Femtosecond dynamics of final-state effects in the valence band photoemission of silver clusters on a graphite substrate,
Europ. Phys. J. D **9**, 595 (1999)

[78] Omicron, instruments for surface science,
Channeltron, pulse counting electronics, CPC,
Version 1.0, (1996)

[79] V. Dose,
VUV Isochromat Spectroscopy,
Appl. Phys. **14**, 117 (1977)

[80] N. Miroslawski,
Geometrisch und electronisch magische Cluster,
Diploma thesis, Technische Universität Dortmund (2010)

[81] Omicron, instruments for surface science,
VUV discharge lamp HIS 13,
Version 1.6, (1996)

[82] M. Budke, M. Donath,
Ar gas discharge lamp with heated LiF window: a monochramatized light source for photoemission,
App. Phys. Lett. **92**, 231918 (2008)

[83] S. Suga et al,
High resolution low hv photoelectron spectroscopy with the use of a microwave excited rare gas lamp and ionic crystal filters,
Rev. Sci. Instr. **81**, 102111 (2010)

[84] O. Cheshnovsky, K.J. Taylor, J. Conceicao, R.E. Smalley,
Ultraviolet photoelectron spectra of mass selected copper clusters: Evolution of the 3d band,
Phys. Rev. Let. **64**, 1785 (1990)

[85] K.J. Taylor, C.L. Pettiette-Hall, O. Cheshnoysky, R.E. Smally,
Ultraviolet photoelectron spectra of coinage metal clusters,
J. Chem. Phys. **96**, 3319 (1992)

[86] P. Kruit, F.H. Read,
Magnetic field paralleliser for 2π electron-spectrometer and electron-image magnifier,
J. Phys. E: Sci. Instrum. **16**, 313 (1983)

[87] G. Wrigge, M.A. Hofmann, B. von Issendorff,
Photoelectron spectroscopy of sodium clusters: Direct observation of the electronic shell structure,
Phys. Rev. A **65**, 063201 (2002)

[88] M.A. Hoffmann, G. Wrigge, B. von Issendorff,
Photoelectron spectroscopy of Al^-_{32000}: Observation of a „Coulomb staircase“ in a free cluster,
Phys. Rev. B **66**, 041404 (2002)

[89] Ch. Schröder,
Ultraviolett-Photoelectronenspektroskopie an Metall-Clustern auf Edelgas,
Master thesis, Technische Universität Dortmund (2012)

[90] T. Irawan et al,
Metal clusters on rare gas layers - growth and spectroscopy,
Appl. Phys. A **82**, 81 (2006)

[91] I. Horcas et al,
WSxM: a software for scanning probe microscopy and a tool for nanotechnology,
Rev. Sci. Instrum. **78**, 013705 (2007)

[92] N. Grönhagen,
Wachstum von Nanostrukturen auf strukturiertem Graphit,
Diploma thesis, Technische Universität Dortmund (2008)

[93] M.A. San-Miguel, J. Oviedo, J.F. Sanz,
Cluster-surface interaction,
Handbook of nanophysics 2, Clusters and Fullerens, 1st edition, edited by K.D. Sattler, CRC Press (2011)

[94] R.M. Nielsen et al,
A comparative STM study of Ru nanoparticles deposited on HOPG by mass-selected gas aggregation versus thermal evaporation,
Surf. Sci. **603**, 3420 (2009)

[95] H. Hövel,
Clusters on surfaces: High-resolution spectroscopy at low temperatures,
Appl. Phys. A **72**, 295 (2001)

[96] B. Wortmann, K. Mende, S. Duffe, N. Grönhagen, B. von Issendorff, H. Hövel,
Ultraviolet photoelectron spectroscopy of supported mass selected silver clusters,
Phys. Stat. Sol. B **247**, 1116 (2010)

[97] R. Courths, H. Schulz, S. Hüfner,
High resolution photoemission spectra from a Cu(111) surface,
Solid State Comm. **29**, 667 (1979)

[98] S. Di Nardo et al,
UPS and XPS studies of Cu clusters on graphite,
Surf. Sci. **307**, 922 (1994)

[99] G.K. Wertheim, S.B. DiCenzo, S.E. Youngquist,
Unit charge on supported gold clusters in photoemission final state,
Phys. Rev. Let. **51**, 2310 (1983)

[100] G.K. Wertheim, S.B. DiCenzo, D.N.E. Buchanan,
Noble- and transition-metal clusters: The d bands of silver and palladium,
Phys. Rev. B **33**, 5384 (1986)

[101] J. Li, W.-D. Schneider, S. Crampin, R. Berndt,
Tunneling spectroscopy of surface state scattering and confinement,
Surf. Sci. **422**, 95 (1999)

[102] P. Nolte et al,
Combinatorial high-energy x-ray microbeam study of the size-dependent oxidation of Pd nanoparticles on MgO(100),
Phys. Rev. B **77**, 115444 (2008)

[103] J. Kliewer, R. Berndt, J. Minár, H. Ebert,
Scanning tunnelling microscopy and electronic structure of Mn clusters on Ag(111),
Appl. Phys. A **82**, 63 (2006)

[104] G. Henkelman, B.P. Uberuaga, H. Jónsson,
A climbing image nudged elastic band method for finding saddle points and minimum energy paths,
J. Chem. Phys. **113**, 9901 (2000)

[105] G. Kresse, J. Furthmüller,
Efficient iterative schemes for ab initio total-energy calculations using plane-wave basis set,
Phys. Rev. B **54**, 11169 (1996)

[106] T.T. Järvi, A. Kuronen, K. Meinander, K. Nordlund,
Contact epitaxy by deposition of Cu, AG, Au, Pt, and Ni nanoclusters on (100) surfaces: Size limits and mechanics,
Phys. Rev. B **75**, 115422 (2007)

[107] M. Pivetta,
Adsorbate- substrate interactions and electron confinement at surfaces,
Dissertaition, Université de Lausanne (2003)

[108] M. Pivetta et al,
Gap opening in the surface electronic structureof graphite induced by adsorption of alkali atoms: Photoemission experiments and density functional calculations,
Phys. Rev. B **71**, 165430 (2005)

[109] A. Savitzky, M.J.E. Golay,
Smoothing and differentiation of data by simplified least squares procedures,
Anal. Chem. **36**, 1627 (1964)

[110] G. Bader, G. Perluzzo, L.G. Caron, L. Sanche,
Elestic and inelastic mean-free-path determination in solid xenon from electron transmission experiments,
Phys. Rev. B **26**, 6019 (1982)

[111] B. Wortmann,
Spektroskopie von massenselektierten Clusters auf Oberflächen,
Diploma thesis, Technische Universität Dortmund (2009)

[112] N.V. Smith,
Phase analysis of image states and surface states associated with nearly-free-electron band gaps,
Phys. Rev. B **32**, 3549 (1985)

[113] T. Andreev, I. Barke, H. Hövel,
Adsorbed rare-gas layers on Au(111): Shift of the Shockley surface state studied with ultraviolet photoelectron spectroscopy and scanning tunnelling spectroscopy,
Phys. Rev. B **70**, 205426 (2004)

[114] A. Goldmann,
Noble metals, noble metal halides and nonmagnetic transition metals,
Landolt-Börnstein: Numerical data and functional relationships in science and technology- New series/Condensed matter **23c1** (2003)

[115] T.R. Ohno, J.C. Patrin, U.S. Ayyala, J.H. Weaver,
Ag deposition onto Xe: Clustering, incorporation, and surface attraction,
Phys. Rev. B **44**, 1891 (1991)

[116] H. Cheng, R.S. Berry, R.L. Whetten,
Electronic structure and binding energies of aluminium clusters,
Phys. Rev. B **43**, 10647 (1991)

[117] S. Peters, S. Peredkov, M. Neeb, W. Eberhardt, M. Al-Hada,
Size-dependent XPS spectra of small supported Au-clusters,
Surf. Scie. **608**, 129 (2013)

[118] M. Seidl, J.P. Perdew,
Size-dependent ionization energy of a metallic cluster: Resolution of the classical image-potential paradox,
Phys. Rev. B **50**, 5744 (1994)

[119] G. Wrigge, M. A. Hoffmann, B. von Issendorff, H. Haberland,
Ultraviolett photoelectron spectroscopy of Nb^-_4 to Nb^-_{200},
Eur. Phys. J. D **24**, 23 (2003)

[120] S. Degen, C. Becker, K. Wandelt,
Thin alumina films on $Ni_3Al(111)$: A template for nanostructured Pd cluster growth,
Faraday Discuss. **125**, 343 (2004)

[121] B. Fultz, J. Howe,
Transmission electron microscopy and diffractometry of materials,
Springer Verlag, 3rd edition (2008)

[122] R.F. Egerton,
Physical principles of electron microscopy,
Springer Verlag, 1st edition (2005)

[123] H. Hövel, A. Hilger, I. Nusch, U. Kreibig,
Experimental determination of deposition induced cluster deformation,
Z. Phys. D **42**, 203 (1997)

12 Acknowledgments

An dieser Stelle möchte ich allen, die zum erfolgreichen Gelingen dieser Arbeit beigetragen haben, herzlich danken.

Ich danke Herrn Prof. Dr. Metin Tolan dafür, diese Arbeit an seinem Lehrstuhl anfertigen zu dürfen.

Besonders herzlich möchte ich mich bei apl. Prof. Dr. Heinz Hövel bedanken. Durch seine große Fachkompetenz und gute Betreuung hat er wesentlich zum Erfolg dieser Arbeit beigetragen. Seine humorvolle und freundschaftliche Art schafften eine angenehme Arbeitsatmosphäre, in der ich sehr gerne gearbeitet habe.

Herrn Prof. Dr. Markus Betz danke ich für das Interesse an meiner Arbeit und die Bereitschaft das Zweitgutachten anzufertigen.

Weiterhin möchte ich Dr. Bärbel Siegmann für das Interesse an meiner Arbeit danken.

Unseren Kooperationspartnern Prof. Dr. Michael Moseler, Dr. Tommi Järvi und Prof. Dr. Bernd von Issendorff danke ich für die gelungene Zusammenarbeit. Michael Moseler und Tommi Järvi danke ich besonders für die Erstellung von MD und DFT Simulationen, die wesentlich zum Verständnis der experimentellen Daten beigetragen haben. Bernd von Issendorff danke ich für die Bereitstellung der experimentellen Daten aus Freistrahlexperimenten und die kompetente Beratung und Hilfestellung bei Fragen.

Weiterhin möchte ich Prof. Dr. Peter A. van Aken und Dr. Wilfried Sigle vom Max Planck Institut (MPI) in Stuttgart für die nette Zusammenarbeit und für die Durchführung der TEM Messungen danken.

Dr. Niklas Grönhagen, Dipl. Phys. David Engemann (ehem. Schützenkönig von Wulmeringhausen), M. Sc. Christoph Schröder und M. Sc. Paul Salmen möchte ich für die gelungene Zusammenarbeit und die anregenden Gespräche danken. Sie alle haben viel zum erfolgreichen Gelingen dieser Arbeit beigetragen und keinen Arbeitstag langweilig werden lassen. Ich freue mich besonders, dass die Clusterstrahlanlage mit Christoph als meinen Nachfolger in guten Händen ist.

Des Weiteren möchte ich mich bei allen Diplomanden, Masterstudenten, Doktoranden und Mitarbeitern des Lehrstuhls bedanken, die durch ihre freundschaftliche Art und den anregenden Austausch von Fachwissen ein effektives Arbeitsklima geschaffen haben.

Manuela Linke und Monika Voits-Besli danke ich für die Hilfe bei allen administrativen Aufgaben, sowie Thorsten Witt und Georg Jülicher für die Hilfe bei technischen Fragen aller Art.

Herrn Wiegers möchte ich für die freundliche Bereitstellung von flüssigem und gasförmigem Stickstoff und flüssigem Helium danken, vor allem, wenn es mal wieder schnell gehen musste.

Acknowledgments

Bei der mechanischen und elektronischen Werkstatt bedanke ich mich für die Hilfe, den Bau und die Reparatur von Geräten und Werkstoffen.

Ein besonderer Dank gilt meiner Familie, besonders meinen Eltern, und meinen Freunden, die mich während meines Studiums und meiner Promotion begleitet und unterstützt haben, insbesondere der *dorph*-Gruppe und meinen Mädels.

Besonders danken möchte ich noch meinem Freund Stefan, der mich mit seiner ruhigen und verständnisvollen Art immer wieder aufgebaut hat, wenn es mal nicht so gut lief, und mich immer unterstützt hat.

Eidesstattliche Versicherung

Hiermit erkläre ich an Eides Statt, dass die vorliegende Dissertationsschrift – abgesehen von der Beratung durch meine wissenschaftlichen Betreuer – nach Inhalt und Form meine eigene Arbeit ist. Ich habe keine anderen als die angegebenen Quellen und Hilfsmittel benutzt sowie wörtliche und sinngemäße Zitate kenntlich gemacht. Sie hat in gleicher oder ähnlicher Form noch keiner Prüfungsbehörde vorgelegen.

Dortmund, den

_ _

(Natalie J. Miroslawski)